# Title: Targeting an alternate Wilms Tumor Antigen-1 peptide bypasses immunoproteasome dependency

**Authors:** Miranda C. Lahman[1,2,3†], Thomas M. Schmitt[1,2†], Kelly G. Paulson[1,2,4,5†], Nathalie Vigneron[6†], Denise Buenrostro[1,2†], Felecia D. Wagener[1,2], Valentin Voillet[7,8], Lauren Martin[1,2], Raphael Gottardo[7,9], Jason Bielas[3,9,10], Julie M. McElrath[2,4,7], Derek L. Stirewalt[2,4], Era L. Pogosova-Agadjanyan[2], Cecilia C. Yeung[2,3,4], Robert H. Pierce[1,2,3,11], Daniel N. Egan[2,4,12], Merav Bar[2,4], Paul C. Hendrie[4], Sinéad Kinsella[1,2], Aesha Vakil[1,2], Jonah Butler[1,2], Mary Chaffee[1,2], , Jonathan Linton[1,2], Megan S. McAfee[1,2], Daniel S. Hunter[1,2],Marie Bleakley[1,2,13], Anthony Rongvaux[1,2,14], Benoit J. Van den Eynde[6,15], Aude G. Chapuis[1,2,3,4, †*], and Philip D. Greenberg[1,2,4,14†].

**Affiliations:**

[1]Program in Immunology, Fred Hutchinson Cancer Research Center, Seattle, WA, USA.

[2]Clinical Research Division, Fred Hutchinson Cancer Research Center, Seattle, WA, USA.

[3]Department of Pathology, University of Washington, Seattle, WA, USA.

[4]University of Washington School of Medicine, Seattle, WA, USA.

[5]Current Affiliations: Swedish Cancer Institute, Seattle, WA USA and Washington State University College of Medicine, Everett, WA USA.

[6]Ludwig Institute for Cancer Research, Brussels, Belgium; de Duve Institute, Université Catholique de Louvain, Brussels, Belgium.

[7]Vaccine and Infectious Disease Division, Fred Hutchinson Cancer Research Center, Seattle, WA, USA.

[8]Hutchinson Centre Research Institute of South Africa, Cape Town, South Africa.

[9]Public Health Sciences Division, Fred Hutchinson Cancer Research Center, Seattle, WA, USA.

[10]Human Biology Division, Fred Hutchinson Cancer Research Center, Seattle, WA, USA.

[11]Current Affiliation: Sensei Biotherapeutics, Boston, MA, USA.

[12]Current Affiliation: Swedish Cancer Institute Medical Oncology – Seattle, WA, USA.

[13]University of Washington School of Medicine, Department of Pediatrics, Seattle, WA, USA.

[14]Department of Immunology, University of Washington, Seattle, WA, USA

[15]Ludwig Institute for Cancer Research, Nuffield Department of Medicine, University of Oxford, Oxford United Kingdom

.

[†]Contributed equally

*Corresponding Author; achapuis@fredhutch.org

Fred Hutchinson Cancer Research Center (FHCRC)

1100 Fairview Ave N, Mail Stop: D3-100, Seattle, WA 98109

**One Sentence Summary:** Targeting the alternate Wilms Tumor-1 (WT1) epitope $WT1_{37\text{-}45}$ circumvents engineered T cell receptor gene therapy resistance by acquisition of immunoproteasome deficiency in acute myeloid leukemia.

**Abstract:**

Designing effective anti-leukemic immunotherapy will require elucidating mechanisms underlying tumor control or resistance. Here we report a new mechanism of escape from immunologic targeting in an AML patient, who relapsed one year following T cell immunotherapy with engineered T cells expressing an HLA-A2 restricted T cell receptor specific for a Wilms' Tumor Antigen 1 epitope ($WT1_{126\text{-}134}$). Resistance occurred despite persistence of functional therapeutic T cells and continuous expression of WT-1 and HLA-A2 by the patient's AML. Analysis of the recurrent AML revealed expression of the standard proteasome (SP), but limited expression of the immunoproteasome (IP), specifically beta subunit 1i (β1i) which is required for presentation of $WT1_{126\text{-}134}$. To determine if the WT1 protein continued to be processed and presented in the absence of IP processing, we identified and tested a TCR targeting an alternative, HLA-A2 restricted $WT1_{37\text{-}45}$ epitope, which was found to be generated by IP deficient cells including WT1 expressing solid tumor lines. T cells expressing this TCR ($T_{TCR37\text{-}45}$) killed the patients' relapsed AML resistant to targeting the $WT1_{126\text{-}134}$ epitope and other primary AML *in vitro*. $T_{TCR37\text{-}45}$ controls solid tumor line which lacks IP subunits both *in vitro* and in an NSG mouse model. Defining and preferentially targeting such proteasome independent epitopes can maximize therapeutic efficacy and potentially circumvent proteasome-related immunoediting resulting in AML immune evasion.

## Introduction

Allogenic hematopoietic cell transplant (HCT) can cure some patients with high-risk acute myeloid leukemia (AML), which is largely a result of donor T cells eliminating leukemia by recognizing minor histocompatibility antigens or less commonly leukemia-associated antigens (*1*). This graft-versus-leukemia (GVL) effect is sporadic, entirely reliant on donor immune cell recognition of differences between host and donor cells, and has not been predictable pre-HCT. Leukemic relapse post-HCT remains the leading cause of death, especially in patients who enter HCT with features of high-risk AML, in part due to the inability to ensure a GVL effect.

Adoptive therapy can provide T cells re-directed towards defined tumor-associated antigens. Most notably, chimeric antigen receptors (CARs) targeting surface proteins, such as CD19 or BCMA, have shown stunning clinical results in B cell malignancies (*2, 3*). For AML, identifying surface proteins that are unique or safely targetable remains a challenge (*4*). By contrast, T cell receptors (TCRs) can recognize a broader set of peptides, which can be derived from intracellular and surface proteins (*5*). To achieve consistent antileukemic activity, we sought to target Wilms' Tumor Antigen 1 (WT1), an intracellular transcription factor detected at very high levels in most leukemic cells but at very low levels in normal adult tissues (*6-9*). Although not present routinely in peptide elution sets (*10*), suggesting there may not be abundant presentation of the processed peptide, the $WT1_{126\text{-}134}$ peptide was successfully eluted from an HLA-A*02:01 leukemia confirming presentation (*11*). T cells targeting $WT1_{126\text{-}134}$ have contributed to maintenance of sustained complete responses in vaccine trials and exhibited a direct anti-leukemic effect in our group's prior clinical study in which donor-derived WT1-specific $CD8^+$ T cell clones were transferred into patients post-HCT (*12-15*).

Based on these results, we isolated a high affinity TCR restricted to human leukocyte antigen (HLA)-A*02:01 and specific for the $WT1_{126\text{-}134}$ epitope, denoted TCR-C4, and cloned it into a clinically-validated lentiviral vector. Donor Epstein Barr Virus (EBV)-specific $CD8^+$ T cells were selected as substrates to both minimize risk of graft-versus-host disease (GVHD) and enhance survival of therapeutic cells – EBV-specific $CD8^+$ T cells transduced with TCR-C4 ($T_{TCR\text{-}C4}$) (*16, 17*) (NCT01640301). Following prophylactic administration to HLA-matched high-risk AML patients post-HCT, $T_{TCR\text{-}C4}$ demonstrated *in vivo* persistence and sustained remissions were achieved in all patients despite risk of relapse that exceeded 50% (*18*). However, a formal assessment of direct anti-tumor activity of $T_{TCR\text{-}C4}$ was challenging as leukemia was undetectable at the time of $T_{TCR\text{-}C4}$ transfer.

By re-directing T cell recognition towards a known tumor epitope, adoptive therapy trials offer the added benefit of limiting the tumor-T cell interaction to a defined target. Paradoxically, the requirements for a therapeutic response can often be better elucidated not in patients with complete sustained responses but rather in patients whose tumors acquire resistance to the immune intervention. This can reveal critical response and evasion mechanisms (*19*).

Tumor escape after CAR- T infusions has commonly reflected loss of the targeted antigen epitope from the cell surface (*20*). For TCR-mediated interventions this would be best paralleled by loss of expression of the targeted antigen or the MHC restricting-allele (*21*). HLA loss has rarely been associated with post-HCT relapse in AML (*21*) and WT1 mutation has not been a major contributor to immune escape in AML patients who received WT1 peptide vaccination (*22*) or infusions of clonal WT1-specific T cells in our previous study (*15*). Instead, and specific to targeted TCR-T cell therapy, presentation of the targeted epitope can be impacted by

proteasome processing (*23*). Indeed, $TCR_{C4}$'s targeted $WT1_{126\text{-}134}$ epitope is reliant on the immunoproteasome (IP) (*24*), the dominant isoform in hemopoietic cells (*25, 26*).

To investigate potential mechanisms of AML resistance to $T_{TCR\text{-}C4}$, one patient was identified who relapsed post second transplant, experienced an apparent sustained remission after receiving $T_{TCR\text{-}C4}$ but then relapsed one year later, despite large numbers of persistent transferred $T_{TCR\text{-}C4}$ was identified. We performed high-dimensional analysis of the persistent T cells and recurrent AML, which confirmed $T_{TCR\text{-}C4}$ were functional and AML continued to express both restricting HLA Class I allele (HLA-A*02) and unmutated WT1. Further in-depth analysis and observations in a second patient who received $T_{TCR\text{-}C4}$ with circulating $WT1^{+}$ AML point to a previously undescribed mechanism of *in vivo* AML escape from a targeted T cell response, involving changes in antigen-processing of the targeted epitope.

We then pursued an alternative HLA-A*02:01-restricted epitope, $WT1_{37\text{-}45}$, that is less susceptible to the observed mechanism of resistance and thus represents a promising TCR-T cell immunotherapy target. Our data underscore the necessity of elucidating acquired resistance mechanisms to inform rational design of more effective TCR-T cell therapy not only for AML but immunotherapy more broadly.

**Results**

*An unusual clinical course warranting deeper investigation*

A 27-year-old patient developed recurrent AML with both extramedullary chloromas and minimal residual disease (MRD) in the marrow 7 months after receiving a second matched, unrelated donor HCT for relapsed refractory disease (**Fig. 1A** and **Supplementary Methods**).

The patient was treated with local radiation and systemic salvage chemotherapy, which achieved remission as evidenced by no evaluable disease (NED), and then received infusion of donor-derived $T_{TCR\text{-}C4}$ on this study (*18*). Based on the history of relapsing after a second allo-HCT, he was at extremely high risk of early relapse and death (AML relapse post-HCT is associated with a median survival of ~3 months (*27*)). Surprisingly, the patient remained in remission without further therapy for 368 days before exhibiting recurrent AML with both a bladder chloroma and flow-cytometric evidence of MRD (0.04% AML cells) in the marrow. He then received reinduction chemotherapy followed by a second $T_{TCR\text{-}C4}$ infusion on day 471 after the 1st infusion with T cells derived from the same pool of transduced cells originally infused, but the leukemia continued to relentlessly progress. This unusual clinical course with a long 1-year remission after multiple relapses led us to investigate potential immunologically-related mechanisms of remission and relapse.

*Phenotypically similar, functional $T_{TCR\text{-}C4}$ persist through remission and relapse.*

Both infusions of $10^{10}$ $T_{TCR\text{-}C4}/m^2$ (on days 0 and 471) were administered without prior lymphodepleting chemotherapy. $T_{TCR\text{-}C4}$ in peripheral blood (PB) reached peak frequencies of 8.2% and 56% of $CD8^+$ T cells after the 1st and 2nd infusion, respectively (**Fig. 1B** and **Supplementary Methods**). Overall, $T_{TCR\text{-}C4}$ frequency remained >3% with sustained, robust absolute $T_{TCR\text{-}C4}$ counts (**Fig. S1A**). Comparable high $T_{TCR\text{-}C4}$ frequencies were observed in the bone marrow at days 28 and 368 (**Fig. 1B, green circles**). These high levels of persistent transferred $T_{TCR\text{-}C4}$ cells are analogous to results obtained in patients who received $T_{TCR\text{-}C4}$ post-HCT prophylactically to prevent relapse (*18*). Both infusion products were expanded immediately prior to infusion from identical pre-infusion aliquots (*28*). Infusions consisted primarily (>75%) of a single expanded clonotype that also comprised majority of persistent $T_{TCR\text{-}C4}$ after both

infusions (**Fig. 1C and Fig. S1B**). $T_{TCR\text{-}C4}$ surface expression of memory-associated markers (CD45RO, CD27, CD28, and CD62L (*29*)) remained similar after both $T_{TCR\text{-}C4}$ infusions (**Fig. 1D, Fig. S2A**). *Ex vivo* analysis of recovered $T_{TCR\text{-}C4}$ revealed the cells were functional, maintaining cytokine production in response to targets presenting the cognate $WT1_{126\text{-}134}$ peptide during the period of apparent remission (day 114) and in the context of progressive AML (day 70 or day 541 after the 2nd or 1st infusion, respectively) (**Fig. 1E, Fig S2B**).

*scRNAseq reveals $T_{TCR\text{-}C4}$ transcriptome during remission is compatible with recent activation*

To investigate if transcriptomes of circulating $T_{TCR\text{-}C4}$ differed between clinical remission and relapse, single-cell RNA sequencing (scRNAseq) (*30*) was performed on available peripheral blood mononuclear cells (PBMC) 100 days after the 1st $T_{TCR\text{-}C4}$ infusion (remission) and 110 days after the 2nd infusion (relapse), which represents 581 days after the 1st infusion (**Fig. 1B, dotted red lines).** Data were generated from a single sequencing run containing both samples, reads were aggregated together, clusters were delineated (**Fig. 2A, Fig. S3**), and then visualized separately, based on barcodes unique to the timepoint (**Fig. 2B**). Surprisingly, during clinical remission, $CD8^+$ cells grouped into 2 separate and distinct clusters in an unsupervised transcriptional profile analysis (**Fig. 2C, light blue and purple clusters**), but the light blue cluster was nearly absent at relapse (**Fig. 2D**). During remission 96% of $T_{TCR\text{-}C4}$, identified by TCR-C4 transgene expression, were grouped in the light blue cluster whereas endogenous $CD8^+$ T cells grouped in the purple cluster (**Fig. 2E)**. In contrast, during relapse in the presence of circulating blasts, 91% of $T_{TCR\text{-}C4}$ grouped with the purple endogenous $CD8^+$ cells (**Fig. 2F**). To probe for differences between $T_{TCR\text{-}C4}$ at remission and relapse, an unsupervised differential gene expression analysis was performed. The 10 most significantly differentially expressed genes found in remission $T_{TCR\text{-}C4}$ comprised genes associated with T cell activation, including

lymphotoxin-β [*LTB*], granzyme K [*GZMK*], human leukocyte antigen DR [*HLA-DR*] and CD74 [*CD74*], which mediates assembly and trafficking of Class II complexes (**Fig. 2G**) (*31-34*). Gene set analysis of effector cytokine/chemokine genes (*35, 36*) (Interferon gamma (IFNγ) [*IFNG*], C-X-C motif chemokine receptor 1 [*CX3CR1*], C-C Motif Chemokine Ligand 5 [*CCL5*] and Tumor Necrosis Factor alpha (TNFα) [*TNF*]), cytolytic effector genes (*36*) (granzymes A [*GZMA*], B [*GZMB*] and H [G*ZMH*] and perforin [*PRF1*]), activation/proliferation genes (*37*) (Jun proto-oncogene [*JUN*], Fos proto-oncogene [*FOS*], CD69 [*CD69*], nuclear receptor subfamily 4 group A member 1 [*NR4A1*], interleukin 2 receptor subunit gamma [*IL2RG*], and interleukin 2 receptor subunit alpha [*IL2RA*]) and activation/exhaustion genes (Programmed Cell Death Receptor-1 [*PDCD1*], T-Cell Immunoreceptor With Ig and ITIM Domains, [*TIGIT*], Lymphocyte Activating 3 [*LAG3*], and Cytotoxic T-Lymphocyte Associated Protein 4, [*CTLA4*]) were significantly enriched in $T_{TCR\text{-}C4}$ at remission vs. relapse ($p=2.98 \times 10^{-8}$, $p=3.25 \times 10^{-3}$, $p=2.11 \times 10^{-2}$ and $p=1.87 \times 10^{-4}$ respectively) (**Fig. 2H**), suggesting repetitive stimulation/activation during remission. Although not every gene in each composite gene-set was individually statistically significant, each of the total gene-sets were significantly different. For example, expression of IFNγ and TNFα assessed individually did not quite achieve statistical significance but were significant as part of the effector cytokine/chemokine gene-set, which may reflect both the known decline in expression of these genes after dissociation from the activating signal (*38*) and potential decline of polyfunctionality from repetitive activation events.

Furthermore, comparison of endogenous $CD8^+$ T cells from the same sample to remission $T_{TCR\text{-}C4}$ transcriptomes again revealed significant enrichment for the effector cytokine/chemokine, activation/proliferation and activation/exhaustion gene-sets in $T_{TCR\text{-}C4}$ ($p=4.89 \times 10^{-2}$, $p=4.89 \times 10^{-2}$ and $p=0.007$ respectively) (**Fig. S4**), suggesting the profile represents antigen-specific events

rather than global activation of T cells in the host. As previously evidenced, $T_{TCR\text{-}C4}$ remained functional at both timepoints (**Fig. 1E**), consistent with the T cells being in an activated but not exhausted state. The differences in gene expression (Log2-fold change) observed at remission between $T_{TCR\text{-}C4}$ and endogenous cells were lost at relapse (**Fig. S5**).

As $T_{TCR\text{-}C4}$ also contains an endogenous EBV-specific TCR, the patient was screened for evidence of EBV reactivation as a potential explanation for T cell activation. A very low level of viral genomes was detectable immediately after the 1st $T_{TCR\text{-}C4}$ infusion (*18*), but were not detected by day 7 or at serial timepoints thereafter (**Table S1**). The results suggest $T_{TCR\text{-}C4}$ may have lysed/eliminated an EBV reservoir shortly after infusion. Although the possibility of low level EBV antigen presentation leading to signaling through the endogenous EBV-specific TCR cannot be eliminated and could explain T cell activation during the prolonged period of clinical remission, this appears unlikely as $T_{TCR\text{-}C4}$ at relapse, a time when systemic illness might be more likely to lead to EBV reactivation, no longer exhibited evidence of activation. This in turn infers $T_{TCR\text{-}C4}$ at relapse were not recognizing/responding to leukemia and/or low level EBV antigen. Consequently, we next evaluated the antigenicity of the patient's leukemia.

*AML during relapse demonstrates expression of unmutated WT1 and HLA-A*02:01*

AML samples for immunohistochemistry (IHC) were obtained from a bone marrow aspirate during relapse after the first allo-HCT and prior to the first $T_{TCR\text{-}C4}$ infusion (**Fig. 3A,B)**, from a bladder chloroma at the time of relapse after the 1st $T_{TCR\text{-}C4}$ infusion (**Fig. 3A,C)**, and from a bone marrow aspirate 71 days after the 2nd $T_{TCR\text{-}C4}$ infusion (**Fig. 3A,D)**. All specimens showed abundant WT1 protein expression in the majority (>90%) of leukemic blasts (**Fig. 3B,C,D)**. Clinical-grade next-generation sequencing performed at relapse after $T_{TCR\text{-}C4}$ (day 58 after the 2nd

$T_{TCR\text{-}C4}$ infusion) found no WT1 sequence mutations (see **Supplementary Methods**). However, $CD8^+$ T cells were not enriched in the chloroma (**Fig. 3C**), consistent with the lack of an effective T cell response at relapse. To assess potential differences in epitope presentation, Class I protein expression was evaluated. On AML prior to the second HCT, IHC could be performed only for total Class I expression, which was positive (**Fig. 3B**). HLA-A expression was evaluable in the cervical chloroma at relapse before any $T_{TCR\text{-}C4}$ infusions, using bulk RNA sequencing on residual clinical material from an archival formalin fixed, paraffin embedded (FFPE) specimen. As control, HLA-A was also analyzed from PBMC obtained 110 days after the $2^{nd}$ $T_{TCR\text{-}C4}$ infusion (the same sample on which scRNAseq was performed). HLA-A expression was detected in the samples (**Fig. 3E**), both of which contained ≥80% AML. Note, the NanoString platform utilized permitted only probing for HLA-A and not a specific allele (see **Supplementary Methods**). However, HLA-A2 expression was directly evaluable on relapsed AML cells present in PBMC obtained 110 days after the $2^{nd}$ $T_{TCR\text{-}C4}$ infusion (**Fig. 3F**). The presence of Class I at all time points and specifically HLA-A2 at the last relapse suggests HLA-A*02:01 expression was retained throughout the disease. The expression of both unmutated target protein and restricting HLA allele at late relapse excludes antigen loss/mutation or restricting HLA loss/downregulation as the cause of AML immune escape in the presence of abundant, potentially reactive, functional $T_{TCR\text{-}C4}$.

*scRNAseq reveals relapsed AML after $T_{TCR\text{-}C4}$ infusions had low expression of immunoproteasome subunits, potentially hampering $WT1_{126\text{-}132}$ processing and presentation.*

We next investigated antigen processing components in relapsed AML after $T_{TCR\text{-}C4}$ infusions to account for the presumed failure of recognition. Evaluation by scRNAseq of the top 100 most significantly differentially expressed genes in AML versus non-AML hematopoietic cells (in the

same sample) revealed that the AML cells had significantly lower expression of the immunoproteasome subunit gene β1i [*PSMB9*] (**Fig. 3G, red arrow)**, which was confirmed by very low to undetectable β1i protein expression in relapsed AML (**Fig. S6**).

Due to the absence of a viably frozen pre-treatment AML sample, it was difficult to directly address if this patient's leukemia expressed the immunoproteasome before $T_{TCR\text{-}C4}$ targeting $WT1_{126\text{-}134}$ were initially infused. Therefore, we used residual clinical material from the cervical chloroma FFPE specimen (before the 1st $T_{TCR\text{-}C4}$ administration) and PBMC obtained 110 days after the 2nd $T_{TCR\text{-}C4}$ infusion (**Fig. 3E**) to assess changes in proteasome subunit expression. Compared to pre-$T_{TCR\text{-}C4}$, AML post-$T_{TCR\text{-}C4}$ had more transcripts encoding proteins ubiquitously present in the caps of all 26S proteasomes (ATPase 2 [*PSMC2*] and non-ATPase 7 [*PSMD7*]) (**Fig. 3H, black bars**), suggesting comparatively increased total proteasome in AML post-$T_{TCR\text{-}C4}$ (*23*). However, AML post-$T_{TCR\text{-}C4}$ had less transcripts associated with the IP subunits, β5i (fold change -0.14) and β1i (fold change -0.67), which would restrict IP formation. Although β2i was not decreased (fold change +0.25), its incorporation into an IP requires β1i, as its presence alone cannot drive IP formation (**Fig. 3H, blue bars**) (*39*). In contrast, although β1 was unavailable for assessment (see **Supplementary Methods**), an increase in β2 (fold change +0.63) and minimal change in β5 (fold change -0.1) was detected suggesting the AML may have preferentially formed the SP (**Fig. 3H, purple bars**). The decrease in β1i resulted in minimally detectable transcripts in the post-$T_{TCR\text{-}C4}$ specimen (**Fig. S7)**, confirmed by absent β1i protein expression (**Fig. S6).** Furthermore, expression level of transcripts encoding proteins constituting the active proteolytic site of the immunoproteasome (β5i [*PSMB8*], β1i [*PSMB9*], and β2i [*PSMB10*]) were significantly ($p<0.01$) decreased, whereas those constituting the active

proteolytic site of the standard proteasome (β5 [*PSMB5*], β1 [*PSMB6*] and β2 [*PSBM7*]) were significantly increased ($p<0.01$) in the AML cells compared to other hematopoietic cells (**Fig. 3I)**. Likewise, the frequency of cells expressing IP subunits β1i [*PSMB9*], and β2i [*PSMB10*] were markedly lower in the relapsed AML while the frequency of cells expressing SP subunits β5 [*PSMB5*], β1 [*PSMB6*] and β2 [*PSBM7*] in these cells was increased in comparison to other hematopoietic cells. IP subunit β5i [*PSMB8*], however, opposed this trend with 50% of relapsed AML cells expressing the transcript compared to 28% of other hematopoietic cells. Reduced [*PSMB9*] expression was not a result of gene mutation, as whole exome sequencing on the relapsed AML did not reveal any pathogenic mutations in *[PSMB9]* (See **Supplementary Methods**). Moreover, the relapsed AML retained expression of IFNγ response genes at similar levels to other cells in the PBMC suggesting cytokine responsiveness remained intact (**Fig. S8**).

To confirm that PSMB9 is required for $WT1_{126\text{-}134}$ processing and $T_{TCR\text{-}C4}$ recognition, $T_{TCR\text{-}C4}$ were co-cultured with cells lines genetically modified to express the IP, SP, an intermediate proteasome with a single immunoproteasome subunit (β5i, β1, β2, (sIP)), or an intermediate with two immunoproteasome subunits (β5i, β1i, β2, (dIP)) (*40*). Indeed, $T_{TCR\text{-}C4}$ were found to only recognize cell lines expressing proteasome isoforms containing β1i (**Fig. 3J**).

To assess whether low PSMB9 may be present in other AML specimens, which would suggest this may be a more common phenomenon, we compared the relapsed leukemia to data from six normal-donor mobilized peripheral blood stem cell samples and 38 enriched primary AML blast samples obtained from the Fred Hutch-University of Washington Hematopoietic Diseases Repository. PSMB9 (β1i) RNA expression in this patient's relapse AML was markedly lower

compared to other AML specimens, but this reduction was not rare, as 8 other AMLs also had reduced levels (**Fig. 3K**). With the caveat that adequate AML cells prior to the final relapse were unavailable, for detailed analysis, the data suggests the absence of β1i in this patient's AML at relapse may have compromised recognition be $T_{TCR\text{-}C4}$.

*$T_{TCR\text{-}C4}$ preferentially eliminates WT1+ AML blasts co-expressing* β1i.

A second patient (Patient 2) on this trial was identified who received $T_{TCR\text{-}C4}$ and had blasts available before and after T cell infusion (**Fig. 4A** and **Supplementary Methods**). This patient's AML constituted 70.2% of PBMC at the time of $T_{TCR\text{-}C4}$ infusion. Although the absolute blast count moderately decreased immediately after infusion, the AML eventually progressed despite persistence of $T_{TCR\text{-}C4}$ at >3% of peripheral $CD8^+$ T cells, and he succumbed to progressive disease 15 days after transfer (**Fig. 4B, Fig. S90**). ScRNAseq on PBMC obtained before $T_{TCR\text{-}C4}$ infusion showed the AML blasts were heterogenous and formed 7 leukemic clusters (**Fig. 4C, Fig. S10**), all expressing one or more of the AML-associated genes CD34, CCND1, CDK6, FLT3, NPM1 and RUNX1(**Fig. 4D, Fig. S11**). Five days after infusion, clusters "AML Blasts 2" and "AML Blasts 3" decreased whereas clusters "AML Blasts 1" and "monocytic AML1" expanded (**Fig 4E**). The expression of AML-associated genes were unchanged (**Fig. S11**). HLA-A also remained expressed (**Fig. 4F**). However, the frequency of WT1-expressing cells decreased from 27% to 2.5% after $T_{TCR\text{-}C4}$ exposure, with the most noticeable reduction in the 2 clusters that expressed the highest levels of WT1 (**Fig. 4G, left**). WT1 loss was confirmed by IHC (**Fig. 4G, right**). In all blast populations expressing WT1 and β1i ([PSMB9]), but especially in the expanding clusters ("AML Blasts 1" and "monocytic AML1"), only the proportion of cells that co-expressed WT1 and β1i ([PSMB9]) was reduced after $T_{TCR\text{-}C4}$ exposure (25.1% to 1.3% or a 19-fold reduction), whereas the proportion of cells that only

expressed WT1 remained proportionately similar (24.6% to 28.6%)(**Fig. 4I**). These data supports the hypothesis that $T_{TCR\text{-}C4}$ exposure only efficiently eliminates WT1+ blasts that also express β1i.

*Targeting $WT1_{37\text{-}45}$ can overcome absence of WT1 immunoproteasome processing and expand therapeutic potential to solid tumors.*

We next investigated whether targeting alternative HLA-A*02:01-restricted WT1 epitopes could have a therapeutic potential towards $IP^{low}$ AML presumed resistant to $T_{TCR\text{-}C4}$ recognition or solid tumors that generally lack IP processing. Identifying epitopes not requiring a specific proteasome isoform might avoid potential immunotherapy resistance and thereby broaden the clinical translation of targeting WT1, since loss of the IP doesn't appear to impact leukemia viability and has been shown to promote oncogenicity in some solid tumors (*41, 42*). We generated T cell lines from 15 healthy donors (two shown) recognizing eight previously described HLA-A*02:01-restricted WT1 epitopes (**Fig. 5A**) (*43-45*). Our screen identified $WT1_{37\text{-}45}$ and $WT1_{235\text{-}243}$ as promising immunogenic candidates. Cell lines targeting $WT1_{37\text{-}45}$ and $WT1_{235\text{-}243}$ were sorted on tetramer positivity (**Fig. 5B**) and assessed for reactivity towards the $WT1^+$ K562 cell line which primarily expresses the SP and is not lysed by T cells targeting $WT1_{126\text{-}134}$, transfected with HLA-A*02:01 (**Fig. 5C, D**).(*24, 46*) A high affinity TCR reactive to $WT1_{37\text{-}45}$ ($TCR_{37\text{-}45}$) was isolated from the cell lines and inserted into a lentiviral backbone (see **Supplementary Methods**). $CD8^+$ T cells expressing $TCR_{37\text{-}45}$ ($T_{TCR37\text{-}45}$) recognized (**Fig. S13**) and lysed HLA-A2- and WT1-transduced HEK-293 cell lines (endogenous SP expression) +/- engineered to express the IP (**Fig. 5E, F**, see **Supplementary Methods**) (*47*). Of note, WT1 expression was not uniform (*48*) in the cells from the WT1-transduced IP and SP cell lines (**Fig. 5F**), which limited the maximal lytic activity achieved in this assay. $CD8^+$ T cells expressing either $TCR_{C4}$

or $TCR_{37\text{-}45}$ lysed HLA-$A2^+WT1^+$primary AML cells (**Fig. 5G**), but only $TCR_{37\text{-}45}$ induced caspase 3 cleavage in the first patient's (**Figs 1-3**) $T_{TCR\text{-}C4}$-resistant AML (**Fig. 5H**). Furthermore, only $TCR_{37\text{-}45}$ reduced growth of the WT1 expressing solid tumor cell lines PANC-1(*49*) and HLA-A*02:01-transduced MDA-MD-683(*50*) in a live tumor visualization assay (**Fig. 5I,** see **Supplementary Methods**). Exposing the PANC-1 cell line to the inflammatory cytokine IFNγ for 48 hours increased β1i expression (**Fig. S13A)** and enhanced recognition by $TCR_{C4}$ (**Fig. S13B**).

In anticipation of targeting $WT1_{37\text{-}45}$ for future clinical translation in both solid and liquid tumors, we sought to maximize the clinical efficacy by also modeling the engagement of both $CD4^+$ and $CD8^+$ T cells as has proven efficient for CAR-T cells approaches with a 1:1 ratio $CD8^+$:$CD4^+$ (*51*). Antigen-specific $CD4^+$ T cells, restricted by class II, enhance $CD8^+$ T cell survival, proliferation and function (*52*). As class II expression is not always expressed by tumors (*53*), an alternative is to impart tumor recognition to $CD4^+$ T cells through expression of a class I-restricted TCR that would co-localize engineered $CD8^+$ and $CD4^+$ T cells on the same tumor target without requiring class II expression. Although high affinity TCRs can engage $CD4^+$ T cells without CD8αβ binding, this is rarely the case for TCRs targeting self-proteins such as WT1 with such high affinity are rarely detectable (*54*). To engineer functional $CD4^+$ T cells targeting $WT1_{37\text{-}45}$ we incorporated CD8αβ along with $TCR_{37\text{-}45}$ into a lentiviral vector (see **Supplementary Methods**). Transduction with this vector generated cells with additional CD8 on the surface yielding 'enhanced' $CD8^+$ T cells ($eCD8^+$) and $CD4^+$ T cells co-expressing CD8 and CD4 (double positive $CD4^+$, $dpCD4^+$). We next assessed the relative contribution of the CD8αβ to the function of $CD8^+$ and $CD4^+$ T cells individually and in combination by intentionally decreasing the effector to target ratio from 10:1 to 4:1 and repetitively adding tumor cells to

"stress" the engineered T cells. Increased expression of CD8αβ did not significantly improve tumor control by eCD8$^+$ cells compared to TCR-transduced CD8$^+$ T cells (**Fig. 5J**), but dpCD4$^+$ did mediate a sustained antitumor response, whereas CD4$^+$ T cells transduced with the TCR alone were ineffective (**Fig 5K**). Furthermore, a 1:1 mixture of eCD8$^+$/dpCD4$^+$ $T_{TCR37\text{-}45}$ cells more effectively controlled both solid tumor cell lines, PANC-1 and HLA-A*02:01-transduced MDA-MB-468, than either eCD8$^+$ or dpCD4$^+$ $T_{TCR37\text{-}45}$ cells alone (**Fig. 5L**). Of note, none of these combinations were effective in clearing PANC-1 targets when CD8αβ was added to $TCR_{C4}$ in CD4 and CD8 T cells suggesting the addition of CD8αβ does not rescue reactivity in the context of limited antigen processing (**Fig S145**). DpCD4$^+$ T cells, when compared to eCD8$^+$ T cells alone, generally secreted abundant inflammatory cytokines (IFNγ, TNFα, IL-2), cytokines associated with a helper function (IL-6, IL-17 and IL-21) or a Th2 response (IL-4, IL-13) and limited IL-10 associated with regulatory function (*55*). Although co-cultures of eCD8$^+$/dpCD4$^+$ resulted in less abundant cytokines compared to dpCD4$^+$ T cells alone; with the exception of IL-6, the amount of cytokines was significantly greater than for eCD8$^+$ T cells alone (**Fig. S16**). Together, these *in vitro* data suggest TCRs targeting $WT1_{37\text{-}45}$ might be efficient against AMLs and solid tumors which have limited IP expression (*23*).

*$T_{TCR37\text{-}45}$ cells but not $T_{TCR\text{-}C4}$ reduce the tumor burden of PANC-1, a solid tumor that expresses limited β1i.*

We next investigated whether eCD8$^+$/dpCD4$^+$ *$T_{TCR37\text{-}45}$* could reduce the burden of established PANC-1 tumor, which in the absence of prolonged exposure to IFNγ, incorporates limited β11 into the proteasome in comparison to the THP-1 AML cell line (**Fig. S13A**). An NSG mouse model with an 'established' PANC-1 tumor was used to compare the activity of eCD8$^+$/dpCD4$^+$ with *$T_{TCR37\text{-}45}$* or *$T_{TCR\text{-}C4}$* or irrelevant control (*$T_{TCR\text{-}irr}$*) (**Fig 6A**). Indeed, eCD8$^+$/dpCD4$^+$ $T_{TCR37\text{-}}$

$_{45}$ effectively reduced detectable tumor in 4/5 mice but $T_{TCR-C4}$ and $T_{TCR-Irr}$ were unable to reduce established tumor (**Fig. 6B, C**). Thus, $T_{TCR37-45}$ was the only transduced T cell to significantly reduce PANC-1 tumor compared to tumor alone (**Fig. 6D**). Moreover, $eCD8^+/dpCD4^+$ $T_{TCR-37-45}$ T cells also controlled PANC-1 tumor outgrowth ($P<0.0001$) in a 'preventive' NSG mouse model (**Fig. S16**).

**Discussion**

Here, we show evidence pointing to a previously undescribed mechanism of AML resistance to immunologic targeting that is proteasome dependent. Proteasomes are responsible for the degradation of proteins into peptides subsequently presented in class I HLA molecules, and the enzymatic composition of the proteasome can determine precisely which peptides are presented (*56*). In our first clinical case, escape under the immunologic pressure of a focused antigen-specific T cell response may have resulted in selection of leukemic cells with altered protein processing machinery, leading to failure of the leukemic cells to present the targeted epitope.

The standard proteasome (SP) is expressed in all somatic cells and contains a catalytic core composed of three enzymatic subunits (β1, β2, and β5). The immunoproteasome (IP) by contrast is expressed in hematopoietic cells and can be induced in most somatic cells by IFNγ. It has a different catalytic core comprised of distinct enzymatic β-subunits (β1i, β2i, and β5i). The IP and SP each produce a broad spectrum of peptides, including many identical peptides, but the IP produces a more diverse set of peptides that are generally considered more immunogenic (*56, 57*). Proteasomes assemble in a cooperative fashion; incorporation of β5i into the pro-form of the proteasome promotes subsequent incorporation of β1i and β2i to form a functional IP (*58*). For SP formation, β5 incorporation leads to preferential incorporation of β1 and β2 (*59*). Formation of IP is more efficient and takes precedence over SP formation, which is evident by the dominant

presence of intact IPs in cells that express the catalytic components of both proteasome types (*59, 60*). Unlike solid tumors which preferentially express the SP, hematopoietic cells including AMLs generally predominantly express the IP, and thus largely display peptides that have been processed by the IP (*61*). As generation of the $WT_{126\text{-}134}$ peptide appears to be exquisitely dependent on the presence of β1i as integral part of the IP, processing of this epitope would be severely hampered following loss or downregulation of β1i.

Our study has limitations and raises questions that warrant future elucidation. We only observed one such 'resistant' case in this small initial trial, no conclusions can be derived as to the frequency of this mechanism either under natural immunologic pressure or as a result of immunotherapy. The timing of the clinical sampling for the first patient and the unavailable 'fresh' leukemia prior to $T_{TCR\text{-}C4}$ infusion, hampered the ability to unequivocally demonstrate the recurrence was due to the loss of β1i. The presence of other leukemias with low levels of β1i and the progression of the second patient's' AML with reduced WT1/β1i co-expression after $T_{TCR\text{-}C4}$ suggests there are many other potential obstacles to efficacy with engineered T cells. Establishing a murine model that can recapitulate loss of β1i as a result of immunological pressure or more generally the study of AML in the presence of T cell infusions to investigate escape mechanisms is warranted, especially as TCR gene therapy becomes more common.

The proteolytic machinery of tumor cells has been shown to impact the outcome of epitope-specific immunotherapies, and immunoproteasome deficiency is a feature of lack of response to immunotherapy in solid tumors (*41, 62*). For example, a MAGE-A3 HLA-B40 restricted peptide was previously shown to be exclusively presented by tumor cells expressing the IP (*63*), and the targeted $WT1_{126\text{-}134}$ epitope was shown to be poorly or not presented by solid tumor lines (*24*).

By contrast, efficient presentation of the melanoma-antigen 1 (MART1) epitope, $MART1_{26-35}$, and of a renal cell carcinoma antigen, depends on SP processing and is obstructed by induction of the IP, which no longer produces these epitopes and thus paradoxically can allow tumors to evade elimination by antigen-specific T cells that are producing IFNγ following target recognition (*64, 65*). Alternative processing defects can also be responsible for tumor evasion. In mice that lack expression of the endoplasmic reticulum aminopeptidase 1 (ERAP1), a component of the antigen processing machinery that trims peptides in the ER to fit in the binding groove of HLA class I molecules, HLA Class I-positive, IFNγ-responsive tumors progressed despite the presence of functional, antigen-specific cytotoxic T lymphocytes due to failure to present trimming-dependent epitopes (*66*). Consistent with our results, these findings highlight how changes in a tumor cell's antigen processing machinery can disrupt immune recognition, particularly if a single epitope is targeted.

The results underscore the importance of epitope selection for T cell therapy or vaccination strategies, in which the goal is to enhance the magnitude of T cell responses to selected epitopes (*67, 68*). In particular, epitopes commonly identified in public databases reflect responses to epitopes expressed by target cells in inflammatory conditions or presented by professional antigen-presenting cells, both of which likely express the IP, which can lead to selection of potentially sub-optimal targets. Strategies targeting multiple proteins or epitopes using engineered T cells will likely be necessary in the face of tumor heterogeneity. Additionally targeting epitopes efficiently processed by both the SP and IP may increase the chances of circumventing proteasome-dependent immune-evasion (*23*). We pursued exactly the latter strategy in searching for an epitope not exclusively dependent on the IP. Our results suggest that selecting T cells/TCRs recognizing $WT1_{37-45}$ rather than $WT1_{126-134}$ should assure that changes in

the relative levels of expression of the IP or SP cannot abrogate presentation of WT1-expressing cells and allow for immune evasion, thus promoting successful clinical translation both for vaccines and TCR-engineered T cell therapies.

**Materials and Methods:**

**Clinical protocol.** The trial was approved by the Fred Hutchinson Cancer Research Center (FHCRC) Institutional Review Board, the U.S. Food and Drug Administration, and the National Institutes of Health Recombinant DNA Advisory Committee. It is registered at clinicaltrials.org as NCT1640301. Individuals with features of 'high-risk' AML and their respective fully HLA-matched (10/10) related or unrelated donors expressing HLA-A*0201 (HLA-A2) were eligible for treatment.

**Patient Selection.** HLA-A2 genotype was confirmed by high-resolution typing(*69*) prior to pre-HCT formal enrollment. High-risk features included: AML with adverse genetic abnormalities,(*70*) AML beyond 1$^{st}$ remission, primary refractory AML, therapy-related AML, AML arising in patients with antecedent hematologic disorders, and/or AML with evidence of minimal residual disease (MRD) or overt disease at time of HCT (*70-72*). Exclusion criteria included: active CNS disease, HIV seropositivity, grade ≥3 graft-versus-host disease (GVHD), and no available EBV-seropositive matched donor. On this 2-arm clinical trial, patients with no detectable disease post-HCT received treatment with $T_{TCR\text{-}C4}$ on the Prophylactic Arm, and patients with evidence of disease post-HCT received $T_{TCR\text{-}C4}$ on the Treatment Arm (*18*).

**Additional methods in supplementary methods.**

**Supplementary materials**

**Supplementary Methods**

Detailed case report Patient 1.

Detailed case report Patient 2.

Assessment of disease status.

Isolation of $TCR_{C4}$ and lentiviral vector construction.

Generation of $T_{TCR\text{-}C4}$.

T cell tracking by $WT1_{126\text{-}134}$ peptide/HLA tetramers.

Clonotype identification in the pre-infusion product and tracking by high throughput TCRβ sequencing.

Flow cytometry on T cells.

Intracellular cytokine staining.

Serum EBV and CMV quantitation

Single Cell RNA Sequencing (scRNAseq).

Computational analysis for scRNAseq on Patient 1.

Statistical analysis for scRNA-seq on patient 1 PBMC.

Computational and statistical analysis for scRNA-seq on patient 2.

Immunohistochemistry (IHC).

AML HLA-A2 flow cytometry.

Gene expression analysis from archived formalin fixed paraffin embedded (FFPE) samples and peripheral blood.

WT1 sequencing.

Whole Exome sequencing.

T cell isolation, activation, and transduction for cytotoxicity assays, live tumor-cell killing assays, and *in vivo* studies.

Assessment of $WT1_{126\text{-}134}$ dependence on specific immunoproteasome subunits.

Collection, sorting, and RNA extraction of normal donor peripheral blood stem cells and primary AMLs.

RNA sequencing on viable leukemia blasts and normal mobilized peripheral blood stem cells.

Identification of the HLA A*0201-restricted WT1-specific $TCR_{37\text{-}45}$.

1. Generation of WT1 epitope-specific T cell lines.
2. Sort-purification of WT1 specific T cell lines.
3. Evaluation of antigen-specific cytokine production in response to $A2^+$ K562 cells.
4. Isolation and expression of a $WT1_{37\text{-}45}$-specific TCR.
5. Lysis of $A2^+$ K562 cells by primary T cells expressing WT1-specific TCRs.

Immunoblot of proteasome catalytic subunits from patient sample or HEK-293 cell lines expressing specific proteasome isoforms.

Transduction of HEK-293 cells expressing the IP or SP with WT1 and HLA A*02:01.

Cytokine analysis of $eCD8^+$ and $dpCD4^+$ $T_{TCR37\text{-}45}$ cells.

Cytotoxicity assays of HEK-293 IP and SP cell lines.

AML cell death Assays.

1. T cell induced AML lysis.
2. T cell induced AML apoptosis.

CRISPR-Cas9 Gene editing by electroporation.

Live tumor-cell killing assays.

*In vivo* $T_{TCR37\text{-}45}$ therapy model.

**Supplementary Figures:**



**Supplementary Tables:**

Table S1: Detection of CMV and EBV viremias after infusions.

**References and Notes:**


1. A. M. Dickinson, J. Norden, S. Li, I. Hromadnikova, C. Schmid, H. Schmetzer, H. Jochem-Kolb, Graft-versus-Leukemia Effect Following Hematopoietic Stem Cell Transplantation for Leukemia. *Front Immunol* **8**, 496 (2017).
2. D. Sermer, R. Brentjens, CAR T-cell therapy: Full speed ahead. *Hematol Oncol* **37 Suppl 1**, 95-100 (2019).
3. S. P. Susanibar Adaniya, A. D. Cohen, A. L. Garfall, Chimeric antigen receptor T cell immunotherapy for multiple myeloma: A review of current data and potential clinical applications. *Am J Hematol* **94**, S28-S33 (2019).
4. F. Perna, S. H. Berman, R. K. Soni, J. Mansilla-Soto, J. Eyquem, M. Hamieh, R. C. Hendrickson, C. W. Brennan, M. Sadelain, Integrating Proteomics and Transcriptomics for Systematic Combinatorial Chimeric Antigen Receptor Therapy of AML. *Cancer Cell* **32**, 506-519 e505 (2017).
5. J. D. Stone, D. M. Kranz, Role of T cell receptor affinity in the efficacy and specificity of adoptive T cell therapies. *Frontiers in immunology* **4**, 244 (2013).
6. H. D. Menssen, H. J. Renkl, U. Rodeck, J. Maurer, M. Notter, S. Schwartz, R. Reinhardt, E. Thiel, Presence of Wilms' tumor gene (wt1) transcripts and the WT1 nuclear protein in the majority of human acute leukemias. *Leukemia* **9**, 1060-1067 (1995).
7. H. Sugiyama, WT1 (Wilms' tumor gene 1): biology and cancer immunotherapy. *Jpn J Clin Oncol* **40**, 377-387 (2010).
8. J. F. Armstrong, K. Pritchard-Jones, W. A. Bickmore, N. D. Hastie, J. B. Bard, The expression of the Wilms' tumour gene, WT1, in the developing mammalian embryo. *Mech Dev* **40**, 85-97 (1993).
9. P. N. Baird, P. J. Simmons, Expression of the Wilms' tumor gene (WT1) in normal hemopoiesis. *Exp Hematol* **25**, 312-320 (1997).
10. R. Narayan, N. Olsson, L. E. Wagar, B. C. Medeiros, E. Meyer, D. Czerwinski, M. S. Khodadoust, L. Zhang, L. Schultz, M. M. Davis, J. E. Elias, R. Levy, Acute myeloid leukemia immunopeptidome reveals HLA presentation of mutated nucleophosmin. *PLoS One* **14**, e0219547 (2019).
11. C. Berlin, D. J. Kowalewski, H. Schuster, N. Mirza, S. Walz, M. Handel, B. Schmid-Horch, H. R. Salih, L. Kanz, H. G. Rammensee, S. Stevanovic, J. S. Stickel, Mapping the HLA ligandome landscape of acute myeloid leukemia: a targeted approach toward peptide-based immunotherapy. *Leukemia* **29**, 647-659 (2015).
12. Y. Oka, H. Sugiyama, WT1 peptide vaccine, one of the most promising cancer vaccines: its present status and the future prospects. *Immunotherapy* **2**, 591-594 (2010).
13. V. F. Van Tendeloo, A. Van de Velde, A. Van Driessche, N. Cools, S. Anguille, K. Ladell, E. Gostick, K. Vermeulen, K. Pieters, G. Nijs, B. Stein, E. L. Smits, W. A. Schroyens, A. P. Gadisseur, I. Vrelust, P. G. Jorens, H. Goossens, I. J. de Vries, D. A. Price, Y. Oji, Y. Oka, H. Sugiyama, Z. N. Berneman, Induction of complete and molecular remissions in acute myeloid leukemia by Wilms' tumor 1 antigen-targeted dendritic cell vaccination. *Proc Natl Acad Sci U S A* **107**, 13824-13829 (2010).
14. S. Ochsenreither, A. Fusi, A. Busse, S. Bauer, C. Scheibenbogen, D. Stather, E. Thiel, U. Keilholz, A. Letsch, "Wilms Tumor Protein 1" (WT1) peptide vaccination-induced complete remission in a patient with acute myeloid leukemia is accompanied by the

emergence of a predominant T-cell clone both in blood and bone marrow. *J Immunother* **34**, 85-91 (2011).
15. A. G. Chapuis, G. B. Ragnarsson, H. N. Nguyen, C. N. Chaney, J. S. Pufnock, T. M. Schmitt, N. Duerkopp, I. M. Roberts, G. L. Pogosov, W. Y. Ho, S. Ochsenreither, M. Wolfl, M. Bar, J. P. Radich, C. Yee, P. D. Greenberg, Transferred WT1-Reactive CD8+ T Cells Can Mediate Antileukemic Activity and Persist in Post-Transplant Patients. *Science translational medicine* **5**, 174ra127 (2013).
16. V. Appay, P. R. Dunbar, M. Callan, P. Klenerman, G. M. Gillespie, L. Papagno, G. S. Ogg, A. King, F. Lechner, C. A. Spina, S. Little, D. V. Havlir, D. D. Richman, N. Gruener, G. Pape, A. Waters, P. Easterbrook, M. Salio, V. Cerundolo, A. J. McMichael, S. L. Rowland-Jones, Memory CD8+ T cells vary in differentiation phenotype in different persistent virus infections. *Nat Med* **8**, 379-385 (2002).
17. C. Berger, M. C. Jensen, P. M. Lansdorp, M. Gough, C. Elliott, S. R. Riddell, Adoptive transfer of effector CD8+ T cells derived from central memory cells establishes persistent T cell memory in primates. *J Clin Invest* **118**, 294-305 (2008).
18. A. G. Chapuis, D. N. Egan, M. Bar, T. M. Schmitt, M. S. McAfee, K. G. Paulson, V. Voillet, R. Gottardo, G. B. Ragnarsson, M. Bleakley, C. C. Yeung, P. Muhlhauser, H. N. Nguyen, L. A. Kropp, L. Castelli, F. Wagener, D. Hunter, M. Lindberg, K. Cohen, A. Seese, M. J. McElrath, N. Duerkopp, T. A. Gooley, P. D. Greenberg, T cell receptor gene therapy targeting WT1 prevents acute myeloid leukemia relapse post-transplant. *Nat Med* **25**, 1064-1072 (2019).
19. P. Sharma, S. Hu-Lieskovan, J. A. Wargo, A. Ribas, Primary, Adaptive, and Acquired Resistance to Cancer Immunotherapy. *Cell* **168**, 707-723 (2017).
20. M. Ruella, M. V. Maus, Catch me if you can: Leukemia Escape after CD19-Directed T Cell Immunotherapies. *Comput Struct Biotechnol J* **14**, 357-362 (2016).
21. M. Waterhouse, D. Pfeifer, M. Pantic, F. Emmerich, H. Bertz, J. Finke, Genome-wide profiling in AML patients relapsing after allogeneic hematopoietic cell transplantation. *Biol Blood Marrow Transplant* **17**, 1450-1459 e1451 (2011).
22. A. Busse, A. Letsch, C. Scheibenbogen, A. Nonnenmacher, S. Ochsenreither, E. Thiel, U. Keilholz, Mutation or loss of Wilms' tumor gene 1 (WT1) are not major reasons for immune escape in patients with AML receiving WT1 peptide vaccination. *J Transl Med* **8**, 5 (2010).
23. N. Vigneron, J. Abi Habib, B. J. Van den Eynde, Learning from the Proteasome How To Fine-Tune Cancer Immunotherapy. *Trends Cancer* **3**, 726-741 (2017).
24. A. Jaigirdar, S. A. Rosenberg, M. Parkhurst, A High-avidity WT1-reactive T-Cell Receptor Mediates Recognition of Peptide and Processed Antigen but not Naturally Occurring WT1-positive Tumor Cells. *J Immunother* **39**, 105-116 (2016).
25. F. Parlati, S. J. Lee, M. Aujay, E. Suzuki, K. Levitsky, J. B. Lorens, D. R. Micklem, P. Ruurs, C. Sylvain, Y. Lu, K. D. Shenk, M. K. Bennett, Carfilzomib can induce tumor cell death through selective inhibition of the chymotrypsin-like activity of the proteasome. *Blood* **114**, 3439-3447 (2009).
26. D. J. Kuhn, R. Z. Orlowski, The immunoproteasome as a target in hematologic malignancies. *Semin Hematol* **49**, 258-262 (2012).

27. N. M. Moukalled, M. A. Kharfan-Dabaja, What is the role of a second allogeneic hematopoietic cell transplant in relapsed acute myeloid leukemia? *Bone Marrow Transplant* **55**, 325-331 (2020).
28. W. Y. Ho, H. N. Nguyen, M. Wolfl, J. Kuball, P. D. Greenberg, In vitro methods for generating CD8+ T-cell clones for immunotherapy from the naive repertoire. *J Immunol Methods* **310**, 40-52 (2006).
29. N. P. Restifo, L. Gattinoni, Lineage relationship of effector and memory T cells. *Curr Opin Immunol* **25**, 556-563 (2013).
30. G. X. Zheng, J. M. Terry, P. Belgrader, P. Ryvkin, Z. W. Bent, R. Wilson, S. B. Ziraldo, T. D. Wheeler, G. P. McDermott, J. Zhu, M. T. Gregory, J. Shuga, L. Montesclaros, J. G. Underwood, D. A. Masquelier, S. Y. Nishimura, M. Schnall-Levin, P. W. Wyatt, C. M. Hindson, R. Bharadwaj, A. Wong, K. D. Ness, L. W. Beppu, H. J. Deeg, C. McFarland, K. R. Loeb, W. J. Valente, N. G. Ericson, E. A. Stevens, J. P. Radich, T. S. Mikkelsen, B. J. Hindson, J. H. Bielas, Massively parallel digital transcriptional profiling of single cells. *Nature communications* **8**, 14049 (2017).
31. J. L. Gommerman, J. L. Browning, C. F. Ware, The Lymphotoxin Network: orchestrating a type I interferon response to optimize adaptive immunity. *Cytokine Growth Factor Rev* **25**, 139-145 (2014).
32. Y. Guo, J. Chen, T. Zhao, Z. Fan, Granzyme K degrades the redox/DNA repair enzyme Ape1 to trigger oxidative stress of target cells leading to cytotoxicity. *Molecular immunology* **45**, 2225-2235 (2008).
33. B. M. Peterlin, Transcriptional regulation of HLA-DRA gene. *Res Immunol* **142**, 393-399 (1991).
34. B. Schroder, The multifaceted roles of the invariant chain CD74--More than just a chaperone. *Biochim Biophys Acta* **1863**, 1269-1281 (2016).
35. J. F. Ashouri, A. Weiss, Endogenous Nur77 Is a Specific Indicator of Antigen Receptor Signaling in Human T and B Cells. *J Immunol* **198**, 657-668 (2017).
36. T. C. Greenough, J. R. Straubhaar, L. Kamga, E. R. Weiss, R. M. Brody, M. M. McManus, L. K. Lambrecht, M. Somasundaran, K. F. Luzuriaga, A Gene Expression Signature That Correlates with CD8+ T Cell Expansion in Acute EBV Infection. *J Immunol* **195**, 4185-4197 (2015).
37. C. Y. Chen, L. W. Forman, D. V. Faller, Calcium-dependent immediate-early gene induction in lymphocytes is negatively regulated by p21Ha-ras. *Mol Cell Biol* **16**, 6582-6592 (1996).
38. M. K. Slifka, F. Rodriguez, J. L. Whitton, Rapid on/off cycling of cytokine production by virus-specific CD8+ T cells. *Nature* **401**, 76-79 (1999).
39. M. Groettrup, S. Standera, R. Stohwasser, P. M. Kloetzel, The subunits MECL-1 and LMP2 are mutually required for incorporation into the 20S proteasome. *Proc Natl Acad Sci U S A* **94**, 8970-8975 (1997).
40. J. Abi Habib, E. De Plaen, V. Stroobant, D. Zivkovic, M. P. Bousquet, B. Guillaume, K. Wahni, J. Messens, A. Busse, N. Vigneron, B. J. Van den Eynde, Efficiency of the four proteasome subtypes to degrade ubiquitinated or oxidized proteins. *Sci Rep* **10**, 15765 (2020).
41. S. C. Tripathi, H. L. Peters, A. Taguchi, H. Katayama, H. Wang, A. Momin, M. K. Jolly, M. Celiktas, J. Rodriguez-Canales, H. Liu, C. Behrens, Wistuba, II, E. Ben-Jacob, H. Levine, J. J.

Molldrem, S. M. Hanash, E. J. Ostrin, Immunoproteasome deficiency is a feature of non-small cell lung cancer with a mesenchymal phenotype and is associated with a poor outcome. *Proc Natl Acad Sci U S A* **113**, E1555-1564 (2016).
42. S. Ariyaratana, D. M. Loeb, The role of the Wilms tumour gene (WT1) in normal and malignant haematopoiesis. *Expert Rev Mol Med* **9**, 1-17 (2007).
43. I. Bellantuono, L. Gao, S. Parry, S. Marley, F. Dazzi, J. Apperley, J. M. Goldman, H. J. Stauss, Two distinct HLA-A0201-presented epitopes of the Wilms tumor antigen 1 can function as targets for leukemia-reactive CTL. *Blood* **100**, 3835-3837 (2002).
44. C. Chaise, S. L. Buchan, J. Rice, J. Marquet, H. Rouard, M. Kuentz, G. E. Vittes, V. Molinier-Frenkel, J. P. Farcet, H. J. Stauss, M. H. Delfau-Larue, F. K. Stevenson, DNA vaccination induces WT1-specific T-cell responses with potential clinical relevance. *Blood* **112**, 2956-2964 (2008).
45. E. Doubrovina, T. Carpenter, D. Pankov, A. Selvakumar, A. Hasan, R. J. O'Reilly, Mapping of novel peptides of WT-1 and presenting HLA alleles that induce epitope-specific HLA-restricted T cells with cytotoxic activity against WT-1(+) leukemias. *Blood* **120**, 1633-1646 (2012).
46. K. S. Anderson, W. Zeng, T. Sasada, J. Choi, A. B. Riemer, M. Su, D. Drakoulakos, Y. J. Kang, V. Brusic, C. Wu, E. L. Reinherz, Impaired tumor antigen processing by immunoproteasome-expressing CD40-activated B cells and dendritic cells. *Cancer Immunol Immunother* **60**, 857-867 (2011).
47. B. Guillaume, J. Chapiro, V. Stroobant, D. Colau, B. Van Holle, G. Parvizi, M. P. Bousquet-Dubouch, I. Theate, N. Parmentier, B. J. Van den Eynde, Two abundant proteasome subtypes that uniquely process some antigens presented by HLA class I molecules. *Proc Natl Acad Sci U S A* **107**, 18599-18604 (2010).
48. A. D. Bandaranayake, C. Correnti, B. Y. Ryu, M. Brault, R. K. Strong, D. J. Rawlings, Daedalus: a robust, turnkey platform for rapid production of decigram quantities of active recombinant proteins in human cell lines using novel lentiviral vectors. *Nucleic Acids Res* **39**, e143 (2011).
49. W. Glienke, L. Maute, J. Wicht, L. Bergmann, Wilms' tumour gene 1 (WT1) as a target in curcumin treatment of pancreatic cancer cells. *Eur J Cancer* **45**, 874-880 (2009).
50. D. M. Loeb, E. Evron, C. B. Patel, P. M. Sharma, B. Niranjan, L. Buluwela, S. A. Weitzman, D. Korz, S. Sukumar, Wilms' tumor suppressor gene (WT1) is expressed in primary breast tumors despite tumor-specific promoter methylation. *Cancer Res* **61**, 921-925 (2001).
51. C. J. Turtle, L. A. Hanafi, C. Berger, T. A. Gooley, S. Cherian, M. Hudecek, D. Sommermeyer, K. Melville, B. Pender, T. M. Budiarto, E. Robinson, N. N. Steevens, C. Chaney, L. Soma, X. Chen, C. Yeung, B. Wood, D. Li, J. Cao, S. Heimfeld, M. C. Jensen, S. R. Riddell, D. G. Maloney, CD19 CAR-T cells of defined CD4+:CD8+ composition in adult B cell ALL patients. *J Clin Invest* **126**, 2123-2138 (2016).
52. R. E. Tay, E. K. Richardson, H. C. Toh, Revisiting the role of CD4(+) T cells in cancer immunotherapy-new insights into old paradigms. *Cancer Gene Ther*, (2020).
53. J. Thibodeau, M. C. Bourgeois-Daigneault, R. Lapointe, Targeting the MHC Class II antigen presentation pathway in cancer immunotherapy. *Oncoimmunology* **1**, 908-916 (2012).
54. M. Ecsedi, M. S. McAfee, A. G. Chapuis, The Anticancer Potential of T Cell Receptor-Engineered T Cells. *Trends Cancer* **7**, 48-56 (2021).

55. I. Raphael, S. Nalawade, T. N. Eagar, T. G. Forsthuber, T cell subsets and their signature cytokines in autoimmune and inflammatory diseases. *Cytokine* **74**, 5-17 (2015).
56. R. M. Spaapen, J. Neefjes, Immuno-waste exposure and further management. *Nat Immunol* **13**, 109-111 (2012).
57. R. E. Toes, A. K. Nussbaum, S. Degermann, M. Schirle, N. P. Emmerich, M. Kraft, C. Laplace, A. Zwinderman, T. P. Dick, J. Muller, B. Schonfisch, C. Schmid, H. J. Fehling, S. Stevanovic, H. G. Rammensee, H. Schild, Discrete cleavage motifs of constitutive and immunoproteasomes revealed by quantitative analysis of cleavage products. *J Exp Med* **194**, 1-12 (2001).
58. A. J. Sijts, T. Ruppert, B. Rehermann, M. Schmidt, U. Koszinowski, P. M. Kloetzel, Efficient generation of a hepatitis B virus cytotoxic T lymphocyte epitope requires the structural features of immunoproteasomes. *J Exp Med* **191**, 503-514 (2000).
59. M. Bai, X. Zhao, K. Sahara, Y. Ohte, Y. Hirano, T. Kaneko, H. Yashiroda, S. Murata, Assembly mechanisms of specialized core particles of the proteasome. *Biomolecules* **4**, 662-677 (2014).
60. S. Khan, M. van den Broek, K. Schwarz, R. de Giuli, P. A. Diener, M. Groettrup, Immunoproteasomes largely replace constitutive proteasomes during an antiviral and antibacterial immune response in the liver. *J Immunol* **167**, 6859-6868 (2001).
61. A. Rouette, A. Trofimov, D. Haberl, G. Boucher, V. P. Lavallee, G. D'Angelo, J. Hebert, G. Sauvageau, S. Lemieux, C. Perreault, Expression of immunoproteasome genes is regulated by cell-intrinsic and -extrinsic factors in human cancers. *Sci Rep* **6**, 34019 (2016).
62. P. G. Coulie, B. J. Van den Eynde, P. van der Bruggen, T. Boon, Tumour antigens recognized by T lymphocytes: at the core of cancer immunotherapy. *Nat Rev Cancer* **14**, 135-146 (2014).
63. E. S. Schultz, J. Chapiro, C. Lurquin, S. Claverol, O. Burlet-Schiltz, G. Warnier, V. Russo, S. Morel, F. Levy, T. Boon, B. J. Van den Eynde, P. van der Bruggen, The production of a new MAGE-3 peptide presented to cytolytic T lymphocytes by HLA-B40 requires the immunoproteasome. *J Exp Med* **195**, 391-399 (2002).
64. M. Keller, F. Ebstein, E. Burger, K. Textoris-Taube, X. Gorny, S. Urban, F. Zhao, T. Dannenberg, A. Sucker, C. Keller, L. Saveanu, E. Kruger, H. J. Rothkotter, B. Dahlmann, P. Henklein, A. Voigt, U. Kuckelkorn, A. Paschen, P. M. Kloetzel, U. Seifert, The proteasome immunosubunits, PA28 and ER-aminopeptidase 1 protect melanoma cells from efficient MART-126-35 -specific T-cell recognition. *Eur J Immunol* **45**, 3257-3268 (2015).
65. S. Morel, F. Levy, O. Burlet-Schiltz, F. Brasseur, M. Probst-Kepper, A. L. Peitrequin, B. Monsarrat, R. Van Velthoven, J. C. Cerottini, T. Boon, J. E. Gairin, B. J. Van den Eynde, Processing of some antigens by the standard proteasome but not by the immunoproteasome results in poor presentation by dendritic cells. *Immunity* **12**, 107-117 (2000).
66. A. Textor, K. Schmidt, P. M. Kloetzel, B. Weissbrich, C. Perez, J. Charo, K. Anders, J. Sidney, A. Sette, T. N. Schumacher, C. Keller, D. H. Busch, U. Seifert, T. Blankenstein, Preventing tumor escape by targeting a post-proteasomal trimming independent epitope. *J Exp Med* **213**, 2333-2348 (2016).
67. U. Sahin, O. Tureci, Personalized vaccines for cancer immunotherapy. *Science* **359**, 1355-1360 (2018).

68. S. Krishna, K. S. Anderson, T-Cell Epitope Discovery for Therapeutic Cancer Vaccines. *Methods Mol Biol* **1403**, 779-796 (2016).
69. M. M. Horowitz, High-resolution typing for unrelated donor transplantation: how far do we go? *Best Pract Res Clin Haematol* **22**, 537-541 (2009).
70. H. Dohner, E. Estey, D. Grimwade, S. Amadori, F. R. Appelbaum, T. Buchner, H. Dombret, B. L. Ebert, P. Fenaux, R. A. Larson, R. L. Levine, F. Lo-Coco, T. Naoe, D. Niederwieser, G. J. Ossenkoppele, M. Sanz, J. Sierra, M. S. Tallman, H. F. Tien, A. H. Wei, B. Lowenberg, C. D. Bloomfield, Diagnosis and management of AML in adults: 2017 ELN recommendations from an international expert panel. *Blood* **129**, 424-447 (2017).
71. D. Araki, B. L. Wood, M. Othus, J. P. Radich, A. B. Halpern, Y. Zhou, M. Mielcarek, E. H. Estey, F. R. Appelbaum, R. B. Walter, Allogeneic Hematopoietic Cell Transplantation for Acute Myeloid Leukemia: Time to Move Toward a Minimal Residual Disease-Based Definition of Complete Remission? *J Clin Oncol* **34**, 329-336 (2016).
72. P. Armand, H. T. Kim, B. R. Logan, Z. Wang, E. P. Alyea, M. E. Kalaycio, R. T. Maziarz, J. H. Antin, R. J. Soiffer, D. J. Weisdorf, J. D. Rizzo, M. M. Horowitz, W. Saber, Validation and refinement of the Disease Risk Index for allogeneic stem cell transplantation. *Blood* **123**, 3664-3671 (2014).
73. Y. Zhou, B. L. Wood, Methods of Detection of Measurable Residual Disease in AML. *Current hematologic malignancy reports* **12**, 557-567 (2017).
74. M. Festuccia, H. J. Deeg, T. A. Gooley, K. Baker, B. L. Wood, M. Fang, B. M. Sandmaier, B. L. Scott, Minimal Identifiable Disease and the Role of Conditioning Intensity in Hematopoietic Cell Transplantation for Myelodysplastic Syndrome and Acute Myelogenous Leukemia Evolving from Myelodysplastic Syndrome. *Biol Blood Marrow Transplant* **22**, 1227-1233 (2016).
75. M. Fang, B. Storer, B. Wood, B. Gyurkocza, B. M. Sandmaier, F. R. Appelbaum, Prognostic impact of discordant results from cytogenetics and flow cytometry in patients with acute myeloid leukemia undergoing hematopoietic cell transplantation. *Cancer* **118**, 2411-2419 (2012).
76. S. Jones, P. D. Peng, S. Yang, C. Hsu, C. J. Cohen, Y. Zhao, J. Abad, Z. Zheng, S. A. Rosenberg, R. A. Morgan, Lentiviral vector design for optimal T cell receptor gene expression in the transduction of peripheral blood lymphocytes and tumor-infiltrating lymphocytes. *Hum Gene Ther* **20**, 630-640 (2009).
77. A. G. Chapuis, J. A. Thompson, K. A. Margolin, R. Rodmyre, I. P. Lai, K. Dowdy, E. A. Farrar, S. Bhatia, D. E. Sabath, J. Cao, Y. Li, C. Yee, Transferred melanoma-specific CD8+ T cells persist, mediate tumor regression, and acquire central memory phenotype. *Proc Natl Acad Sci U S A*, (2012).
78. A. G. Chapuis, C. Desmarais, R. Emerson, T. M. Schmitt, K. Shibuya, I. Lai, F. Wagener, J. Chou, I. M. Roberts, D. G. Coffey, E. Warren, H. Robbins, P. D. Greenberg, C. Yee, Tracking the Fate and Origin of Clinically Relevant Adoptively Transferred CD8+ T Cells In Vivo. *Sci Immunol* **2**, (2017).
79. J. Zhou, M. E. Dudley, S. A. Rosenberg, P. F. Robbins, Persistence of multiple tumor-specific T-cell clones is associated with complete tumor regression in a melanoma patient receiving adoptive cell transfer therapy. *J Immunother* **28**, 53-62 (2005).
80. P. C. Tumeh, C. L. Harview, J. H. Yearley, I. P. Shintaku, E. J. Taylor, L. Robert, B. Chmielowski, M. Spasic, G. Henry, V. Ciobanu, A. N. West, M. Carmona, C. Kivork, E.

Seja, G. Cherry, A. J. Gutierrez, T. R. Grogan, C. Mateus, G. Tomasic, J. A. Glaspy, R. O. Emerson, H. Robins, R. H. Pierce, D. A. Elashoff, C. Robert, A. Ribas, PD-1 blockade induces responses by inhibiting adaptive immune resistance. *Nature* **515**, 568-571 (2014).

81. H. Horton, E. P. Thomas, J. A. Stucky, I. Frank, Z. Moodie, Y. Huang, Y. L. Chiu, M. J. McElrath, S. C. De Rosa, Optimization and validation of an 8-color intracellular cytokine staining (ICS) assay to quantify antigen-specific T cells induced by vaccination. *Journal of immunological methods* **323**, 39-54 (2007).
82. G. Moncunill, H. Han, C. Dobano, M. J. McElrath, S. C. De Rosa, OMIP-024: pan-leukocyte immunophenotypic characterization of PBMC subsets in human samples. *Cytometry. Part A : the journal of the International Society for Analytical Cytology* **85**, 995-998 (2014).
83. A. P. Limaye, M. L. Huang, E. E. Atienza, J. M. Ferrenberg, L. Corey, Detection of Epstein-Barr virus DNA in sera from transplant recipients with lymphoproliferative disorders. *J Clin Microbiol* **37**, 1113-1116 (1999).
84. M. Boeckh, M. Huang, J. Ferrenberg, T. Stevens-Ayers, L. Stensland, W. G. Nichols, L. Corey, Optimization of quantitative detection of cytomegalovirus DNA in plasma by real-time PCR. *J Clin Microbiol* **42**, 1142-1148 (2004).
85. A. Dobin, C. A. Davis, F. Schlesinger, J. Drenkow, C. Zaleski, S. Jha, P. Batut, M. Chaisson, T. R. Gingeras, STAR: ultrafast universal RNA-seq aligner. *Bioinformatics* **29**, 15-21 (2013).
86. A. Butler, P. Hoffman, P. Smibert, E. Papalexi, R. Satija, Integrating single-cell transcriptomic data across different conditions, technologies, and species. *Nat Biotechnol* **36**, 411-420 (2018).
87. T. Stuart, A. Butler, P. Hoffman, C. Hafemeister, E. Papalexi, W. M. Mauck, 3rd, Y. Hao, M. Stoeckius, P. Smibert, R. Satija, Comprehensive Integration of Single-Cell Data. *Cell* **177**, 1888-1902 e1821 (2019).
88. T. Ilicic, J. K. Kim, A. A. Kolodziejczyk, F. O. Bagger, D. J. McCarthy, J. C. Marioni, S. A. Teichmann, Classification of low quality cells from single-cell RNA-seq data. *Genome Biol* **17**, 29 (2016).
89. G. Finak, A. McDavid, M. Yajima, J. Deng, V. Gersuk, A. K. Shalek, C. K. Slichter, H. W. Miller, M. J. McElrath, M. Prlic, P. S. Linsley, R. Gottardo, MAST: a flexible statistical framework for assessing transcriptional changes and characterizing heterogeneity in single-cell RNA sequencing data. *Genome Biol* **16**, 278 (2015).
90. C. Hafemeister, R. Satija, Normalization and variance stabilization of single-cell RNA-seq data using regularized negative binomial regression. *Genome Biol* **20**, 296 (2019).
91. M. H. Veldman-Jones, R. Brant, C. Rooney, C. Geh, H. Emery, C. G. Harbron, M. Wappett, A. Sharpe, M. Dymond, J. C. Barrett, E. A. Harrington, G. Marshall, Evaluating Robustness and Sensitivity of the NanoString Technologies nCounter Platform to Enable Multiplexed Gene Expression Analysis of Clinical Samples. *Cancer Res* **75**, 2587-2593 (2015).
92. C. C. Pritchard, S. J. Salipante, K. Koehler, C. Smith, S. Scroggins, B. Wood, D. Wu, M. K. Lee, S. Dintzis, A. Adey, Y. Liu, K. D. Eaton, R. Martins, K. Stricker, K. A. Margolin, N. Hoffman, J. E. Churpek, J. F. Tait, M. C. King, T. Walsh, Validation and implementation of targeted capture and sequencing for the detection of actionable mutation, copy number

variation, and gene rearrangement in clinical cancer specimens. *J Mol Diagn* **16**, 56-67 (2014).
93. J. E. Park, L. Ao, Z. Miller, K. Kim, Y. Wu, E. R. Jang, E. Y. Lee, K. B. Kim, W. Lee, PSMB9 codon 60 polymorphisms have no impact on the activity of the immunoproteasome catalytic subunit B1i expressed in multiple types of solid cancer. *PLoS One* **8**, e73732 (2013).
94. J. D. Buenrostro, P. G. Giresi, L. C. Zaba, H. Y. Chang, W. J. Greenleaf, Transposition of native chromatin for fast and sensitive epigenomic profiling of open chromatin, DNA-binding proteins and nucleosome position. *Nat Methods* **10**, 1213-1218 (2013).
95. B. Guillaume, J. Chapiro, V. Stroobant, D. Colau, B. Van Holle, G. Parvizi, M. P. Bousquet-Dubouch, I. Theate, N. Parmentier, B. J. Van den Eynde, Two abundant proteasome subtypes that uniquely process some antigens presented by HLA class I molecules. *Proc. Natl. Acad. Sci. USA* **107**, 18599-18604 (2010).
96. N. Vigneron, A. Ooms, S. Morel, W. Ma, G. Degiovanni, B. J. Van den Eynde, A peptide derived from melanocytic protein gp100 and presented by HLA-B35 is recognized by autologous cytolytic T lymphocytes on melanoma cells. *Tissue Antigens* **65**, 156-162 (2005).
97. E. L. Pogosova-Agadjanyan, A. Moseley, M. Othus, F. R. Appelbaum, T. R. Chauncey, I. L. Chen, H. P. Erba, J. E. Godwin, M. Fang, K. J. Kopecky, A. F. List, G. L. Pogosov, J. P. Radich, C. L. Willman, B. L. Wood, S. Meshinchi, D. L. Stirewalt, Impact of Specimen Heterogeneity on Biomarkers in Repository Samples from Patients with Acute Myeloid Leukemia: A SWOG Report. *Biopreserv Biobank* **16**, 42-52 (2018).
98. L. Wang, S. Wang, W. Li, RSeQC: quality control of RNA-seq experiments. *Bioinformatics* **28**, 2184-2185 (2012).
99. Y. Liao, G. K. Smyth, W. Shi, featureCounts: an efficient general purpose program for assigning sequence reads to genomic features. *Bioinformatics* **30**, 923-930 (2014).
100. A. Frankish, M. Diekhans, A. M. Ferreira, R. Johnson, I. Jungreis, J. Loveland, J. M. Mudge, C. Sisu, J. Wright, J. Armstrong, I. Barnes, A. Berry, A. Bignell, S. Carbonell Sala, J. Chrast, F. Cunningham, T. Di Domenico, S. Donaldson, I. T. Fiddes, C. Garcia Giron, J. M. Gonzalez, T. Grego, M. Hardy, T. Hourlier, T. Hunt, O. G. Izuogu, J. Lagarde, F. J. Martin, L. Martinez, S. Mohanan, P. Muir, F. C. P. Navarro, A. Parker, B. Pei, F. Pozo, M. Ruffier, B. M. Schmitt, E. Stapleton, M. M. Suner, I. Sycheva, B. Uszczynska-Ratajczak, J. Xu, A. Yates, D. Zerbino, Y. Zhang, B. Aken, J. S. Choudhary, M. Gerstein, R. Guigo, T. J. P. Hubbard, M. Kellis, B. Paten, A. Reymond, M. L. Tress, P. Flicek, GENCODE reference annotation for the human and mouse genomes. *Nucleic Acids Res* **47**, D766-D773 (2019).
101. M. D. Robinson, D. J. McCarthy, G. K. Smyth, edgeR: a Bioconductor package for differential expression analysis of digital gene expression data. *Bioinformatics* **26**, 139-140 (2010).
102. M. D. Robinson, A. Oshlack, A scaling normalization method for differential expression analysis of RNA-seq data. *Genome Biol* **11**, R25 (2010).
103. L. Findlay, D. Eastwood, R. Stebbings, G. Sharp, Y. Mistry, C. Ball, J. Hood, R. Thorpe, S. Poole, Improved in vitro methods to predict the in vivo toxicity in man of therapeutic monoclonal antibodies including TGN1412. *J Immunol Methods* **352**, 1-12 (2010).

104. S. R. Riddell, K. S. Watanabe, J. M. Goodrich, C. R. Li, M. E. Agha, P. D. Greenberg, Restoration of viral immunity in immunodeficient humans by the adoptive transfer of T cell clones. *Science* **257**, 238-241 (1992).
105. I. Jedema, N. M. van der Werff, R. M. Barge, R. Willemze, J. H. Falkenburg, New CFSE-based assay to determine susceptibility to lysis by cytotoxic T cells of leukemic precursor cells within a heterogeneous target cell population. *Blood* **103**, 2677-2682 (2004).
106. D. N. Nguyen, T. L. Roth, P. J. Li, P. A. Chen, R. Apathy, M. R. Mamedov, L. T. Vo, V. R. Tobin, D. Goodman, E. Shifrut, J. A. Bluestone, J. M. Puck, F. C. Szoka, A. Marson, Polymer-stabilized Cas9 nanoparticles and modified repair templates increase genome editing efficiency. *Nat Biotechnol* **38**, 44-49 (2020).
107. X. Cao, E. W. Shores, J. Hu-Li, M. R. Anver, B. L. Kelsall, S. M. Russell, J. Drago, M. Noguchi, A. Grinberg, E. T. Bloom, et al., Defective lymphoid development in mice lacking expression of the common cytokine receptor gamma chain. *Immunity* **2**, 223-238 (1995).

**Acknowledgments:** We thank Fred Hutch Good Manufacturing Practice Cell Processing Facility for generating $T_{TCR\text{-}C4}$, Immune Monitoring Laboratory for generating tetramers, Flow Cytometry Facility for providing instruments and assistance in flow cytometry assays, Genomics Core for sequencing and data processing, Program in Immunology, Immunotherapy Integrated Research Center, Seattle Cancer Care Alliance Immunotherapy Clinic staff, and The Fred Hutch/University of Washington Hematopoietic Disease Repository for providing primary AML samples, patients and their family**. Funding**: P01CA18029-41 (PDG.), SITC-Merck Immunotherapy Fellowship (KGP). National Institutes of Health -T32CA080416 (MCL), National Institutes of Health -5K08CA169485 (AGC), Immunotherapy Integrated Research Center at FHCRC (AGC.), Damon Runyon (AGC), Guillot Family Zach Attacks Leukemia Foundation (AGC., PDG.), Juno Therapeutics (PDG). **Author contributions**: Conception and design: PDG, AGC, TMS, KGP, AR. Collection and assembly of data: MCL, KGP, TMS, DB, MSM, DSH, FDW, JMM, DS, EPA, CY, RHP, DNE, MB, PH, JB, MC, LM, JL, SK, AV, NV. Data analysis and interpretation: NV, VV, RG, AR, JB, BJVE. Manuscript writing: All authors. Final Approval of manuscript: All authors. **Competing interests**: AGC and PDG have received support from Juno Therapeutics. PDG was a consultant, has received support from, and had ownership interest in Juno Therapeutics. He consults and has ownership interest in RAPT Bio., Elpiscience, Celsius, and Nextech. PDG, TMS, and the Fred Hutch have intellectual property related to $TCR_{C4}$. AGC and KP have received reagents from 10X Genomics. RG has received consulting income from Juno Therapeutics, Takeda, Infotech Soft, Celgene, Merck and has received research support from Janssen Pharmaceuticals and Juno Therapeutics, and declares ownership in CellSpace Biosciences. The authors declare no other competing interests. **Data and materials availability**: All requests for raw and analyzed data and materials are promptly reviewed by the Fred Hutchinson cancer Research Center to verify if the request is subject to any

intellectual property confidential obligations. Patient-related data not included in the paper were generated as part of a clinical trial and may be subject to patient confidentiality. Any data and materials that can be shared will be released via a Material Transfer Agreement. PBMC scRNAseq data for the remission and relapse timepoints as well as the R code to generate the UMAP plots using Seurat software packages, primary AML blasts RNA sequencing and NanoString datasets, will be available at the National Center for Biotechnology Information Gene Expression Omnibus (NCBI GEO).

**Figures and Legends.**

**Fig. 1: $T_{TCR\text{-}C4}$ persist and remain functional in the presence of relapsed AML. (A)** Timeline of patient's treatment regimens. Chemo: chemotherapy; Radiation: radiation therapy. IT chemo: Intrathecal chemotherapy. **(B)** Percent multimer$^+$ of CD8$^+$ T cells in PBMCs (solid circles) and bone marrow (green circles) collected before and at defined timepoints after $T_{TCR\text{-}C4}$ infusions. Orange shaded area indicates presence of AML. Dotted red lines represent days 100 and 110 (or day 581 after the 1$^{st}$) after 1$^{st}$ and 2$^{nd}$ infusion respectively. **(C)** Pie chart representing individual clonotypes composing the pre-infusion $T_{TCR\text{-}C4}$ product (left) and at indicated timepoints (right) after both infusions. **(D)** Percent expression of CD45RO, CD27, CD28 and CD62L on infusion products (bar graphs to the left) and at days 4, 42, 114, 289, 393, 478, 508 and 542 after the 1$^{st}$ infusion (graphs to the right). The three last timepoints are also days 7, 35 and 71 after the second infusion. Timing of infusions are indicated by black arrows. **(E)** Percent expression of IFNγ, TNFα and IL-2 (functional markers) in response to *ex vivo* stimulation $WT1_{126\text{-}134}$ peptide (1nM) during remission (day 114 after 1$^{st}$ infusion) and relapse (day 581 after 1$^{st}$ infusion, day 110 after 2$^{nd}$). Maximum and minimal cytokine expression following exposure to Staphylococcal enterotoxin B (SEB) and dimethylsufoxide (DMSO) are shown for each cytokine.

**Fig. 2: $T_{TCR\text{-}C4}$ present an activated transcription profile during remission but not during relapse. (A)** UMAP visualization of PBMC from both the remission (100 days after 1st infusion) and relapse (110 days after the second infusion or 581 days after the 1st) (red dotted lines **Fig. 1A**) samples visualized together (see **Supplementary Methods**). PBMC (n=7704) clustered into populations as indicated by labels. Clustering biostatistical analysis is described in Supplementary Methods and representative marker genes are shown in **Fig. S3**. **(B)** UMAP visualization of the separated PBMC obtained at remission (left) and relapse (right). **(C)** Close-up of clusters containing T cells during remission with identification of two (light blue and purple) distinct $CD8^+$ T cell clusters based on their transcriptional programs. **(D)** Close-up of clusters containing T cells during relapse revealing the $CD8^+$ T cells are predominantly in the purple cluster. **(E)** Localization of $T_{TCR\text{-}C4}$ (dark blue dots) cells during remission. **(F)** Localization of $T_{TCR\text{-}C4}$ (dark blue dots) cells during relapse. Percentage of the total $T_{TCR\text{-}C4}$ cells in each cluster are indicated. **(G)** Heat map of significantly differentially expressed genes (DEG) comparing $T_{TCR\text{-}C4}$ during remission (n=501) to those during relapse (n=33). **(H)** Analysis of gene-sets representing effector cytokines, cytolytic effector genes activation and exhaustion genes were compared in $T_{TCR\text{-}C4}$ during remission (light blue) and relapse (darker blue) with each transcript in the gene-set is shown as a violin plot. The shape of the violin displays frequencies of values. Model-based Analysis of Single Cell Transcriptomics (MAST – See **Supplementary Methods**) was used to determine the significance shown above each plot. Significance thresholds were set *a priori* at a threshold of false discovery rate of 5% and positive or negative fold change > log2(1.3).

**Fig. 3: Analysis of immunoproteasome expression in relapsed AML (A)** Bone marrow aspirate, myeloid chloroma or blood obtained relative to the timeline of successive therapies. Presence of AML is indicated in orange. **(B)** Pre-$T_{TCR\text{-}C4}$ AML Hematoxylin and Eosin (H&E) (top panel), immunohistochemistry (IHC) of WT1 expression (middle panel) and class I expression (bottom panel). **(C)** H&E (top panel), WT1 IHC expression (middle panel) and CD3 infiltration (bottom panel) of bladder chloroma obtained early post-$T_{TCR\text{-}C4}$ relapse. **(D)** Post-$T_{TCR\text{-}C4}$ AML H&E (top panel) and WT1 IHC (bottom panel). **(E)** Normalized counts (y-axis) of bulk RNA expression of HLA-A obtained from the pre-$T_{TCR\text{-}C4}$ cervical chloroma and a post-$T_{TCR\text{-}C4}$ PBMC, both containing >89% AML. **(F)** HLA-A2 protein expression detected by flow cytometry of the post-$T_{TCR\text{-}C4}$ blood. **(G)** Heat map of the 100 most significantly differentially expressed genes (DEG) comparing AML (n=2,447) during relapse after T cell therapy to other cells in the sample (n=306). Red arrow indicates immunoproteasome subunit β1i [*PSBM9*] **(H)** Fold change (*y axis*) of transcripts encoding proteasome cap ([*PSMC2*] and [*PSMD7*]; black bars), immuno-proteasome (β5i [*PSMB8*], β1i [*PSMB9*] and β2i [*PSMB10*]; blue bars) and standard proteasome (β5 [*PSMB5*], and β2 [*PSMB7*]; purple bars) sub-units comparing expression in the post-$T_{TCR\text{-}C4}$ obtained from PBMC, to pre-$T_{TCR\text{-}C4}$ AML obtained from a chloroma FFPE sample. Of note, β1 [*PSMB6*] was not available in the commercial RNA probe-set utilized (see **Supplementary Methods**). **(I)**Expression of transcripts encoding genes constituting the active proteolytic site of the immunoproteasome (β5i [*PSMB8]*, β1i [*PSMB9]* and β2i [*PSMB10]*) and the standard proteasome (β5 [*PSMB5]*, β1 [*PSMB6]* and β2 [*PSMB7]*) at relapse comparing AML (n=2,447, orange) and other non-malignant cells (n=306, green) in the sample. Frequencies of cells with the detectable transcript are shown to the right of each violin plot. P values are indicated as well as the log2 fold change. Positive values indicate increased and negative decreased expression in AML. Model-based Analysis of Single Cell

Transcriptomics (MAST – See **Supplementary Methods**) was used to determine significance shown above each plot. Significance thresholds were set *a priori* at a threshold of false discovery rate of 5% and positive or negative fold change > log2(1.3)). **(J)** TNFα production (pg/mL) from T cells expressing $TCR_{C4}$ cultured with cells expressing a specific proteasome isoform and transfected with varying amounts of WT1 cDNA (*40*) or pulsed with $WT1_{126-134}$ peptide as a positive control. (**K**)RNAseq on viable leukemic blasts shows expression of genes constituting the active proteolytic site of the immunoproteasome (β5i [*PSMB8]*, β1i [*PSMB9]* and β2i [*PSMB10]*) in peripheral blood stem cells obtained from healthy donors (n=6, light grey), primary AML samples obtained from the Fred Hutch-University of Washington Hematopoietic Diseases Repository (black, n=38) and the patient (red, n=1). Box and whisker plot represents median, interquartile and range. Dots represent individual patient sample.

**Fig. 4: $T_{TCR-C4}$ preferentially eliminates $WT1^+$ AML co-expressing β1i.** (**A**) Timeline of patient's treatment regimens. Chemo: chemotherapy; NR: no response. (**B**) Percent $multimer^+$ of $CD8^+$ T cells in peripheral blood collected before and at day +1, +4, and +5. Orange shaded area indicates presence of AML. Dotted red lines represent days +0 and +5 after $T_{TCR-C4}$. (**C**) UMAP visualization of scRNAseq on PBMC from both before (D+0, n=7,381) $T_{TCR-C4}$ infusion and 5 days post $1^{st}$ infusion (D+5, n=3,319) (red dotted lines **Fig. 4B**) aggregated into a single UMAP(top) or as individual time points (bottom). (**D,F,G,H**) UMAP of AML clusters on D+0 (top row) or D+5 (bottom row). (**D**) Expression of AML specific markers CD34, CCND1, CDK6, FLT3, NPM1, RUNX1. (**E)** Relative proportions of AML clusters at D+0 and D+5. (**F**) Expression of HLA-A. (**G**) Expression of WT1 transcripts from peripheral AML (left panel) and immunohistochemistry performed on a bone marrow biopsy (D+0) and a PBMC cell pellet (D+5). (**H**) Co-expression of WT1 and the immunoproteasome gene β1i (PSMB9). (**I**) Percent of

cells that express WT1 only (pink bars) or WT1 and β1i ([PSMB9]) (purple bars) before (D+0) and after (D+5) $T_{TCR\text{-}C4}$ infusion. Percent values are indicated above each column.

**Fig. 5: Identification of an alternate HLA-A*02:01-restricted WT1 peptide ($WT1_{37\text{-}45}$) not dependent on immunoproteasome processing.** (**A**) Ten $CD8^+$ T cell lines from 2 HLA-A*02:01-expressing healthy donors were generated against 8 candidate HLA-A*02:01-binding WT1 peptides (x-axis). Each cell line's ability to produce IFNγ following stimulation with the immunoproteasome-deficient but $WT1^+$ HLA-A*02:01-transduced K562 cell line at an E:T of 1:1 was assessed. Two peptides ($WT1_{37\text{-}45}$ and $WT1_{235\text{-}243}$) were identified that, elicited high reactivity from donor T cells as measured by MFI (above the arbitrary threshold of 6000) for the IFNγ positive cells. (**B**) Representative flow plots of $CD8^+$ T cell lines targeting ($WT1_{37\text{-}45}$ and $WT1_{235\text{-}243}$) that were sorted using the corresponding tetramers. (**C**) Sorted T cell lines targeting $WT1_{37\text{-}45}$ had the highest comparative reactivity, assessed by IFNγ MFI, when cultured with HLA A*02:01-tansduced K562 cells. TCRs targeting $WT1_{37\text{-}45}$ were isolated from T cells in these lines. (**D**) Lysis of K562 +/- expressing HLA-A*02:01 by $CD8^+$ T cells from a healthy donor transduced with $TCR_{C4}$ and a TCR targeting $WT1_{37\text{-}45}$ ($TCR_{WT1\text{-}37\text{-}45}$ #1 -see **Supplementary Methods**) confirmed expression of the $WT1_{37\text{-}45}$ peptide was not dependent on IP processing. **(E)** Immunoblot demonstrating protein expression of catalytic proteasome subunits in HEK-293 (endogenous SP expression) +/- engineered to express IP. **(F)** Percent lysis (y-axis) of IP/SP-skewed HEK-293 cells lines by $CD8^+$ T cells transduced to express either $TCR_{C4}$ (blue lines), $TCR_{37\text{-}45}$ (red lines) and untransduced $CD8^+$ T cells (black lines) at indicated effector to target (E:T) ratios (x-axis). Inset depicts WT1 IHC of IP/SP HEK-293 cells transduced with WT1-and HLA-A*02:01. IP/SP cell lines demonstrate heterogeneity of WT1 expression (see **Supplementary Methods**). **(G)** Percent lysis (y-axis) of a primary leukemia by

$CD8^+$ T cells transduced to express either an irrelevant TCR ($TCR_{irr.}$; black lines), $TCR_{C4}$ (blue lines) or $TCR_{37\text{-}45}$ (red lines). **(H)** Percent AML cells expressing cleaved caspase 3 (cl-caspase 3, y-axis) of Patient 1's relapsed AML either alone (grey) or cultured with $CD8^+$ T cells with the endogenous TCR removed using CRISPR-Cas9 and transduced to express either $TCR_{irr.}$ (black), $TCR_{C4}$ (blue), or $TCR_{37\text{-}45}$ (red)(see **Supplementary Methods**). **(I)** Growth kinetics of $WT1^+$ cell lines PANC-1 and HLA-A*02:01-transduced MDA-MD-468 in live tumor-visualization assay in the absence (grey lines), or presence of $CD8^+$ T cells transduced to express either $TCR_{C4}$ (blue lines) or $TCR_{37\text{-}45}$ (red lines). Effector to target (E:T) ratio of 10:1, arrows indicate addition of tumor cells to culture. Standard error of triplicate wells are shown. **(J-L)** Growth kinetics of $WT1^+$ cell lines PANC-1 and HLA-A*02:01-transduced MDA-MB-468 in live tumor-visualization assay in the absence (grey lines), or presence of $T_{TCR37\text{-}45}$ cells. **(J)** $CD8^+$ T cells transduced with only $TCR_{37\text{-}45}$ (light-blue line) or a poly-cistronic construct containing $TCR_{37\text{-}45}$ and CD8αβ (red line, $eCD8^+$). **(K)** $CD4^+$ T cells transduced with only $TCR_{37\text{-}45}$ (blue line) or a poly-cistronic construct containing $TCR_{37\text{-}45}$ and CD8αβ (green line, $dpCD4^+$). **(L)** Comparison of $eCD8^+$ alone (red line), $dpCD4^+$ alone (green line) or $eCD8^+/dpCD4^+$ in combination (1:1 ratio, purple line). For all conditions, arrows indicate addition of tumor cells to culture. Standard error of triplicate wells are shown. 4:1 E:T ratio, total T cells was kept consistent for all conditions.

**Fig 6: $T_{TCR37-45}$ cells reduce PANC-1 solid tumor burden in an NSG mouse model.**

(**A**) Schematic for NSG experimental treatment model. (**B**) IVIS images of mice at Weeks 1, 2, and 8 post PANC-$1_{leu}$ injection. All mice had detectable tumor at the time of adoptive transfer. **(C)** Total flux (p/s) for each treatment group: Tumor (No T cells, n=5); $T_{TCR37-45}$ (n=5); $T_{TCR-C4}$ (n=4) $T_{TCR-Irr.}$ (n=4). **(D)** Fold change (from baseline (Week 1)) at week 8 for each treatment group.

**Figures and Legends.**

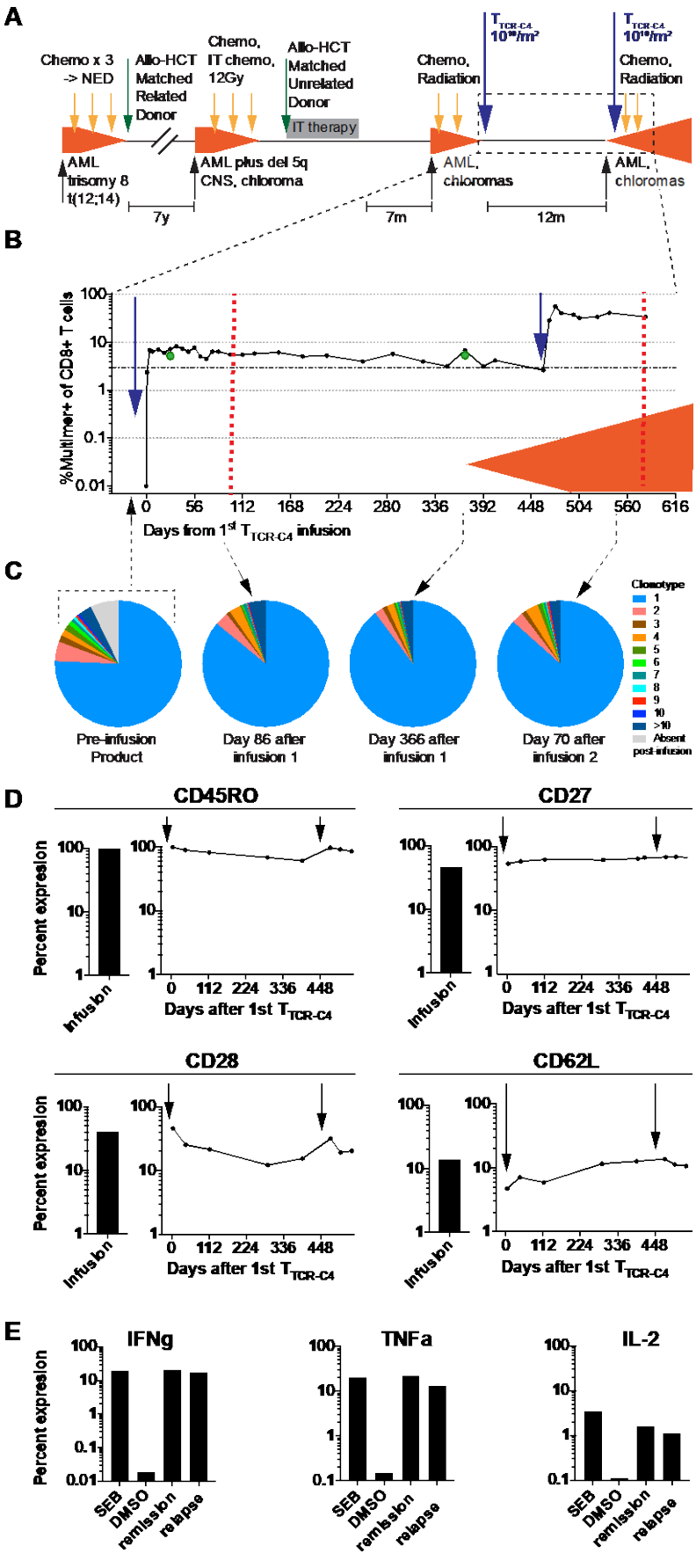
A
Chemo x 3
-> NED
Allo-HCT
Matched
Related
Donor
Chemo,
IT chemo,
12Gy
Allo-HCT
Matched
Unrelated
Donor
IT therapy
Chemo,
Radiation
Chemo,
Radiation
AML
trisomy 8
t(12;14)
AML plus del 5q
CNS, chloroma
AML,
chloromas
AML,
chloromas
7y
7m
12m
B
%Multimer+ of CD8+ T cells
Days from 1st T TCR-C4 infusion
C
Clonotype
Pre-infusion
Product
Day 86 after
infusion 1
Day 366 after
infusion 1
Day 70 after
infusion 2
Absent
post-infusion
D
CD45RO
CD27
CD28
CD62L
Percent expresion
Infusion
Days after 1st T TCR-C4
E
IFNg
TNFa
IL-2
SEB
DMSO
remission
relapse

**Fig. 1: $T_{TCR\text{-}C4}$ persist and remain functional in the presence of relapsed AML. (A)** Timeline of patient's treatment regimens. Chemo: chemotherapy; Radiation: radiation therapy. IT chemo: Intrathecal chemotherapy. **(B)** Percent multimer$^+$ of CD8$^+$ T cells in PBMCs (solid circles) and bone marrow (green circles) collected before and at defined timepoints after $T_{TCR\text{-}C4}$ infusions. Orange shaded area indicates presence of AML. Dotted red lines represent days 100 and 110 (or day 581 after the 1$^{st}$) after 1$^{st}$ and 2$^{nd}$ infusion respectively. **(C)** Pie chart representing individual clonotypes composing the pre-infusion $T_{TCR\text{-}C4}$ product (left) and at indicated timepoints (right) after both infusions. **(D)** Percent expression of CD45RO, CD27, CD28 and CD62L on infusion products (bar graphs to the left) and at days 4, 42, 114, 289, 393, 478, 508 and 542 after the 1$^{st}$ infusion (graphs to the right). The three last timepoints are also days 7, 35 and 71 after the second infusion. Timing of infusions are indicated by black arrows. **(E)** Percent expression of IFNγ, TNFα and IL-2 (functional markers) in response to *ex vivo* stimulation $WT1_{126\text{-}134}$ peptide (1nM) during remission (day 114 after 1$^{st}$ infusion) and relapse (day 581 after 1$^{st}$ infusion, day 110 after 2$^{nd}$). Maximum and minimal cytokine expression following exposure to Staphylococcal enterotoxin B (SEB) and dimethylsufoxide (DMSO) are shown for each cytokine.

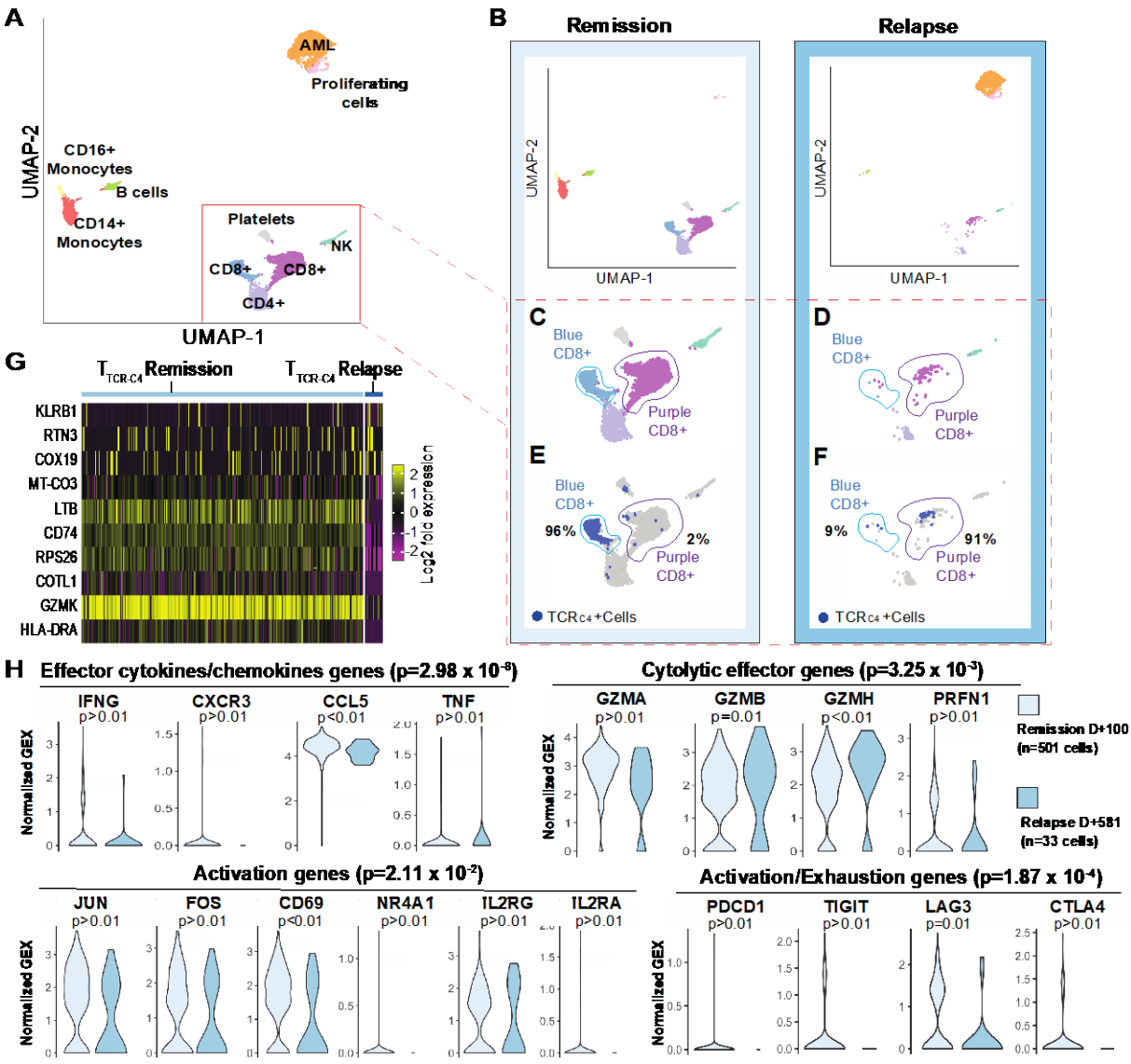


**Fig. 2: $T_{TCR\text{-}C4}$ present an activated transcription profile during remission but not during relapse. (A)** UMAP visualization of PBMC from both the remission (100 days after 1st infusion) and relapse (110 days after the second infusion or 581 days after the 1st) (red dotted lines **Fig. 1A**) samples visualized together (see **Supplementary Methods**). PBMC (n=7704) clustered into populations as indicated by labels. Clustering biostatistical analysis is described in Supplementary Methods and representative marker genes are shown in **Fig. S3**. **(B)** UMAP visualization of the separated PBMC obtained at remission (left) and relapse (right). **(C)** Close-up of clusters containing T cells during remission with identification of two (light blue and

purple) distinct $CD8^+$ T cell clusters based on their transcriptional programs. **(D)** Close-up of clusters containing T cells during relapse revealing the $CD8^+$ T cells are predominantly in the purple cluster. **(E)** Localization of $T_{TCR\text{-}C4}$ (dark blue dots) cells during remission. **(F)** Localization of $T_{TCR\text{-}C4}$ (dark blue dots) cells during relapse. Percentage of the total $T_{TCR\text{-}C4}$ cells in each cluster are indicated. **(G)** Heat map of significantly differentially expressed genes (DEG) comparing $T_{TCR\text{-}C4}$ during remission (n=501) to those during relapse (n=33). **(H)** Analysis of gene-sets representing effector cytokines, cytolytic effector genes activation and exhaustion genes were compared in $T_{TCR\text{-}C4}$ during remission (light blue) and relapse (darker blue) with each transcript in the gene-set is shown as a violin plot. The shape of the violin displays frequencies of values. Model-based Analysis of Single Cell Transcriptomics (MAST – See **Supplementary Methods**) was used to determine the significance shown above each plot. Significance thresholds were set *a priori* at a threshold of false discovery rate of 5% and positive or negative fold change > log2(1.3).

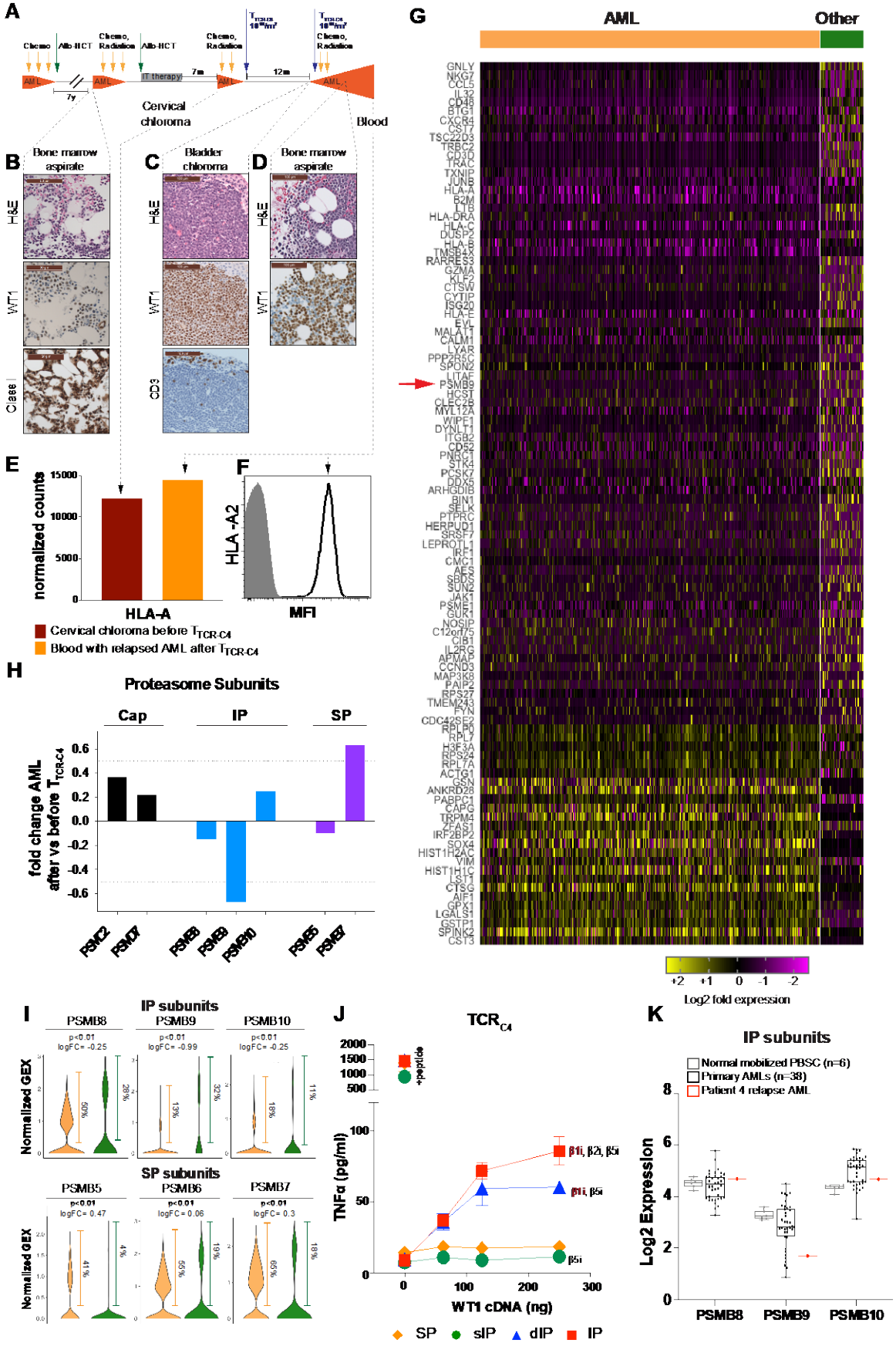
A
Chemo
Allo-HCT
Chemo, Radiation
Allo-HCT
Chemo, Radiation
Chemo, Radiation
AML
7y
AML
IT therapy
7m
AML
12m
AML
Cervical chloroma
Blood
B
Bone marrow aspirate
C
Bladder chloroma
D
Bone marrow aspirate
H&E
WT1
CD3
E
normalized counts
15000
10000
5000
0
HLA-A
F
HLA -A2
MFI
Cervical chloroma before TTCR-C4
Blood with relapsed AML after TTCR-C4
G
AML
Other
GNLY
NKG7
CCL5
IL32
CD48
BTG1
CXCR4
CST7
TSC22D3
TRBC2
CD3D
TRAC
TXNIP
JUNB
HLA-A
B2M
LTB
HLA-DRA
HLA-C
DUSP2
HLA-B
TMSB4X
RARRES3
GZMA
KLF2
CTSW
CYTIP
ISG20
HLA-E
EVL
MALAT1
CALM1
LYAR
PPP2R5C
SPON2
LITAF
PSMB9
HCST
CLEC2B
MYL12A
WIPF1
DYNLT1
ITGB2
CD52
PNRC1
STK4
PCSK7
DDX5
ARHGDIB
BIN1
SELK
PTPRC
HERPUD1
SRSF7
LEPROTL1
IRF1
CMC1
AES
SBDS
SUN2
JAK1
PSME1
GUK1
NOSIP
C12orf75
CIB1
IL2RG
AFMAP
CCND3
MAP3K8
PAIP2
RPS27
TMEM243
FYN
CDC42SE2
RPLP0
RPL7
H3F3A
RPS24
RPL7A
ACTG1
GSN
ANKRD28
PABPC1
CAPG
TRPM4
ZFAS1
IRF2BP2
SOX4
HIST1H2AC
VIM
HIST1H1C
LST1
CTSC
AIF1
GPX1
LGALS1
GSTP1
SPINK2
CST3
+2
+1
0
-1
-2
Log2 fold expression
H
Proteasome Subunits
Cap
IP
SP
fold change AML after vs before TTCR-C4
0.6
0.4
0.2
0.0
-0.2
-0.4
-0.6
PSMC2
PSMD7
PSMB5
PSMB9
PSMB10
PSMB5
PSMB7
I
IP subunits
PSMB8
PSMB9
PSMB10
p<0.01
logFC= -0.25
p<0.01
logFC= -0.99
p<0.01
logFC= -0.25
Normalized GEX
50%
26%
13%
32%
18%
11%
SP subunits
PSMB5
PSMB6
PSMB7
p<0.01
logFC= 0.47
p<0.01
logFC= 0.06
p<0.01
logFC= 0.3
Normalized GEX
41%
4%
55%
19%
66%
18%
J
TCRC4
peptide
2000
1500
1000
500
TNFα (pg/ml)
100
50
0
β1i, β2, β5i
β1i, β5i
β5i
0
100
200
300
WT1 cDNA (ng)
SP
sIP
dIP
IP
K
IP subunits
Normal mobilized PBSC (n=6)
Primary AMLs (n=38)
Patient 4 relapse AML
Log2 Expression
8
6
4
2
0
PSMB8
PSMB9
PSMB10

**Fig. 3: Analysis of immunoproteasome expression in relapsed AML (A)** Bone marrow aspirate, myeloid chloroma or blood obtained relative to the timeline of successive therapies. Presence of AML is indicated in orange. **(B)** Pre-$T_{TCR\text{-}C4}$ AML Hematoxylin and Eosin (H&E) (top panel), immunohistochemistry (IHC) of WT1 expression (middle panel) and class I expression (bottom panel). **(C)** H&E (top panel), WT1 IHC expression (middle panel) and CD3 infiltration (bottom panel) of bladder chloroma obtained early post-$T_{TCR\text{-}C4}$ relapse. **(D)** Post-$T_{TCR\text{-}C4}$ AML H&E (top panel) and WT1 IHC (bottom panel). **(E)** Normalized counts (y-axis) of bulk RNA expression of HLA-A obtained from the pre-$T_{TCR\text{-}C4}$ cervical chloroma and a post-$T_{TCR\text{-}C4}$ PBMC, both containing >89% AML. **(F)** HLA-A2 protein expression detected by flow cytometry of the post-$T_{TCR\text{-}C4}$ blood. **(G)** Heat map of the 100 most significantly differentially expressed genes (DEG) comparing AML (n=2,447) during relapse after T cell therapy to other cells in the sample (n=306). Red arrow indicates immunoproteasome subunit β1i [*PSBM9*] **(H)** Fold change (*y axis*) of transcripts encoding proteasome cap ([*PSMC2*] and [*PSMD7*]; black bars), immuno-proteasome (β5i [*PSMB8*], β1i [*PSMB9*] and β2i [*PSMB10*]; blue bars) and standard proteasome (β5 [*PSMB5*], and β2 [*PSMB7*]; purple bars) sub-units comparing expression in the post-$T_{TCR\text{-}C4}$ obtained from PBMC, to pre-$T_{TCR\text{-}C4}$ AML obtained from a chloroma FFPE sample. Of note, β1 [*PSMB6*] was not available in the commercial RNA probe-set utilized (see **Supplementary Methods**). **(I)**Expression of transcripts encoding genes constituting the active proteolytic site of the immunoproteasome (β5i [*PSMB8]*, β1i [*PSMB9]* and β2i [*PSMB10]*) and the standard proteasome (β5 [*PSMB5]*, β1 [*PSMB6]* and β2 [*PSMB7]*) at relapse comparing AML (n=2,447, orange) and other non-malignant cells (n=306, green) in the sample. Frequencies of cells with the detectable transcript are shown to the right of each violin plot. P values are indicated as well as the log2 fold change. Positive values indicate increased and negative decreased expression in AML. Model-based Analysis of Single Cell

Transcriptomics (MAST – See **Supplementary Methods**) was used to determine significance shown above each plot. Significance thresholds were set *a priori* at a threshold of false discovery rate of 5% and positive or negative fold change > log2(1.3)). **(J)** TNFα production (pg/mL) from T cells expressing $TCR_{C4}$ cultured with cells expressing a specific proteasome isoform and transfected with varying amounts of WT1 cDNA (*40*) or pulsed with $WT1_{126\text{-}134}$ peptide as a positive control. (**K**)RNAseq on viable leukemic blasts shows expression of genes constituting the active proteolytic site of the immunoproteasome (β5i [*PSMB8]*, β1i [*PSMB9]* and β2i [*PSMB10]*) in peripheral blood stem cells obtained from healthy donors (n=6, light grey), primary AML samples obtained from the Fred Hutch-University of Washington Hematopoietic Diseases Repository (black, n=38) and the patient (red, n=1). Box and whisker plot represents median, interquartile and range. Dots represent individual patient sample.

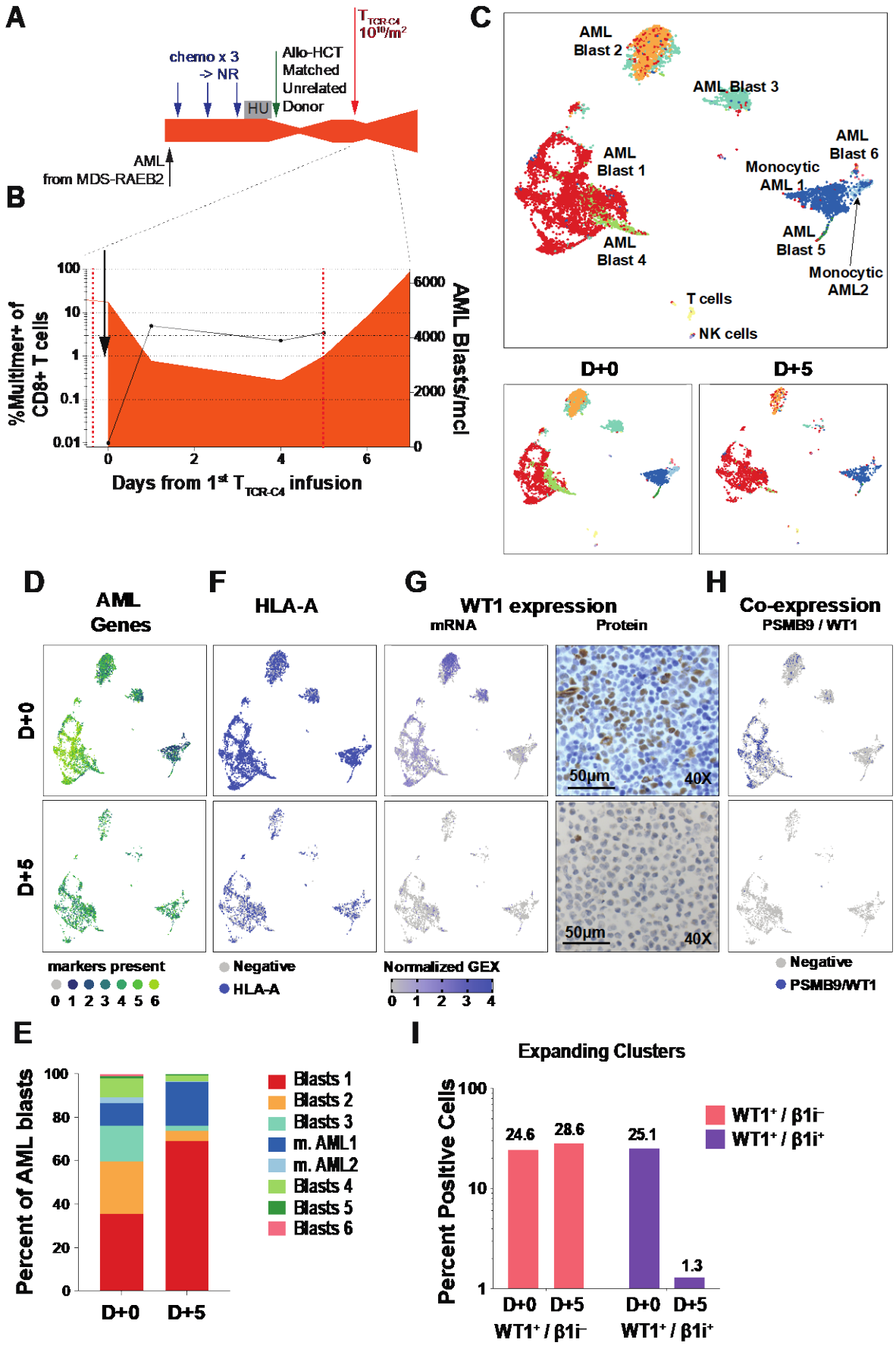
A
chemo x 3
-> NR
HU
Allo-HCT
Matched
Unrelated
Donor
$T_{TCR-C4}$
$10^{10}/m^2$
AML
from MDS-RAEB2
B
%Multimer+ of CD8+ T cells
AML Blasts/mcl
Days from 1st $T_{TCR-C4}$ infusion
C
AML Blast 2
AML Blast 3
AML Blast 1
AML Blast 6
Monocytic AML 1
AML Blast 5
AML Blast 4
Monocytic AML2
T cells
NK cells
D+0
D+5
D
AML Genes
F
HLA-A
G
WT1 expression
mRNA
Protein
H
Co-expression
PSMB9 / WT1
D+0
D+5
50µm
40X
markers present
Negative
HLA-A
Normalized GEX
Negative
PSMB9/WT1
E
Percent of AML blasts
Blasts 1
Blasts 2
Blasts 3
m. AML1
m. AML2
Blasts 4
Blasts 5
Blasts 6
I
Expanding Clusters
Percent Positive Cells
24.6
28.6
25.1
1.3
WT1+ / β1i−
WT1+ / β1i+

**Fig. 4: $T_{TCR\text{-}C4}$ preferentially eliminates $WT1^+$ AML co-expressing β1i.** (**A**) Timeline of patient's treatment regimens. Chemo: chemotherapy; NR: no response. (**B**) Percent multimer$^+$ of $CD8^+$ T cells in peripheral blood collected before and at day +1, +4, and +5. Orange shaded area indicates presence of AML. Dotted red lines represent days +0 and +5 after $T_{TCR\text{-}C4}$. (**C**) UMAP visualization of scRNAseq on PBMC from both before (D+0, n=7,381) $T_{TCR\text{-}C4}$ infusion and 5 days post 1$^{st}$ infusion (D+5, n=3,319) (red dotted lines **Fig. 4B**) aggregated into a single UMAP(top) or as individual time points (bottom). (**D,F,G,H**) UMAP of AML clusters on D+0 (top row) or D+5 (bottom row). (**D**) Expression of AML specific markers CD34, CCND1, CDK6, FLT3, NPM1, RUNX1. (**E**) Relative proportions of AML clusters at D+0 and D+5. (**F**) Expression of HLA-A. (**G**) Expression of WT1 transcripts from peripheral AML (left panel) and immunohistochemistry performed on a bone marrow biopsy (D+0) and a PBMC cell pellet (D+5). (**H**) Co-expression of WT1 and the immunoproteasome gene β1i (PSMB9). (**I**) Percent of cells that express WT1 only (pink bars) or WT1 and β1i ([PSMB9]) (purple bars) before (D+0) and after (D+5) $T_{TCR\text{-}C4}$ infusion. Percent values are indicated above each column.

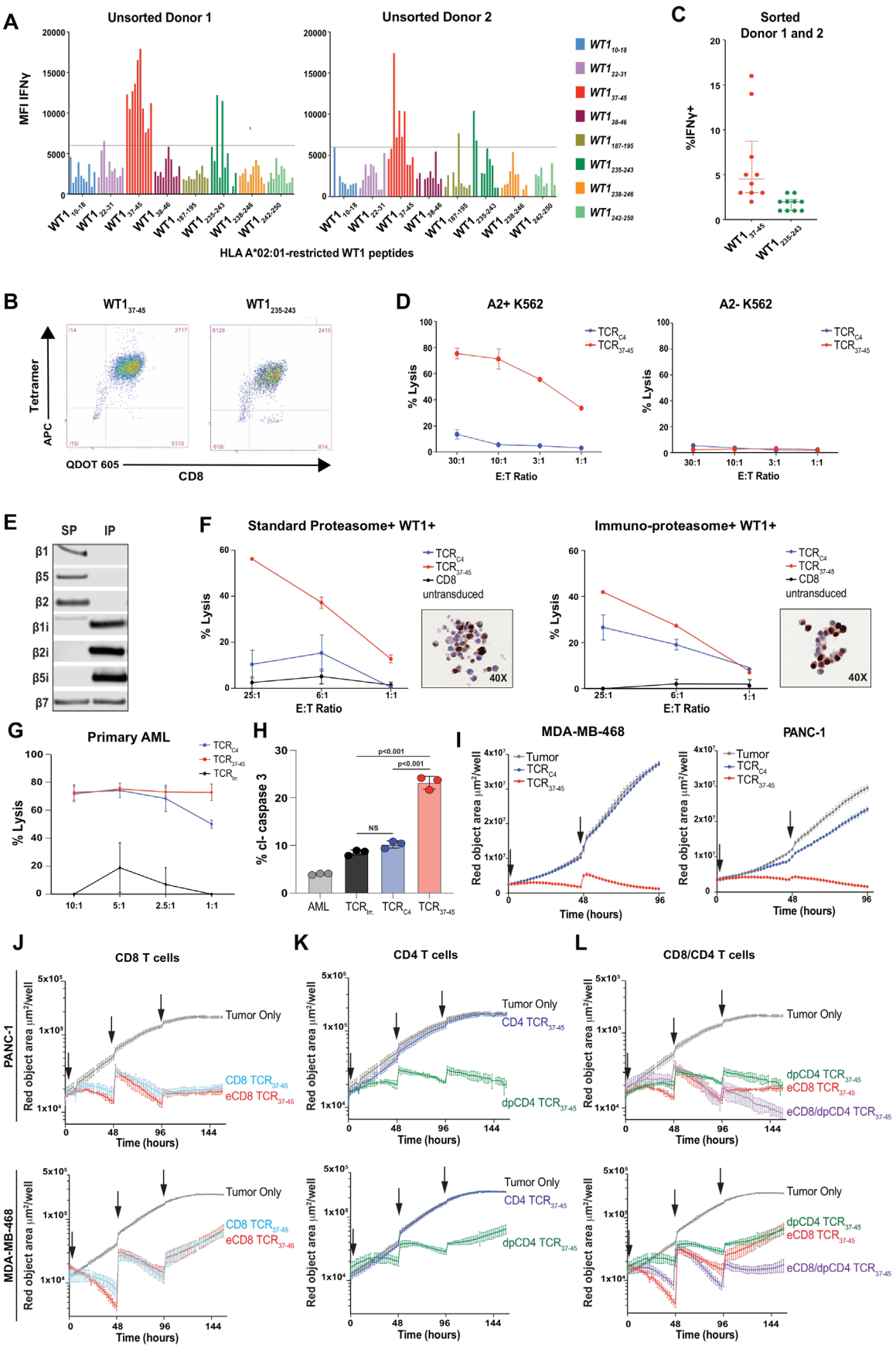
A
Unsorted Donor 1
Unsorted Donor 2
MFI IFNγ
HLA A*02:01-restricted WT1 peptides
C
Sorted Donor 1 and 2
%IFNγ+
B
Tetramer
APC
QDOT 605
CD8
D
A2+ K562
A2- K562
% Lysis
E:T Ratio
E
SP
IP
β1
β5
β2
β1i
β2i
β5i
β7
F
Standard Proteasome+ WT1+
Immuno-proteasome+ WT1+
untransduced
40X
G
Primary AML
H
% cl- caspase 3
p<0.001
NS
AML
I
MDA-MB-468
PANC-1
Red object area µm²/well
Time (hours)
Tumor
J
CD8 T cells
K
CD4 T cells
L
CD8/CD4 T cells
Tumor Only
CD8 TCR37-45
eCD8 TCR37-45
CD4 TCR37-45
dpCD4 TCR37-45
eCD8/dpCD4 TCR37-45

**Fig. 5: Identification of an alternate HLA-A*02:01-restricted WT1 peptide ($WT1_{37\text{-}45}$) not dependent on immunoproteasome processing.** (**A**) Ten $CD8^+$ T cell lines from 2 HLA-A*02:01-expressing healthy donors were generated against 8 candidate HLA-A*02:01-binding WT1 peptides (x-axis). Each cell line's ability to produce IFNγ following stimulation with the immunoproteasome-deficient but $WT1^+$ HLA-A*02:01-transduced K562 cell line at an E:T of 1:1 was assessed. Two peptides ($WT1_{37\text{-}45}$ and $WT1_{235\text{-}243}$) were identified that, elicited high reactivity from donor T cells as measured by MFI (above the arbitrary threshold of 6000) for the IFNγ positive cells. (**B**) Representative flow plots of $CD8^+$ T cell lines targeting ($WT1_{37\text{-}45}$ and $WT1_{235\text{-}243}$) that were sorted using the corresponding tetramers. (**C**) Sorted T cell lines targeting $WT1_{37\text{-}45}$ had the highest comparative reactivity, assessed by IFNγ MFI, when cultured with HLA A*02:01-tansduced K562 cells. TCRs targeting $WT1_{37\text{-}45}$ were isolated from T cells in these lines. (**D**) Lysis of K562 +/- expressing HLA-A*02:01 by $CD8^+$ T cells from a healthy donor transduced with $TCR_{C4}$ and a TCR targeting $WT1_{37\text{-}45}$ ($TCR_{WT1\text{-}37\text{-}45}$ #1 -see **Supplementary Methods**) confirmed expression of the $WT1_{37\text{-}45}$ peptide was not dependent on IP processing. **(E)** Immunoblot demonstrating protein expression of catalytic proteasome subunits in HEK-293 (endogenous SP expression) +/- engineered to express IP. **(F)** Percent lysis (y-axis) of IP/SP-skewed HEK-293 cells lines by $CD8^+$ T cells transduced to express either $TCR_{C4}$ (blue lines), $TCR_{37\text{-}45}$ (red lines) and untransduced $CD8^+$ T cells (black lines) at indicated effector to target (E:T) ratios (x-axis). Inset depicts WT1 IHC of IP/SP HEK-293 cells transduced with WT1-and HLA-A*02:01. IP/SP cell lines demonstrate heterogeneity of WT1 expression (see **Supplementary Methods**). **(G)** Percent lysis (y-axis) of a primary leukemia by $CD8^+$ T cells transduced to express either an irrelevant TCR ($TCR_{irr.}$; black lines), $TCR_{C4}$ (blue lines) or $TCR_{37\text{-}45}$ (red lines). **(H)** Percent AML cells expressing cleaved caspase 3 (cl-caspase 3, y-axis) of Patient 1's relapsed AML either alone (grey) or cultured with $CD8^+$ T cells with the

endogenous TCR removed using CRISPR-Cas9 and transduced to express either $TCR_{irr.}$ (black), $TCR_{C4}$ (blue), or $TCR_{37\text{-}45}$ (red)(see **Supplementary Methods**). **(I)** Growth kinetics of $WT1^+$ cell lines PANC-1 and HLA-A*02:01-transduced MDA-MD-468 in live tumor-visualization assay in the absence (grey lines), or presence of $CD8^+$ T cells transduced to express either $TCR_{C4}$ (blue lines) or $TCR_{37\text{-}45}$ (red lines). Effector to target (E:T) ratio of 10:1, arrows indicate addition of tumor cells to culture. Standard error of triplicate wells are shown. **(J-L)** Growth kinetics of $WT1^+$ cell lines PANC-1 and HLA-A*02:01-transduced MDA-MB-468 in live tumor-visualization assay in the absence (grey lines), or presence of $T_{TCR37\text{-}45}$ cells. **(J)** $CD8^+$ T cells transduced with only $TCR_{37\text{-}45}$ (light-blue line) or a poly-cistronic construct containing $TCR_{37\text{-}45}$ and CD8αβ (red line, $eCD8^+$). **(K)** $CD4^+$ T cells transduced with only $TCR_{37\text{-}45}$ (blue line) or a poly-cistronic construct containing $TCR_{37\text{-}45}$ and CD8αβ (green line, $dpCD4^+$). **(L)** Comparison of $eCD8^+$ alone (red line), $dpCD4^+$ alone (green line) or $eCD8^+/dpCD4^+$ in combination (1:1 ratio, purple line). For all conditions, arrows indicate addition of tumor cells to culture. Standard error of triplicate wells are shown. 4:1 E:T ratio, total T cells was kept consistent for all conditions.

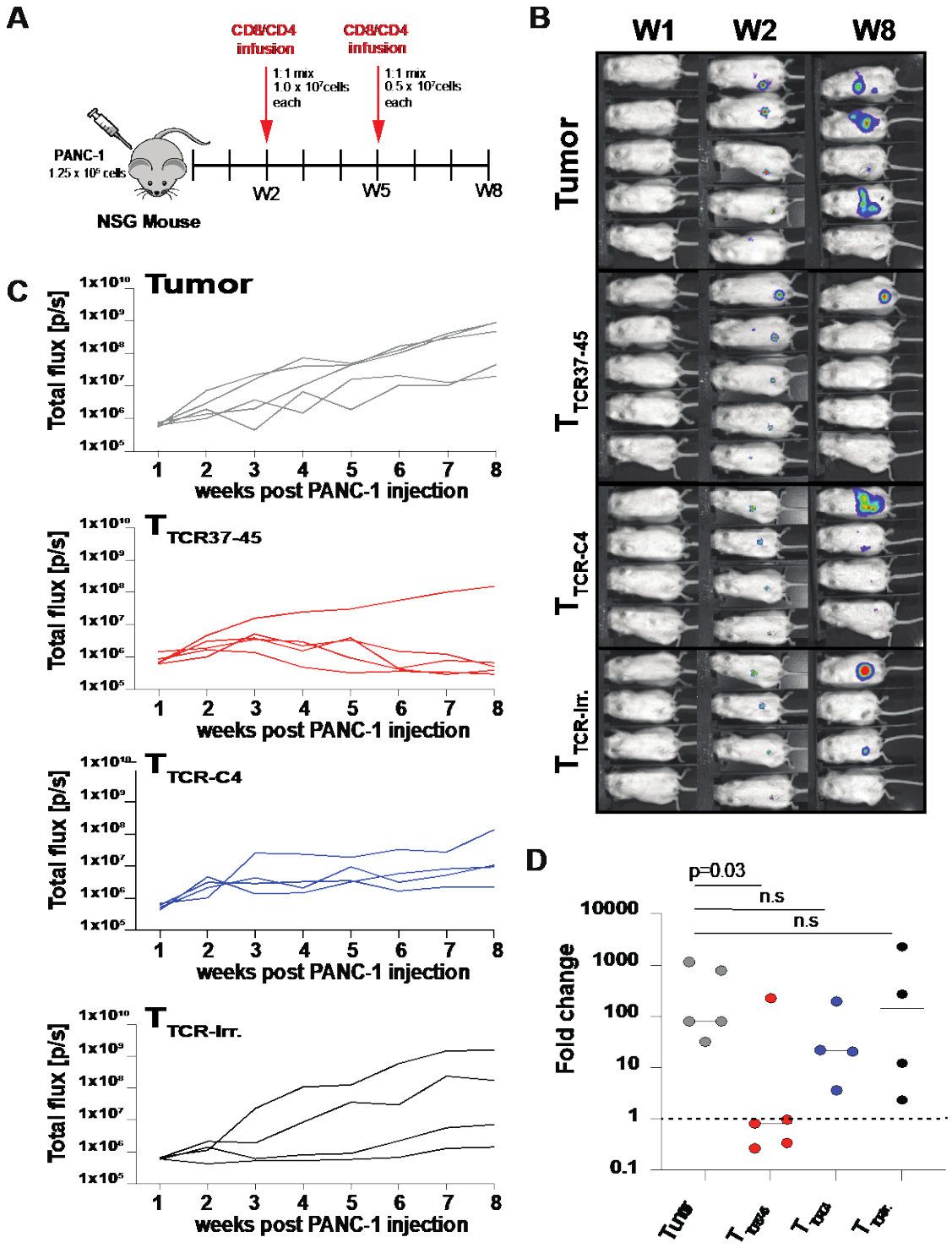


**Fig 6:** $T_{TCR37\text{-}45}$ **cells reduce PANC-1 solid tumor burden in an NSG mouse model.**

(**A**) Schematic for NSG experimental treatment model. (**B**) IVIS images of mice at Weeks 1, 2, and 8 post PANC-$1_{leu}$ injection. All mice had detectable tumor at the time of adoptive transfer.

**(C)** Total flux (p/s) for each treatment group: Tumor (No T cells, n=5); $T_{TCR37\text{-}45}$ (n=5); $T_{TCR\text{-}C4}$ (n=4) $T_{TCR\text{-}Irr.}$ (n=4). **(D)** Fold change (from baseline (Week 1)) at week 8 for each treatment group.

**Supplementary Methods:**

**Detailed case report Patient 1.** The individual described here was a 27-year-old man who, at the age of 15 was diagnosed with AML trisomy 8, translocation (12;14). His AML proved resistant to Daunorubicin, AraC, etoposide and Dex, followed by HiDAC and mitoxantrone induction and finally achieved a complete remission after single agent Mylotarg. He underwent a first 10/10 matched related mobilized allogeneic hematopoietic stem cell transplant (HCT) with a preparative regimen of Samarium 153-ethylene diamine tetramethylene phosphonate ($^{153}$Sm-EDTAP) and Mephalan. HCT was successful with full engraftment and no evaluable disease (NED) detected post-HCT. Unfortunately, his AML relapsed 7 years later at age 23 with a new deletion 5q (23q33) and was now located in the marrow (61% blasts), in the central nervous system (67% blasts) and within a S2-S3 nerve root myelosarcoma. He received systemic re-induction with azacytidine and mylotarg, serial intrathecal methotrexate (IT MTX) and 24 Gy of radiation in 12 fractions to the sacrum which again achieved a CR. He received a second reduced intensity HCT from a 10/10 matched unrelated donor after a preparative regimen of Treosulfan, Fludarabine and 200cGy of total body irradiation. This second HCT achieved 100% donor engraftment and NED post-HCT. He continued to receive IT MTX for 7 months post-HCT and his AML relapsed 7 months after treatment discontinuation with predominantly cervical C5 and C7 myelosarcomas and minimal marrow involvement (0.002% blasts). He received a cycle of systemic azacitine (75mg/m$^2$ x 7 days) and mylotarg (days 8, 11, 14) as well as 24 Gy in 24 fractions to the cervical spine. 2 months after the start of this last treatment, he had no evaluable marrow AML Immediately prior to a first infusion of $10^{10}$ $T_{TCR\text{-}C4}$/m$^2$ on the Treatment Arm. The patient was monitored for and no evidence of GVHD or toxicity to cells expressing low physiologic levels of WT1 including the hematopoietic system, kidneys, lung, heart, liver and

skin were observed. He remained with NED and no additional treatments for 368 days before relapsing with a bladder myelosarcoma. His concurrent marrow aspirate was positive for AML blasts. He received a second infusion of $10^{10}$ $T_{TCR\text{-}C4}/m^2$, radiation to the bladder then additional azacitidine and mylotarg, Filgrastim, Cladribine, Cytarabine, and Mitoxantrone (G-CLAM) chemotherapy and hydroxyurea which did not control his AML. In accordance with the patient and his family, no additional treatments were administered, and he succumbed to progressive AML a year after his 2nd $T_{TCR\text{-}C4}$ infusion. Although the patient was followed closely after the last relapse, the study team respected his wishes for minimal intervention and sample collection, which greatly limited the amount of material obtained.

**Detailed case report Patient 2**. This patient was a 47-year-old man who at the age of 46 was diagnosed with a myelodysplastic syndrome at the stage of refractory anemia with excess blasts (blasts constituted 15.6% of marrow cells). He had multiple cytogenetic abnormalities including translocation of chromosome 11 and 12, trisomy 8 and 21 and deletion of the long arm of chromosome 17. A month later he presented with circulating blasts and received chemotherapy with daunorubicin and cytarabine on a scheduled 7 +3, 2 cycles of decitabine, daunorubicin and cytarabine, and decitabine followed by mitoxantrone, etoposide and cytarabine. All chemotherapy resulted in progressive disease without having achieved a remission. His circulating blast count was then maintained with hydroxyurea. He was enrolled in a transplant protocol specifically designed for patients with residual leukemia and received a myeloablative induction of clofarabine and busulfan prior to the infusion of peripheral blood stem cells from a male matched unrelated donor. Post-transplant immunosuppression consisted of methotrexate on days 1, 3, 6 and 11 as well as tacrolimus which was tapered 56 days later. Twenty eight days after transplant he presented with minimal residual disease with 0.28% abnormal marrow blasts.

He received two 7-day cycles of azacytidine separated by a month but his disease continued to progress. A bone marrow biopsy performed 94 days after HCT showed 12.9% blasts and cytogenetics now showed evidence of clonal evolution with additional inversion of chromosome 7. Chromosome gene array testing performed on the latter marrow (CGAT) showed deletions of chromosomes 9q13q31, 9q32q33 and 17q11.2 in >80% host cells (host cells constituted 80% of the bone marrow cells). Of note, no copy number aberrations, no single nucleotide polymorphisms or copy neutral loss of heterozygosity were detected in WT1. Twelve days prior to the infusion of $10^{10}$ $T_{TCR\text{-}C4}/m^2$ on the protocol Treatment Arm (150 days after HCT), his marrow showed 69% blasts and immediately prior to cell infusion his complete blood count included a total of 8030 white blood cells/mcl with 66% blasts (5310 cells/mcl), 9% neutrophils (720 cells/mcl) and 13% lymphocytes (1040 cells/mcl). Although his absolute blast count moderately decreased immediately after infusion, his AML subsequently progressed despite presistance of $T_{TCR\text{-}C4}$ at >3% CD8 cells in the peripheral lymphocyte compartment and he succumbed to progressive disease 15 days after $T_{TCR\text{-}C4}$ transfer.

**Assessment of disease status.** Morphology, multiparameter flow cytometry,(*73*) standard cytogenetics(*74*) or genomic technologies(*75*) were routinely performed on bone marrow aspirates that were obtained from the patients. Any level of residual disease was considered to indicate positivity for MRD.

**Isolation of $TCR_{C4}$ and lentiviral vector construction.** $TCR_{C4}$ was selected from a screen of more than 1000 T cell clones from more than 50 HLA-$A2^+$ healthy donors based on its comparatively higher functional avidity for the $WT1_{126\text{-}134}$ peptide (RMFPNAPYL) as previously

described (*18*). $TCR_{C4}$ was inserted into the pRRLSIN.cPPT.MSCV/GFP.wPRE vector obtained from the lab of Richard Morgan after excising the green fluorescent protein (GFP) gene (*76*).

**Generation of $T_{TCR\text{-}C4}$.** All *ex vivo* manipulations involving processing of infusion products were performed in the cGMP Cell Processing Facility (CPF) at FHCRC as previously described (*18*). Briefly, substrate $CD8^+$ T cells for generating the $TCR_{C4}$-transduced T cells ($T_{TCR\text{-}C4}$) were obtained from an aliquot the G-CSF stimulated PBMC donation (mobilized leukapheresis) of their corresponding allogeneic stem cell donors. Cells were stimulated with the HLA-A2-restricted EBV ($EBV_{280\text{-}288}$ BMLF1 [GLCTLVAML]) peptide, transduced using the pRRLSIN.cPPT.MSCV/$TCR_{C4}\beta$-P2A-$TCR_{C4}\alpha$/wPRE lentiviral vector and sorted by flow cytometry; cells were labeled with tetramers that selectively bound the WT1-specific TCR (APC) and the EBV-specific TCR (PE), double positive cells were selected followed by a secondary, non-specific expansion and infusion into the patient. Total production time was of 4-6 weeks. Quality control of the infused products included assessment of inserted lentiviral vector copy number per cell (≤5 copies/cell), envelope VSV-G DNA by qPCR as a surrogate marker for RCL (<10copies/50ng DNA) and binding to the $WT1_{126\text{-}134}$ HLA-A2-restricted tetramer (≥30% of live cells).

**T cell tracking by $WT1_{126\text{-}134}$ peptide/HLA tetramers.** HLA-A2/$WT1_{126\text{-}134}$ specific tetramers (produced by the FHCRC immune monitoring core facility) were used to detect $T_{TCR\text{-}C4}$ in PBMCs collected after infusions, with a staining sensitivity of 0.01% of total $CD8^+$ T-cells, as previously described (*77*).

**Clonotype identification in the pre-infusion product and tracking by high throughput TCRβ sequencing**. To identify clonotypes composing infused $T_{TCR\text{-}C4}$, high-throughput TCRβ sequencing (HTTCS) analysis was performed on HLA-A2/$WT1_{126\text{-}134}$ tetramer $^{+}$ cells from the pre-infusion product to obtain >99% purity (*78*). As the $TCR_{C4}$ sequence was codon-optimized, HTTCS could not identify the introduced WT1-specific TCR. Instead, HTTCS identified clonotypes based on the endogenous EBV-specific TCR sequence. To track the identified clonotypes, HTTCS was performed on whole PBMC obtained after transfer (*78*). Briefly, DNA was extracted from T cell products and sorted PBMC using Qiagen Maxi DNA isolation kits (QIAGEN Inc.). TCRβ CDR3 regions were amplified and sequenced from 750ng of extracted DNA by Adaptive Biotechnologies Corp (Seattle, WA) using the ImmunoSEQ assay as previously described using "deep" resolution (*79*). Raw sequence data was filtered using the Adaptive bioinformatic website based on the TCRβ V, D and J gene definitions provided by the International ImMunoGeneTics collaboration (IMGT)(*80*), using the IMGT database (www.imgt.org). Productive nucleotide sequences were used for all tracking experiments. The limit of detection of HTTCS was set at 0.001% of all TCR reads, below which frequency could not be reliably determined (*80*). Only clonotypes present in the infusion products were tracked in PBMC obtained after infusions. Clonotypes in the infusion product that were not detected *in vivo* after infusions and which did not undergo expansion throughout the ex-vivo culture process, signifying bystander clonotypes were eliminated for further analysis (*78*). The frequency of each clonotype detected by HTTCS is based on all TCR Vβ reads which include $CD4^{+}$ and $CD8^{+}$ T cells.

**Flow cytometry on T cells**. $T_{TCR\text{-}C4}$ in infusion products and PBMCs post-transfer were identified by binding to the APC dye-labeled HLA-A2/$WT1_{126\text{-}134}$ tetramer (FHCRC in-house production), and analyzed by flow cytometry after staining with fluorochrome-conjugated mAbs to CD16 (PE-Cy5 clone 3G8, Becton Dickinson), CD19 (PE-Cy5 HIB19, Becton Dickinson) (dump channel), CD4 (BUV 496 clone SK3, Beckton Dickinson) CD8 (Qdot 605 clone 3B5, Life Technologies), CD28 (BV421clone CD28.05, Biolegend), CD27 (FITC clone M-T271, Biolegend), CD62L (PE clone SK11 Becton Dickinson) and CD45RO (Alexa 700, clone UCHL1, BioLegend). A representative example of the initial gating algorithm is shown in **Fig. S2A**.

**Intracellular cytokine staining.** Cryopreserved PBMCs were thawed and rested overnight in RPMI medium, supplemented with 10% fetal bovine serum (FBS) (R10). Intracellular cytokine staining and stimulations were performed using a 15-color staining panel, as previously described (*81, 82*). After addition of the stimulation cocktail containing the $WT1_{126\text{-}134}$ peptide in R10 at a final peptide concentration of 1 μg/mL or the addition of R10 with an equivalent amount of dimethyl sulfoxide (DMSO) used to preserve the peptides (negative control) or staphylococcal endotoxin B (positive control). Modifications to the panel included excluding IL-21, CD56 and CXCR5, changing IL-2 to PE-dazzle 594 (clone MQ1-17H12, Biolegend) and adding granzyme B on alexa 700 (clone GB11, BD Biosciences). Cells were analyzed on an LSRII instrument (Becton Dickinson), using FACS-Diva software. The resulting flow cytometry data was analyzed using FlowJo v9.9.6 (Treestar). Percent cytokine expression (% of tetramer$^+$ cells that are both cytokine$^+$ and tetramer$^+$ in the DMSO only sample [negative control]) was calculated for each sample. Percent tetramer$^+$cytokine$^+$ cells in the presence of DMSO without

peptide varied among samples from 0-2.27% with a median of 0.745%. A representative example of the initial gating algorithm is shown in **Fig. S2B**.

**Serum EBV and CMV quantitation**. EBV PCR: This in-house developed PCR uses primers specific for the EBER gene (*83*). The limit of quantitative detection (the minimum virus level that gives a positive result in 95% of replicates) is 250 IU/mL (2.40 log IU/mL). Quantitative results less than 250 IU/mL are described as very low positive. CMV PCR: This in-house developed PCR uses primers specific for the UL123 and gB genes (*84*). The limit of quantitative detection (the minimum virus level that gives a positive result in 95% of replicates) is 20 IU/mL (1.3 log IU/mL). Quantitative results less than 20 IU/mL are described as very low positive.

**Single Cell RNA Sequencing (scRNAseq)**. Patient 1 :Patient samples, during 'remission' and 'relapse' were selected to be approximately 100 days after the last infusion to minimize changes associated with infusion of large numbers of ex vivo-manipulated cells. Patient 2: Patient samples before $T_{TCR\text{-}C4}$ infusion and five days after were selected. PBMCs for both patients were thawed, washed and labelled using the 10x Genomics 3' Chromium v2.0 (Patient 1) or 5' Chromium v2.0 (Patient 2) platform as per manufacturer's instructions. Library preparation was performed as per manufacturer's protocol with no modifications. Library quality was confirmed by Illumina TapeStation high sensitivity (evaluates library size), qubit (evaluates dsDNA quantity), and KAPA qPCR analysis (KAPA Biosystems, evaluates quantity of amplifiable transcript). Samples were mixed in equimolar fashion and sequenced on an Illumina HiSeq 2500 *rapid run* mode according to standard 10x genomics protocol.

**Computational analysis for scRNAseq on Patient 1.** The Cell Ranger Single-Cell Software Suite (v2.0.0) was used to perform sample demultiplexing, barcode processing and single-cell 3' gene counting (http://10xgenomics.com/). First, raw base BCL files were demultiplexed using the Cell Ranger *mkfastq* pipeline into sample-specific FASTQ files. Second, these FASTQ files were individually processed using the Cell Ranger *count* pipeline. Reads, which contain cDNA inserts, were aligned to the hg38 human reference genome (Ensembl) and the known transgene codon-optimized sequence using STAR (*85*). Aligned reads were then filtered for valid cell barcodes and unique molecular identifiers (UMIs). Cell barcodes with 1-Hamming-distance from a list of known barcodes were examined. UMIs with sequencing quality score > 10% and not homopolymers were retained as valid UMIs. A UMI with 1-Hamming-distance from another UMI with more reads, for a same cell and a same gene was corrected to this UMI with more reads. The default estimated number of cells used were 10,000 cells for both 'remission' and 'relapse' timepoints. Samples from both time points were aggregated using the Cell Ranger *aggr* pipeline resulting in one gene-barcode count matrix to be used for downstream analyses. A correction for sequencing depth was performed during the aggregation.

**Statistical analysis for scRNA-seq on patient 1 PBMC**. Standard analyses were performed using the Seurat R package (*86, 87*). Following sequence alignment and filtering, cells with a percentage of mitochondrial genes > 20%, a unique gene counts < 200 and/or > 15,000 UMIs were removed. Based on these thresholds, 68 cells were discarded, resulting in a data set of 7,688 cells for downstream analyses. Only genes with at least one UMI count detected in at least three cells were kept (16,590 genes). A library-size normalization was performed for each cell. UMI counts were divided by the total number of UMI in each cell followed by a multiplication by

10,000. Data were then log transformed and corrected for unwanted sources of variation such as the number of detected UMIs and percentage of mitochondrial content using the *ScaleData* R function as described in the Seurat manual. As high mitochondrial gene expression might be suggestive of low-quality libraries(*88*), the corrected-normalized gene-barcode matrix was used as input to perform PCA, clustering and UMAP analyses, whereas the normalized gene-cell barcode matrix was used as input for the differential expression analysis as described below. Principal component analysis (PCA) was performed using the top 2,000 most variable genes. The top 20 principal components (PCs) were then down-selected for UMAP visualization and clustering. UMAP with these parameters (n.epochs = 400, min.dist = .2, local.connectivity = 20) was performed using the *RunUMAP* R function. Cell clustering was performed using a graph-based clustering method implemented in Seurat (*FindNeighbors* and *FindClusters* R function) using a resolution of 0.25.

Differential expression analysis was performed using the R package MAST (*89*) implemented within the *FindMarkers* R function from the Seurat R package. MAST provides functionality for significance testing of differential expression using a Hurdle model, gene set enrichment and facilities for visualizing patterns in residuals indicative of differential expression. It is a two-part generalized linear model that simultaneously models the rate of expression over the background of various transcripts (logistic regression), and the positive expression mean (Gaussian). These tests are two sided and adjust for the bimodal nature of single cell RNA sequencing data. Differential expression was performed between clusters, and between conditions (such as transgenic CD8-T vs endogenous CD8-T). In each case, the normalized gene-cell barcode matrix was used as input; and the model included the cellular detection rate (CDR), defined as the total

of UMIs in a given cells, as a covariate to correct for biological and technical nuisance factors that can affect the number of genes detected in a cell (e.g. cell size and amplification bias). Genes were declared significantly differentially expressed at a false discovery rate (FDR) of 5% and a fold-change > 1.5.

**Computational and statistical analysis for scRNA-seq on patient 2**. A relaxed QC strategy was used, and we chose to only exclude cells with large mitochondrial proportions as proxy for cell damage. A stringent cutoffs (2 Median Absolute Deviation (MAD)) for percent of mitochondrial genes was used, resulting in a data set of 10,700 cells for downstream analyses (2,477 cells were filtered out). Only genes with at least one UMI count detected in at least three cells were retained (17,475 genes).

Data integration and standard analyses were performed using the Seurat R package (*87*). Gene expression data integration was performed using the time point as factor, resulting in two different datasets. To integrate the gene expression values, we first separately normalized each of our partitions using the *SCTransform* R function (*90*) with *vars.to.regress = "percent.mito"*. Data integration was then performed using the two R functions *FindIntegrationAnchors* and *IntegrateData* (with *dims = 1:50*). Principal component analysis (PCA) on the integrated dataset was performed using the *RunPCA* R function. The top 50 principal components (PCs) were then used for UMAP visualization and clustering. UMAP with this parameter (*min.dist = .01*) was performed using the *RunUMAP* R function. Cell clustering was performed using a graph-based clustering method implemented in Seurat (*FindNeighbors* and *FindClusters* R function) with different resolutions. Differential expression analysis was performed using the R package MAST

(*89*) implemented within the *FindMarkers* R function from the Seurat R package as described in the *Statistical analysis for scRNA-seq on patient 1 PBMC* section

**Immunohistochemistry (IHC).** WT1 IHC was performed by a College of American Pathologists (CAP) Clinical Laboratory Improvement Amendments (CLIA) certified laboratory with the standard clinical protocol. Paraffin-embedded core bone marrow biopsies or particle preparations were sectioned (4μM) and antigen retrieval performed by heat treatment in 10mM sodium citrate buffer (pH 6) before staining with DAKO mouse anti-WT1 monoclonal antibody (mAb) clone 6F-H2, at a 1:800 dilution. IHC for MHC Class I (HLA-A,B,C) was performed in a CLIA certified laboratory using Paraffin-embedded core bone marrow biopsies or particle preparations were sectioned (4μM). Antigen retrieval was performed at heat treatment at 95 degrees Celsius for 20 min in DIVA citrate buffer (pH 6.0), before staining with mouse monoclonal MHC Class 1 antibody clone EMR8-5 (Abcam, Cambridge, MA) at a 1:1000 dilution.

**AML HLA-A2 flow cytometry.** Patient PBMCs at relapse were assessed for HLA-A2 expression using Flow Cytometry. Briefly, PBMC containing >80% AML were stained for CD34 (BV-421 clone 561, BioLegend) to identify AML blasts and HLA-A2 (APC, BB7.2, Beckton Dickinson).

**Gene expression analysis from archived formalin fixed paraffin embedded (FFPE) samples and peripheral blood.** Tumor tissues was obtained post-second HCT and pre-$T_{TCR\text{-}C4}$ from a malignant chloroma (**Fig. 3A**) and at the time of relapse from PBMC (day 581 after the first $T_{TCR\text{-}C4}$ infusion). Both samples contained ≥89% AML. For FFPE tissues, total RNA was

extracted using the AllPrep DNA/RNA FFPE Kit (Qiagen) and for PBMC RNA was extracted using Blood RNEasy miniprep kit (Qiagen). RNA gene expression quantification was performed using the nCounter Immunology Panel (Human V2, code set NS_Immunology_v2_c2328) which contains 579 immunology related human genes plus 15 internal housekeeping control genes per manufacturer's protocol (NanoString Technologies). The raw counts were normalized using the geometric mean of the internal controls using nSolver software (Version 4.0) and all samples passed QC parameters (**Fig. S6**) (*91*). The normalized counts for the genes encoding the cap proteins ([*PSMC2*] and [*PSMD7*]) catalytic sites of the IP and SP available in the panel (β5i [PSMB8], β1i [PSMB9], β2i [PSMB10], β5 [PSBM5] and β2 [PSMB7]) for the blood sample after $T_{TCR\text{-}C4}$ infusion were expressed as a fold change compared to expression in the cervical chloroma sample obtained before $T_{TCR\text{-}C4}$ infusions. Of note, although the purity of both samples was ≥89% AML, the pre-$T_{TCR\text{-}C4}$ sample was a chloroma and considered to be nearly 100% AML whereas the relapsed PBMC sample on which RNA gene expression was performed contained only 89% AML. Thus, the calculated reduction of [PSMB9] is likely an underestimate due to immune and hematopoietic cells (expressing elevated immunoproteasome genes) in the PBMC sample.

**WT1 sequencing**. Clinical sequencing for oncogenic mutations including for WT1 was performed on a post-relapse bone marrow biopsy specimen from day 58 after 2$^{nd}$ infusion using the University of Washington OncoPlex platform. Performance details and characteristics of this technology have been previously described (*92*). Tumor percentage of studied specimen was 35%. The study quality was "high", full length WT1 was sequenced with good coverage of all exons, and average WT1-specific coverage for this sample was 452x.

**Whole Exome sequencing**. Isolated AML cells were sent to University of Washington Center for Precision Diagnostics for whole exome sequencing. >95% of genes had at least 20X coverage. A single nucleotide polymorphism was detected in [*PSMB9*], which was a G to A transition at position 179 (c.179G>A) yielding a change from an arginine to histidine (p.Arg60His). This polymorphism is reported to occur in 26.8% of the population (NCBI ALFA allele frequency, global population) (*93*).

**T cell isolation, activation, and transduction for cytotoxicity assays, live tumor-cell killing assays, and *in vivo* studies.** $CD8^+$ and/or $CD4^+$ T cells were isolated from healthy HLA-A*02:01 donor PBMCs using the EasySep Human positive selection kits (STEMCELL Technologies) following the manufacturer's protocol. T cells were seeded at $10^6$ T cells/ml with 50 IU/ml IL-2 and were activated with either CTS Dynabeads CD3/CD28 (Life Technologies), T Cell TransAct™, human (Miltenyi Biotec), or 30ng/ml OKT3 antibody according to manufacturer's instructions. After 24-48 hours of stimulation beads, TransACT™ or OKT3 was removed and T-cells were transduced with lentiviral particles encoding $TCR_{C4}$, $TCR_{37\text{-}45}$ or an irrelevant virus-specific TCR. In some cases to enhance transduction efficiency T cells were spinfected at 30°C and 1055 x g for 90 minutes with polybrene (Sigma-Aldrich) at 5 µg/mL or protamine sulfate at 10mg/ml. Because $TCR_{37\text{-}45}$ is dependent on CD8 expression in assays involving use of $CD4^+$ cells, the CD8-alpha and CD8-beta chains were added to the existing lentiviral constructs to generate $dpCD4^+$ and $eCD8^+$ T cells. Cells were maintained every 2-3 days with IL-2 and media supplemented with 5-10% human serum, L-glutamine (Thermo Fischer Scientific) or glutamax (Thermo Fisher Scientific) and antibiotics (penicillin (200U/ml) and streptomycin (0.1mg/ml) (Thermo Fisher Scientific)). After 7 days T cells were selected for

$CD8^+$ and multimer-binding (APC) using flow cytometry and subsequently placed in non-specific rapidly expanding protocol (REP)(*28*) for 9-12 days before use. Cells used for $^{51}Cr$ release assays, live-tumor assays, recognition assays, and in vivo studies were used after sort purification. Cells used in the AML cytotoxicity assays underwent Cas9 electroporation before WT1-specific TCR transduction to knockout both their TCRα and TCRβ chains of the endogenous TCR (see CRISPR methods below).

**Assessment of $WT1_{126-134}$ dependence on specific immunoproteasome subunits.** Four HEK-293 cell lines, each expressing one proteasome subtype (*95*), were used to study processing of the peptide $WT1_{126-135}$ by the four proteasomes. The day before transfection, 30,000 HEK-293 cells were seeded in collagen-treated 96-well plates (Greiner) in 100ul IMDM 10%FBS supplemented with essential amino acids, penicillin (200U/ml) and streptomycin (0.1mg/ml). The next day, 293 cells were transfected in duplicate using LT-transit (Mirus Bio), 50ng HLA-A*0201 and the indicated concentration of the pCMV6-XL4-WT1 variant D cDNA (Origene). As control, 1μM peptide $WT1_{126-135}$ was pulsed on HLA-A2 transfected cells for 30min. Peptide was removed before addition of the CTL. After 24 h, transfected cells were incubated with 10,000 CTL in 200μl IMDM medium supplemented with 10% FBS, essential amino acids, penicillin (200U/ml), streptomycin (0.1mg/ml) and 25 U/ml rIL2. After 20h co-culture, the culture supernatant was collected and TNF released by the CTL was measured using WEHI -164 cl13 cells as previously described (*96*).

**Collection, sorting, and RNA extraction of normal donor peripheral blood stem cells and primary AMLs.** For our study, we had access to historical data from 6 normal donor mobilized peripheral stem cells and peripheral blood or bone marrow samples AMLs from 38 previously

untreated patients. All donors and patients signed the informed consent for Fred Hutch protocol #1690: Fred Hutch/University of Washington Hematopoietic Diseases Repository. Cryopreserved samples were thawed, and RNA was extracted as previously described (*97*). Briefly, after thawing cells were stained with CD45-APC-H7 (to identify lymphoid and myeloid populations, Beckman Coulter, Pasadena, CA), CD34-APC, and CD117-PE (to identify the immunophenotype of leukemic blasts, BioLegend, San Diego, CA) and sorted on a BDFACS Aria II instruments for viable AML blasts. Cells were then lysed in RLT-Plus buffer (Qiagen, Valencia, CA) supplemented with β-mercaptoethanol (Sigma-Aldrich, St. Louis, MO) and RNA from the CD34+ enriched normal donor mobilized peripheral stem cells and leukemic blast populations were extracted by using the AllPrep DNA/RNA Mini kit (Qiagen) and quantified by using the Nanodrop spectrophotometer (Thermofisher Scientific). RNA integrity number (RIN) was determined on Agilent 2200 TapeStation (Agilent Technologies, Santa Clara, CA).

**RNA sequencing on viable leukemia blasts and normal mobilized peripheral blood stem cells.** RiboErase (Roche, Wilmington, MA) was utilized to deplete ribosomal RNA, and transcriptome libraries were generated using KAPA Stranded RNA-Seq Library Preparation Kit. Paired-end 50 bp or 75 bp reads were sequenced on either Illumina HiSeq 2500 instrument or NovaSeq 6000 instruments (Illumina, San Diego, CA). A pipeline of established bioinformatics tools, including FastQC (https://www.bioinformatics.babraham.ac.uk/projects/fastqc/), STAR2, (*85*) RSeQC,(*98*) Subread/featureCounts,(*99*) was used by the FRED HUTCH Bioinformatics Resource to assess data quality, map reads to GRCh37/hg19 and compute gene-level expression based on GENCODE gene annotation V31 (*100*). The expression matrix was processed by edgeR(*101*) and normalized using the Trimmed Mean of M-values (TMM) method (*102*).

**Identification of the HLA A*0201-restricted WT1-specific TCR$_{37\text{-}45}$.**

1. **Generation of WT1 epitope-specific T cell lines.** Antigen-specific T cell lines were generated from two donors that were specific for the following WT1 peptides: WT1$_{10\text{-}18}$ (ALLPAVPSL), WT1$_{22\text{-}31}$ (GGCALPVSGA), WT1$_{37\text{-}45}$ (VLDFAPPGA), WT1$_{38\text{-}46}$ (LDFAPPGAS), WT1$_{187\text{-}195}$ (SLGEQQYSV), WT1$_{235\text{-}243}$ (CMTWNQMNL), WT1$_{238\text{-}246}$ (WNQMNLGAT), and WT1$_{242\text{-}250}$ (NLGATLKGV). 10 lines were generated from each donor targeting each epitope (160 total) as previously described (*28*). Briefly, dendritic cells were derived from the plastic adherent fraction of PBMCs after culture for two days (days -2 to 0) in media supplemented with 1000 U/ml IL-4 and 800 U/ml GM-CSF. On day -1, a maturation cocktail containing 10ng/ml TNFα, 10ng/ml IL-1β, 1000 U/ml IL-6 and 1000ng/ml $PGE_2$ was added. On day 0, DCs were harvested, washed and pulsed with peptide. CD8 T cells were isolated from PBMCs using anti-CD8 microbeads and stimulated with peptide-pulsed DCs in the presence of 30ng/ml IL-21. Cultures were fed every 2-3 days by exchanging half of the medium and adding 12.5 U/ml IL-2, 5ng/ml IL-7 and 5ng/ml IL-15. T cells were re-stimulated every 10 days by culturing at a 1:2 ratio with irradiated, peptide-pulsed, autologous PBMCs.
2. **Sort-purification of WT1 specific T cell lines.** T cell lines from the most responsive donor PBMCs were stained with peptide-HLA-A*0201 tetramers specific for WT1$_{37\text{-}45}$ and WT1$_{235\text{-}243}$. The optimal tetramer concentration for staining was determined by titrating each tetramer on a cell population containing antigen-specific T cells and evaluating specific staining above background (non-specific) T cells. The tetramer-stained cells were sorted for high expression of tetramer and expanded using a modified

rapid expansion protocol with IL2 (50 U/mL), OKT3 (1 mg/mL), and 100-fold excess of irradiated feeder cells in 8 mL of RMPI1640 supplemented with 10% heat inactivated human AB serum, 25 mM HEPES, 12 mM L-glutamine, and 55 μM β-mercaptoethanol. Cultures were maintained with CTL media and 50 U/mL IL-2 every 2-3 days.

3. **Evaluation of antigen-specific cytokine production in response to $A2^+$ K562 cells.** Sorted antigen-specific T cells were co-cultured at a 1:1 ratio with HLA-A2-transduced K562 cells ($A2^+$ K562). After 6 hours of incubation in the presence of golgi-inhibitors (BD GolgiPlug and GolgiStop), cells were surface-stained with anti-CD8 and then fixed (BD Cytofix/Cytoperm) before intracellular labelling with anti-IFNγ in BD Perm/Wash buffer. The cells were then analyzed by flow cytometry to determine the percentage of $IFN\gamma^+$ cells for each sample.
4. **Isolation and expression of a $WT1_{37\text{-}45}$-specific TCR.** T cells from $WT1_{37\text{-}45}$, which exhibited the most robust IFNγ response when cultured with $A2^+$ K562s, were further sorted for the highest population of tetramer binding T cells (~1% of the total population). The sorted $tetramer^{hi}$ population of cells were lysed, RNA was isolated, and full length TRA and TRB genes were amplified by RACE PCR (TakaraBio). A dominant TCRA/TCRB clonotype was evident from the sequencing data, which was confirmed to be $WT1_{37\text{-}45}$ specific by expression in Jurkat cells followed by $WT1_{37\text{-}45}$ specific tetramer staining. This TCR ($TCR_{WT1\text{-}37\text{-}45}$ #1) was then synthesized as a codon-optimized P2A-linked lentiviral expression construct in the pRRLSIN.cPPT.MSCV/GFP.wPRE vector after excising the green fluorescent protein (GFP) gene (*76*).
5. **Lysis of $A2^+$ K562 cells by Primary T cells expressing WT1-specific TCRs**. Target $A2^+$ K562 cells or control ($HLA\text{-}A2^-$) K562 cells were labeled with $^{51}Cr$ (PerkinElmer,

Fremont, CA) overnight, washed and incubated in triplicate with effector T cells expressing either $TCR_{C4}$ or $TCR_{WT1\text{-}37\text{-}45}$ #1 at various effector to target (E:T) ratios. Supernatants were harvested for γ-counting after a 4 h incubation and percent specific lysis was calculated.

**Immunoblot of proteasome catalytic subunits from patient sample or HEK-293 cell lines expressing specific proteasome isoforms.** *Cell lysis*: For relapsed patient sample, PBMCs were depleted of $CD3^+$ cells using EasySep CD3+ selection kit II (StemCell) following manufacturer's instructions. $CD3^+$ cells were discarded leaving an enriched AML blast population. Blasts or HEK-293-EBNA cells expressing either standard proteasome (SP) or the immunoproteasome (IP) were then counted and lysed at 40M cells/mL for 15 min on ice using Pierce IP lysis buffer (Thermo Fisher) with 1X proteasome inhibitor (Thermo Fisher). Lysates were spun at 13,000 xG for 10 min to clear. *Co-immunoprecipitation:* Assembled proteasome complexes were isolated using co-immunoprecipitation with and anti- α2 antibody, MCP21 (Enzo Lifesciences, BML-PW8105) and assessed with immunoblot as previously described using different immunoprecipitation beads (*47*) (*40*). Briefly, Dynabeads M-270 epoxy beads (Invitrogen) were functionalized with MCP21 at 35 μg antibody per mg Dynabeads following manufacturer's instructions. Cleared lysate was quantified using a BCA assay Kit (Thermo Fisher) and 700 ng protein was incubated with 1mg functionalized beads to capture assembled proteasome complexes. Complexes were eluted in 0.1M Glycine buffer pH 2-2.5 and neutralized with equal volume Tris pH 7.5. *Immunoblot:* Proteasome composition assessed by immunoblot. Elution fractions were separated on a denaturing 4-12% polyacrylamide gel and then transferred to a

PVDF (Invitrogen) membrane using the mini-blot module (Invitrogen). Membranes were blocked for 1 h at room temperature in TBS containing 5% of dry milk and 0.1% Tween 20, washed three times in TBS, 0.1% Tween and incubated with the primary antibody. Standard proteasome and immunoproteasome beta subunits were probed 1:500 dilution in a solution of TBS, 5% milk powder, and 0.1% Tween-20 for β1[patient AML (Santa Cruz Bio, sc-374405), HEK293 cell lines (Enzo Life sciences, BLM-PW8140)], β2 (Enzo Lifesciences, BML-PW8145), β5(Enzo Lifesciences, BML- PW8895) β1i (Enzo Lifesciences, BML- PW8840), β2i(Novus, NBP1-8660-), β5i(Enzo Lifesciences, BML- PW8355) and the shared beta-subunit β7(Enzo Lifesciences, BML- PW8135) was used as a loading control.

**Transduction of HEK-293 cells expressing the IP or SP with WT1 and HLA A*02:01.** HEK-239-EBNA cell lines expressing either the IP or SP(*47*) were serially transduced with lentiviral constructs containing HLA A*02:01 then WT1 (pCVL-A) (*48*). Cells were cultured on CELLCOAT® Type I Collagen plates (greiner bio-one) all were grown in IMDM medium supplemented with L-Glutamine, 1% NEAA, 10% FBS. Hygromycin and puromycin were added to select for IP expressing cells. Cells were first transduced with HLA A*02:01 and positive cells (stained with anti-HLA-A2 (APC)) were isolated using the Sony MA900. HLA-$A2^+$ cells were then transduced a second time with full-length WT1 (variant D) in the pCVL-A(*48*) co expressing eGFP. Cells were again stained for HLA-A2 and double positive HLA-$A2^+GFP^+$ cells were selected using the Sony MA900 WT-1 expression was further confirmed by IHC (**See Immunohistochemistry methods**)

**Cytokine analysis of eCD8$^+$ and dpCD4$^+$ T$_{TCR37-45}$ cells.** PBMC were thawed from a healthy donor. CD8$^+$ and CD4$^+$ were selected using CD8 and CD4 positive selection kits from stem cell technologies. CD8$^+$ and CD4$^+$ T cells were transduced with a poly-cistronic construct containing TCR$_{37-45}$ and CD8αβ to yield eCD8$^+$ and dpCD4$^+$ T cells respectively. 5.0 x10$^5$ cells of either eCD8$^+$, dpCD4$^+$, or a combination eCD8$^+$/dpCD4$^+$(1:1 ratio; 2.5 x10$^5$ cells each) were co-cultured with T2 cells exogenously loaded with 10μg WT1$_{37-45}$ peptide at an E:T ratio of 5:1 for 4, 24 or 48 hours before supernatant was collected for analysis. Cytokine concentrations were determined using the R&D systems Luminex (*103*) platform according to manufacturer's instructions. Based on the inability of CD4$^+$ T cells to control tumor without co expression of the CD8αβ co-receptor (**Fig. 5K** and **Fig. S15**), suggesting a lack of TCR activation through TCR signaling, we did not assess the cytokine profile of CD4 T cells alone. Similarly, CD8$^+$ cells expressing only TCR$_{37-45}$ showed identical tumor control as eCD8$^+$ T cells and were not assessed separately.

**Cytotoxicity assays of HEK-293 IP and SP cell lines.** Cytotoxic activity of mock-transduced, T$_{TCR-C4}$ and CD8+ T cells transduced with TCR$_{37-45}$ were examined by assessing the capacity of the T cells to lyse WT1- and HLA-A2-transduced HEK-293-EBNA cell lines expressing either the IP or SP in a 4 hour$^{51}$ Chromium release assay at the indicated effector to target (E:T) ratios as previously described (*104*).

**AML cell death Assays.** Because the WT1-specific TCR is codon optimized, it is not susceptible to the gRNA used. The endogenous TCR can non-specifically react with the patient

sample (only HLA-A2 is matched) necessitating an additional CRISPR step to view specific TCR signaling (see **CRISPR/CAS9 Gene editing by electroporation)**.

1. **T cell induced AML Lysis.** CRISPRed T cells were transduced with $TCR_{37\text{-}45}$, $TCR_{C4}$, and $TCR_{Irr}$ and stained with CFSE and cultured with primary AML cells at the indicated E:T ratios in triplicates for 18 hours as previously described (*105*). Briefly, after the culture period, surviving AML cells were identified by staining for CD45 (PE Texas Red clone 2D1, BioLegend), CD34 (BV421 clone 561, BioLegend), CD38 (BUV395 clone HB7, Beckton Dickinson) and quantified with Flow Count beads (Molecular Probes). Percent killing was calculated by the formula: (Absolute number of AML targets in co-culture / Absolute number of AML targets in target only control well) x 100.
2. **T cell induced AML apoptosis.** T cells with endogenous TCR α and β chains knocked out with CRISPR (see CRISPR-Cas9 below) were transduced with $TCR_{37\text{-}45}$, $TCR_{C4}$, and $TCR_{irr}$ and cultured with PBMC form Pt.1' relapsed AML at a 3:1 E:T ratio ($3.0 \times 10^6$ T cells, $1.0 \times 10^6$ AML) for 1 hour. The cells were harvested and stained with a viability dye (TONBO Biosciences #13-0870-T100) and cell surface markers, CD34 (BioLegend #343610), CD8 (BD Biosciences #557760), CD45 (BioLegend #368510). The cells were fixed with 4% Formaldehyde (CellSignal #47746) and permeabilized with 100% Methanol (CellSignal #13604) according to manufacturer's instructions, followed by intracellular stain for cleaved caspase-3-FITC (CellSignal #96695) and analyzed by flow cytometry. Percent cleaved-caspase 3 expressing $CD8^{-}CD34^{+}$ cells were quantified.

**CRISPR-Cas9 Gene editing by electroporation.** $CD8^{+}$ and $CD4^{+}$ T cells were selected from healthy PBMCs using the EasySep Human CD8 Positive Selection kit II and Human CD4+ T

Cell isolation kit (STEMCELL Technologies). T Cells were seeded at $10^6$ T cells/mL with 50 IU/mL IL-2 and activated with T Cell TransAct, Human (Miltenyi Biotec) according to manufacturer's instructions. 48 hours later, TransAct was removed. Cells were then electroporated with Cas9 complexed with CRISPR-RNA (crRNA) targeting the TCRα and TCRβ to knock out the endogenous TCR, sequences for TRAC Exon 1 and TRBC Exon 1 were 5'-AGAGTCTCTCAGCTGGTACA-3' and 5'- GGAGAATGACGAGTGGACCC -3' respectively. To generate gRNAs, crRNAs and tracrRNAs were thawed, mixed at 1:1 v/v ratio (160μM stock) and incubated at 37°C for 30 minutes. To create the ribonucleoprotein (RNP) mixture, Cas9 protein (MacroLab, Berkeley, 61 μM stock) and poly-L-glutamic acid (Sigma-Aldrich, 100 mg/mL in $H_2O$ stock) were both added to the gRNA at a 1:1 v/v ratio (Poly-L-glutamic Acid:Cas9 protein). Poly-L-glutamic acid increases stability of the Cas9(*106*) T cells were resuspended in Lonza P3 Buffer ($1x10^6$ per 20 μL) and 4 μL of the RNP mixture was added to each sample. The Cell/RNP mixture was transferred to a 16 well nucleocuvette strip (Lonza) and electroporated using the pulse code EH115 (Lonza, Nucleofector™ Device). Following electroporation, 80 μL of prewarmed medium was added and the samples recovered for 15 minutes at 37°C. Cells were then transferred to 1mL of prewarmed media and allowed to rest for one hour at 37°C before transduction with lentivirus encoding $TCR_{C4}$, $TCR_{37\text{-}45}$ or an irrelevant virus-specific TCR. An aliquot of untransduced cells were reserved to assess TCRα/TCRβ knockout efficiency by flow cytometry 3 days later, efficiency determined by percent $CD3^-$. Cells were allowed to grow for 7 days after transduction, then FACS sorted for CD8+, tetramer+ (APC), then placed into a rapid expansion protocol (REP). Cells were ready to use 7-9 days after REP.

**Live tumor-cell killing assays.** T cell killing capacity was monitored using the IncuCyte® S3 Live-Cell Analysis System (Essen BioScience, Ann Arbor, MI). PANC-1 (ATCC®) and MDA-MB-468 (ATCC®) tumors were transduced with the IncuCyte® NucLight Red Lentivirus Reagent (Sartorius) and seeded (10,000 cells/well) in 48-well plates (Corning). When comparing WT1-specific TCRs, wells were cocultured in triplicate at an effector to tumor target ratio of 10:1 with either no T cells, or $CD8^+$ T cells transduced with the indicated TCR construct. When investigating if CD4+ cells could help sustain an anti-tumor response wells were cocultured in triplicate at an effector to tumor target ratio of 4:1 with no T cells, $CD8^+$ T cells, $dpCD4^+$ T cells or a $CD8^+$/$dpCD4^+$ T cell mixture. $CD8^+$ and $CD4^+$ T cells were transduced with a lentiviral construct containing CD8αβ along with $TCR_{37\text{-}45}$. For all assays, red fluorescence was recorded at 2 h intervals for 96 or 156 hours. Tumor rechallenge (10,000 cells/well) was conducted at 48 and 96 hours. Images were analyzed using the IncuCyte® S3 v. 2019b software (Essen BioScience) with total red object area ($\mu m^2$/well) corresponding to the degree of tumor cell death over time.

***In vivo* $T_{TCR37\text{-}45}$ therapy model.** The A2+ WT1+ pancreatic cancer cell line Panc-1 was transduced to express a firefly luciferase (PANC-$1_{Luc}$) individual clones were assessed for high level luciferase expression. Clone#9 was selected as the clone exhibiting the highest level of transgene expression and used in subsequent *in vivo* studies. NSG (NOD-*scid* IL2Rgamma$^{null}$) mice (*107*) of similar age and gender were injected with 1.25 x $10^5$ PANC-$1_{Luc}$ cells Intraperitoneal (I.P.). As a model of adoptive T cell therapy, three days later ('prevention' model) or 14 days later ('treatment' model) mice either received no T cells at all (tumor only), or therapeutic T cells ($T_{TCR37\text{-}46}$ , $T_{TCRC4}$ ,$T_{TCRirr.}$) consisting of each $eCD8^+$/$dpCD4^+$ (2E6 each (prevention model) or 10E6 each (treatment model)). Mice were imaged and weighed weekly. The mice were administered 1uL of Luciferin per gram of body weight at 15 mg/mL of

concentration Intraperitoneal (I.P.), under isoflurane anesthesia. The incubation time was 15 minutes before the mice were imaged, while still under isoflurane anesthesia. At week 4 $T_{TCR37\text{-}45}$ treated mice received a second injection of $T_{TC37\text{-}45}$ T cells ($2.0x10^6$ each $CD4^+$ and $CD8^+$). Mice were sacrificed on week 10.

# Supplementary Figures and Tables

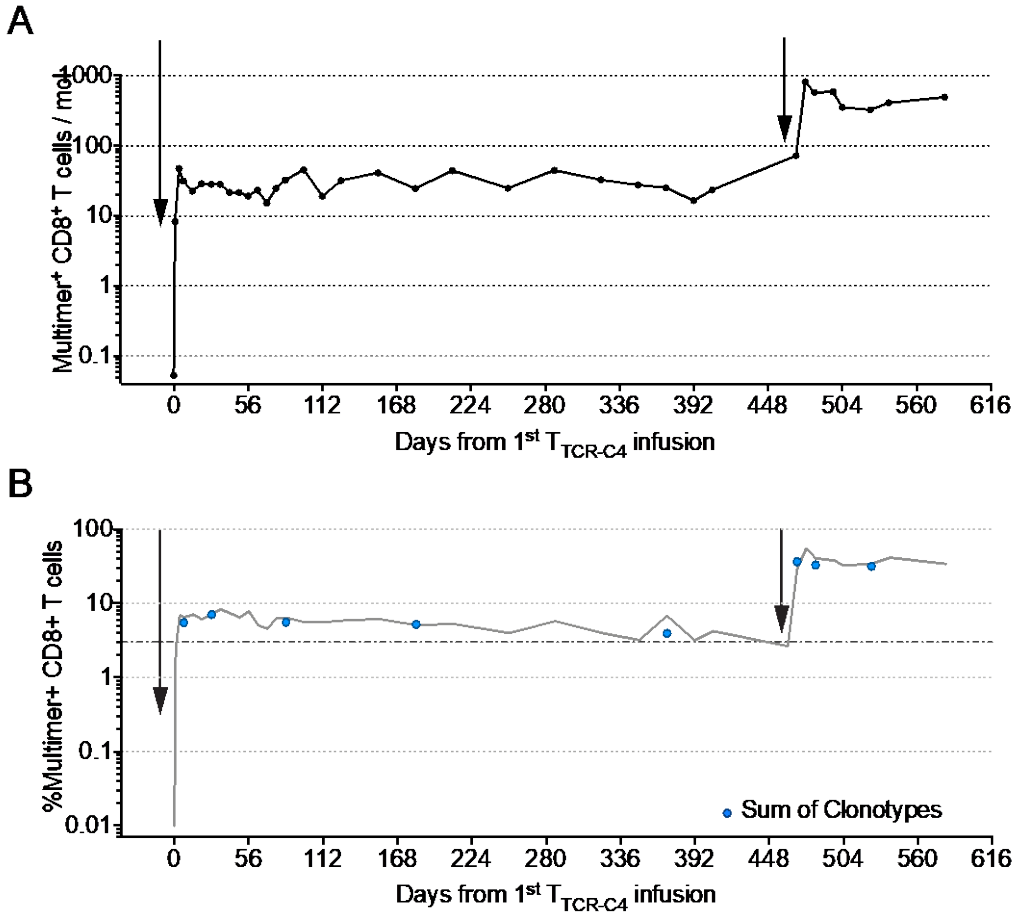


**Fig. S1*: Patient 1 in vivo* persistence kinetics of transferred $T_{TCR\text{-}C4}$. (A)** Multimer$^{+}$CD8$^{+}$ T-cells/µl (y-axis) in PBMCs collected after infusion (x-axis, day relative to first infusion). Time of infusions indicated with black arrows. **(B)** Relationship over time after infusion (x-axis) between the percent multimer$^{+}$CD8$^{+}$T cells (grey line) in PBMC and the sum of detected frequencies of individual infusion product clonotypes (blue circles). Multimer$^{+}$CD8$^{+}$ T-cells/µl (y-axis) in PBMCs collected after infusions (x-axis, day relative to first infusion). Time of infusions indicated with black arrows.

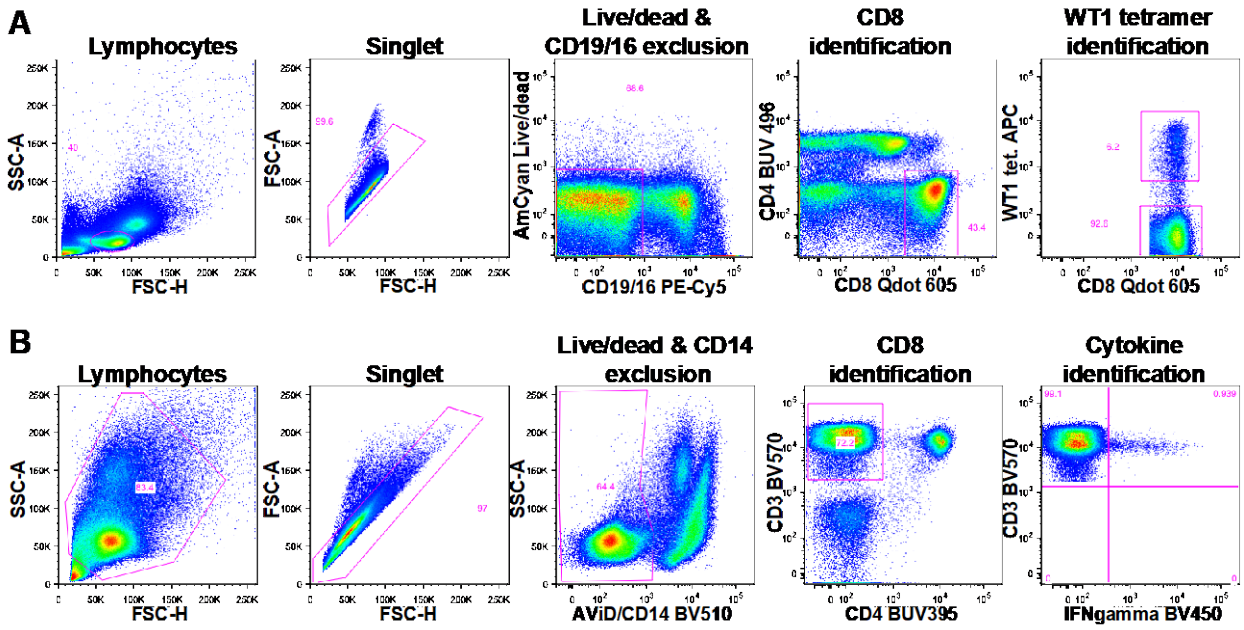


**Fig. S2 Gating strategies for surface and intracellular stains. (A)** Surface stains. Panels from left to right: Initial gating was on lymphocytes (SSC-A vs. FSC-H), followed by singlet exclusion (FSC-A vs FSC-H), followed by exclusion of dead cells and CD19/16-expressing cells (AmCyan Live/dead vs CD19/16 PE-Cy5), followed by CD8 identification (CD4 BUV 496 vs CD8 Qdot605), followed by WT1/HLA-A2 tet$^{+}$ cells identifying $T_{TCR\text{-}C4}$ (WT1 tetramer APC vs CD8 Qdot605). A representative example is shown. **(B)** Intracellular stains. Panels from left to right: Initial gating was on lymphocyte identification (SSC-A vs. FSC-H), followed by singlet exclusion (FSC-A vs. FSC-H), followed by exclusion of dead cells and CD14-expressing antigen presenting cells (SSC-A vs. AViD/CD14 BV510), followed by CD8 identification (CD3 BV570 vs CD4 BUV395), followed by cytokine identification (CD3 BV570 vs IFNgamma BV450). A representative example for IFNγ is shown.

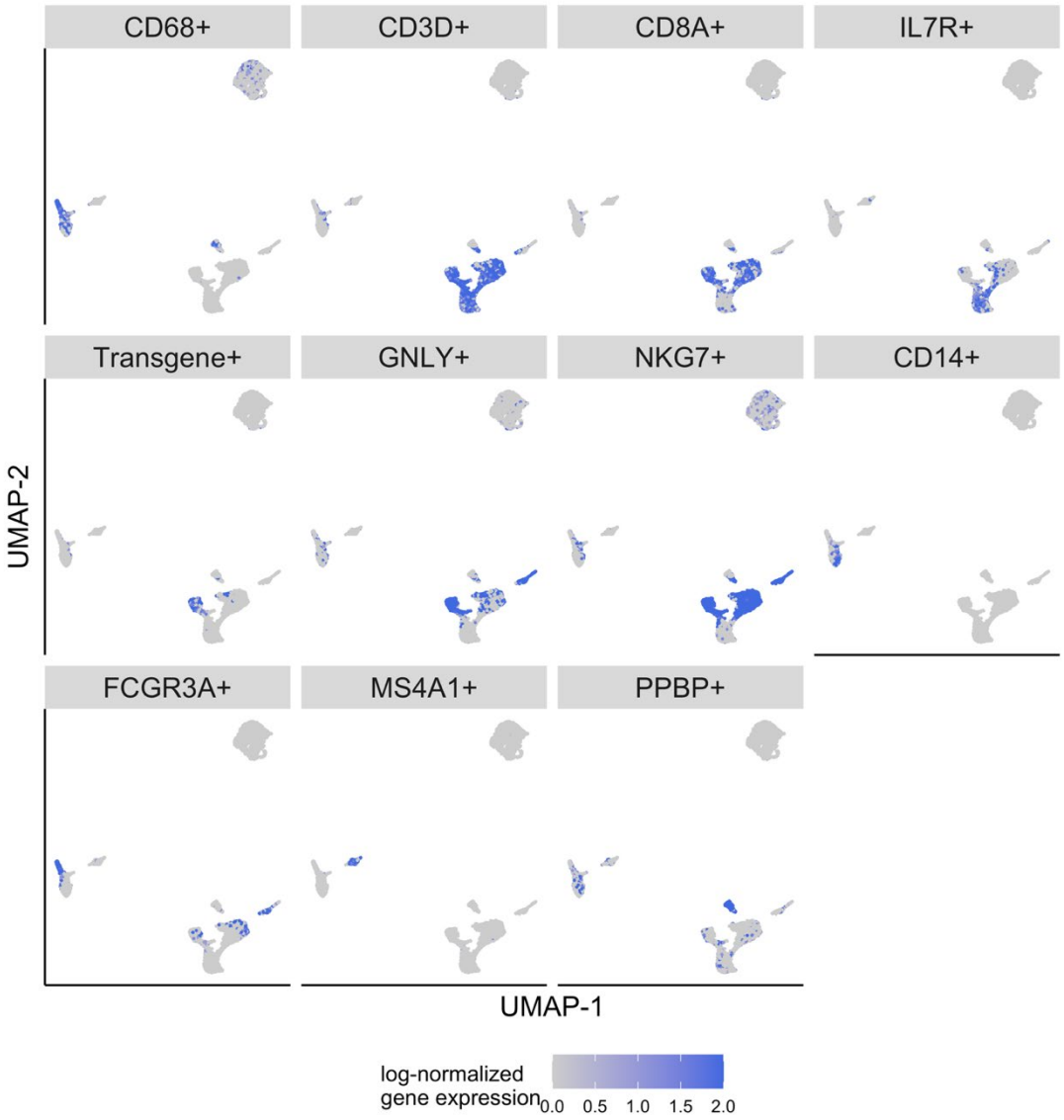


**Fig. S3: Identification of cell populations in patient 1 peripheral blood.** Selection of key markers that assisted in confirmation of clusters identified by principal component analysis and visualized with UMAP for both remission and relapse timepoints combined (n=7704, each represented with a dot). Gene names are shown. Blue color shows cells expressing indicated gene, with darker blue indicating greater expression.

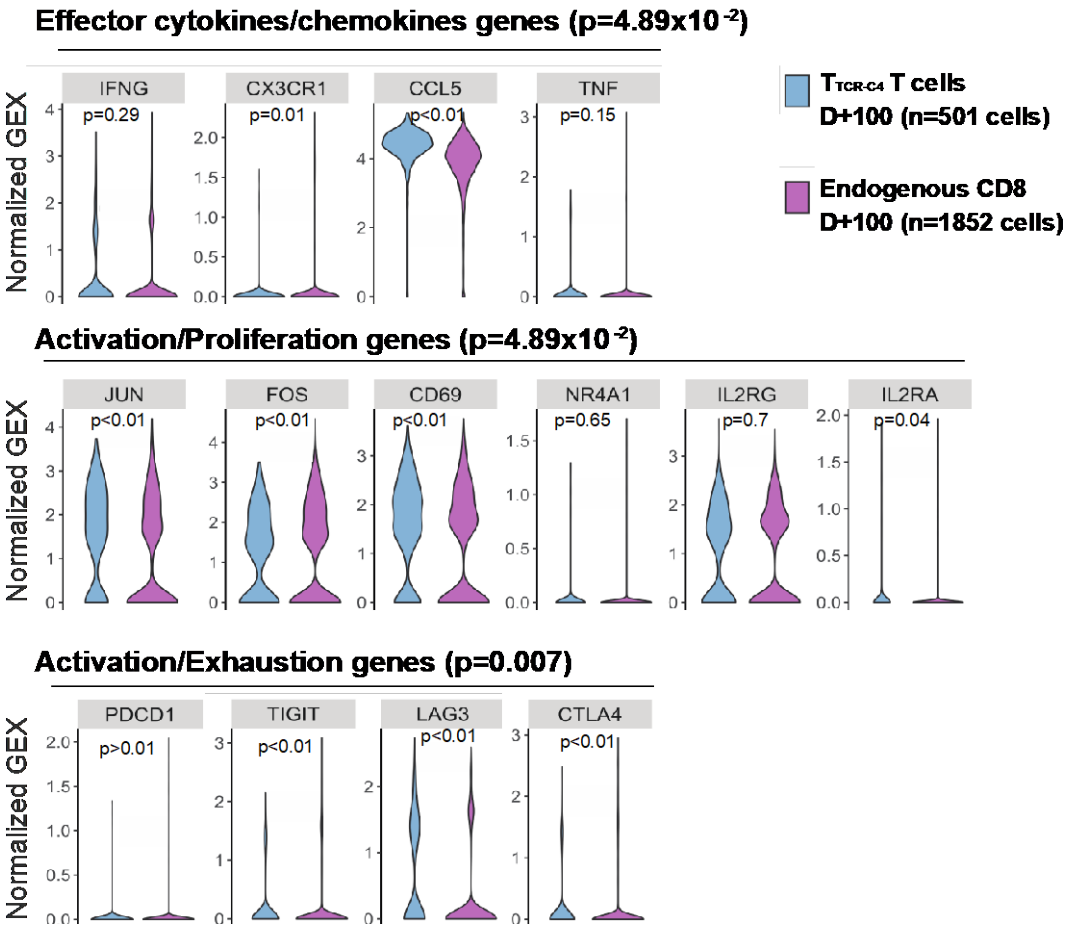


**Fig. S4**: **Gene set differences between $T_{TCR\text{-}C4}$ and endogenous $CD8^+$ T cells at remission.** Expression of transcripts for gene-sets representing effector cytokine/chemokine production and T cell activation at remission for $T_{TCR\text{-}C4}$ (blue, n=501) and endogenous $CD8^+$ T cells (purple, n=1852). All graphs are shown as a violin plot. The shape of the violin displays frequencies of values. Model-based Analysis of Single Cell Transcriptomics (MAST – See **Supplementary Methods**) was used to determine the significance shown on each plot. Significance thresholds were set *a priori* at a threshold of false discovery rate of 5% and positive or negative fold change > log2(1.3). Effector cytokine/chemokine genes: Interferon-γ [*IFNG*], C-X-C motif chemokine receptor 1 [*CX3CR1*], C-C Motif Chemokine Ligand 5 [*CCL5*] and Tumor Necrosis Factor-α[*TNF*]. Activation/Proliferation genes: Jun proto-oncogene [*JUN*], Fos proto-oncogene

[*FOS*], [*CD69*], nuclear receptor subfamily 4 group A member 1 [*NR4A1*], interleukin 2 receptor subunit gamma [*IL2RG*], and interleukin 2 receptor subunit alpha [*IL2RA*].

Activation/Exhaustion genes: Programmed Cell Death Receptor-1 [PDCD1], T-Cell Immunoreceptor with Ig and ITIM domains [TIGIT], Lymphocyte Activating-3 [LAG-3] and Cytotoxic T-Lymphocyte Associated Protein 4 [CTLA4].

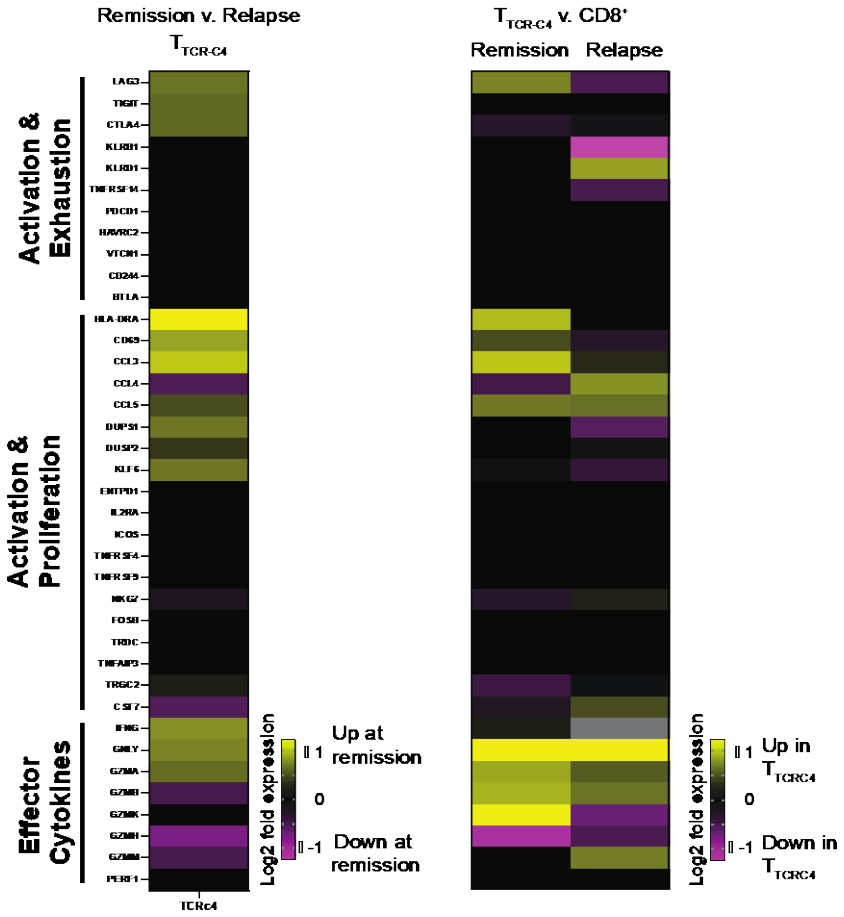


**Fig. S5**: **Gene expression differences between $T_{TCR-C4}$ at remission and relapse and between $T_{TCR-C4}$ and endogenous CD8$^+$ T cells at both remission and relapse.** Heat map of gene expression differences (shown as Log2 fold change) for a large set of activation/exhaustion genes, Activation/proliferation genes, and effector cytokines. Comparisons: between $T_{TCR-C4}$ at remission and at relapse, and $T_{TCR-C4}$ and endogenous CD8$^+$ T cells remission, $T_{TCR-C4}$ and endogenous CD8$^+$ T cells at relapse. Grey indicates Log2 fold change could not be calculated.

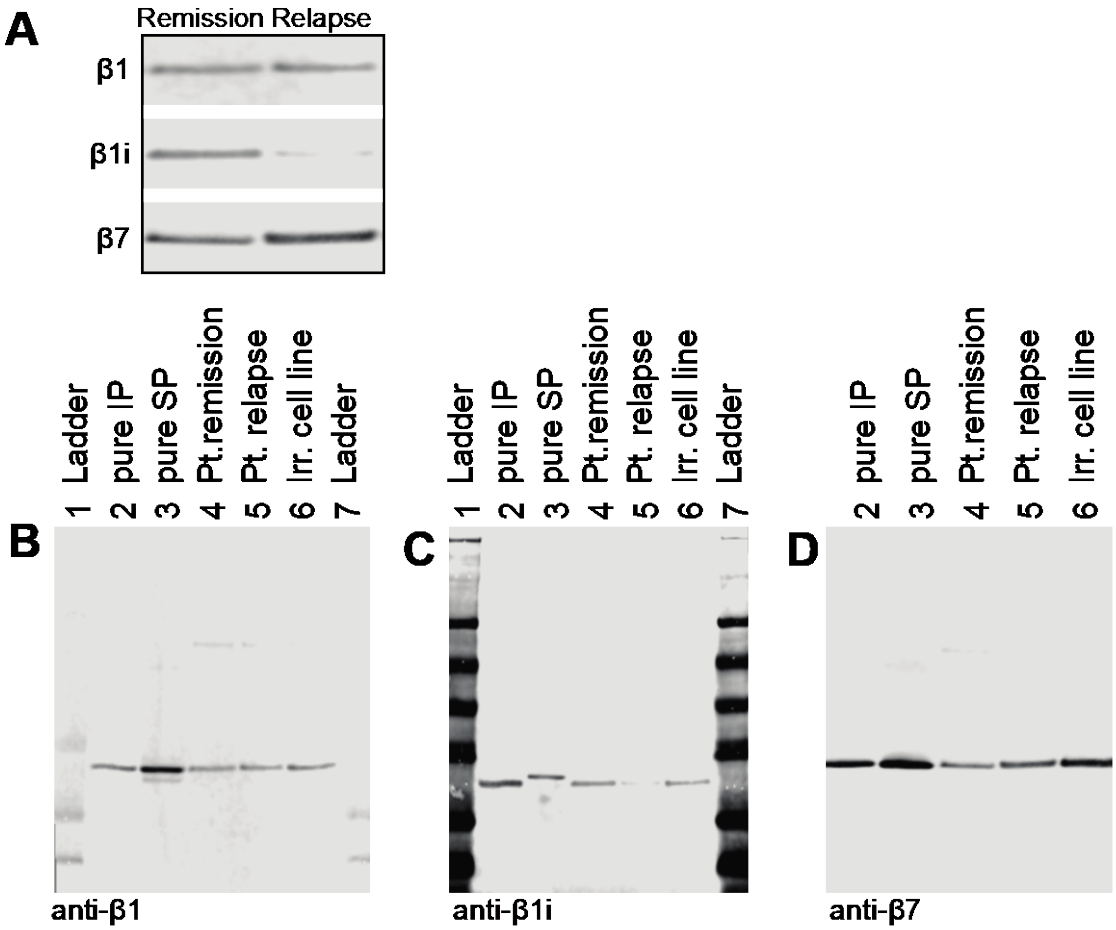


**Fig. S6: Protein expression of proteasome subunits at remission and relapse.** (**A**) Loss of immunoproteasome subunit β1i at relapse was confirmed using immunoblot. Patient PBMCs from remission (complete sample) and CD3 depleted AML from relapse were lysed and assembled proteasome complexes were immunoprecipitated. Subunits were detected using immunoblot (see **Supplementary Methods**). Proteasome subunit β7 is shared between both Immunoproteasome and standard proteasome complexes and serves as a loading control of immunoprecipitated fractions (**B**) Full blots are shown (**B)** anti-β1 (**C**) anti-β1i (**D**) anti-β7. Lanes are 1-Ladder, 2-purified Immunoproteasome (Thermo Fischer), 3-purified Standard proteasome (Novus Biologics), 4-Patient PMBCs at remission 5- Patient AML at relapse, 6-irrelevant cell line, 7-ladder.

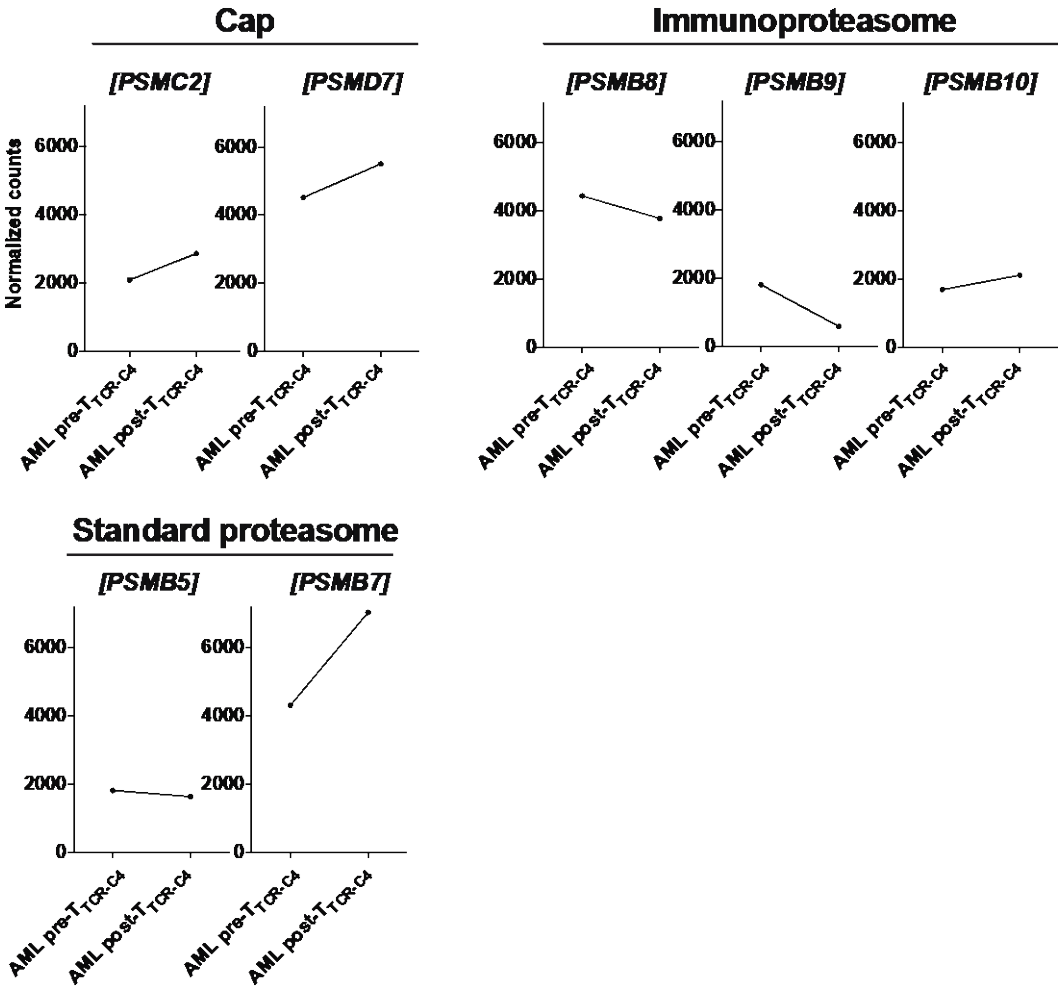


**Fig. S7: Transcript expression of proteasome subunit in AML before and after $T_{TCR\text{-}C4}$ infusions.** Normalized counts showing expression of proteasome beta subunits and two subunits in the regulatory cap. Unfortunately, no PSMB6 (β1) probes were available for the panel used (see **Supplementary Methods**).

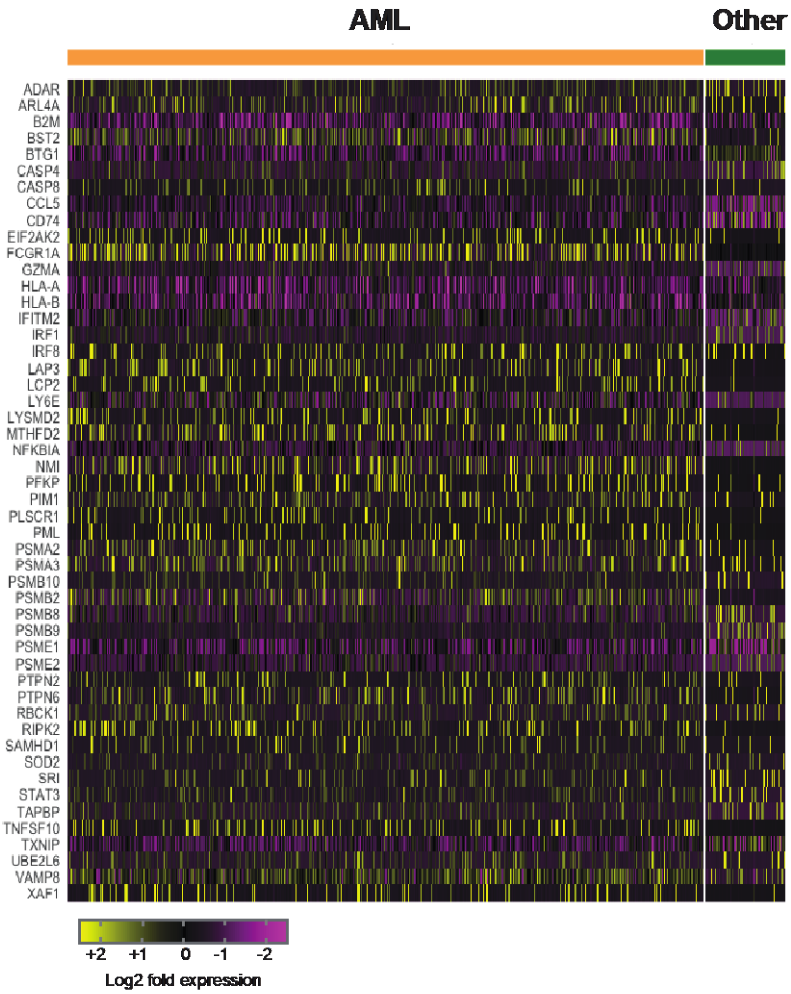


**Fig. S8: IFNγ response genes expressed in Patient 1 relapsed PBMC.** Fifty of the most highly expressed IFNγ response genes in PBMC at relapse in addition to immunoproteasome subunits in Patient 1's AML and other immune cells.

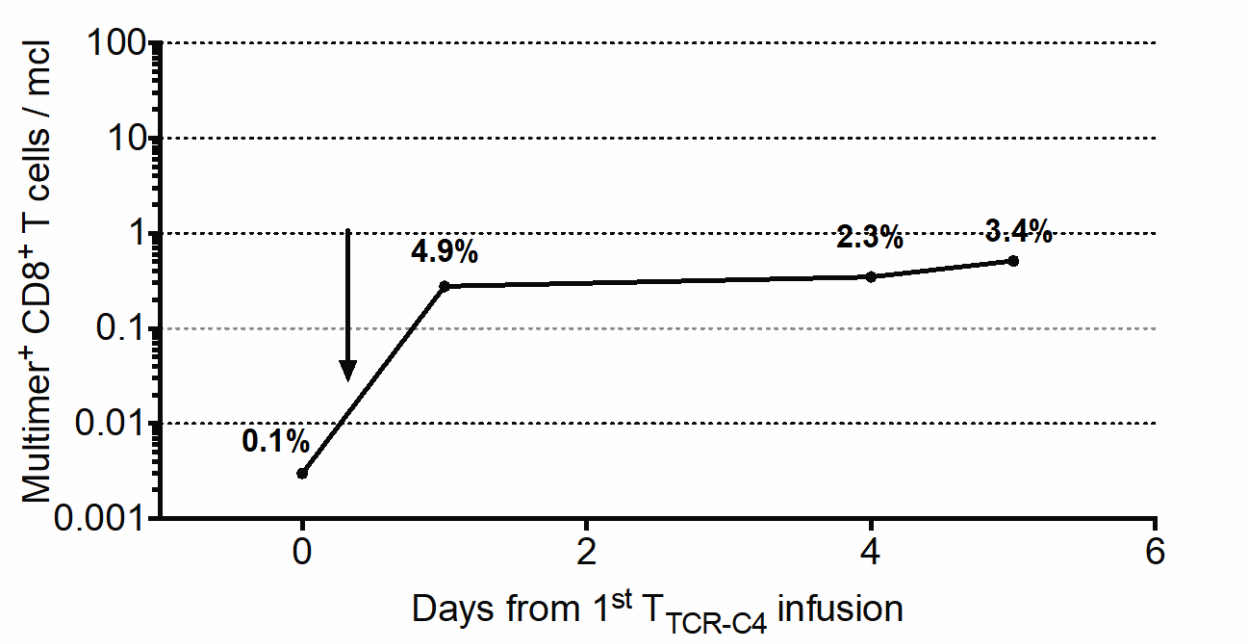


**Fig. S9: Patient 2 *in vivo* persistence kinetics of transferred $T_{TCR\text{-}C4}$.:** Multimer$^{+}$CD8$^{+}$ T-cells/µl (y-axis) in PBMCs collected after infusion (x-axis, day relative to infusion). Time of infusion indicated with black arrow. Percent multimer$^{+}$ of CD8$^{+}$ cells shown above each timepoint.

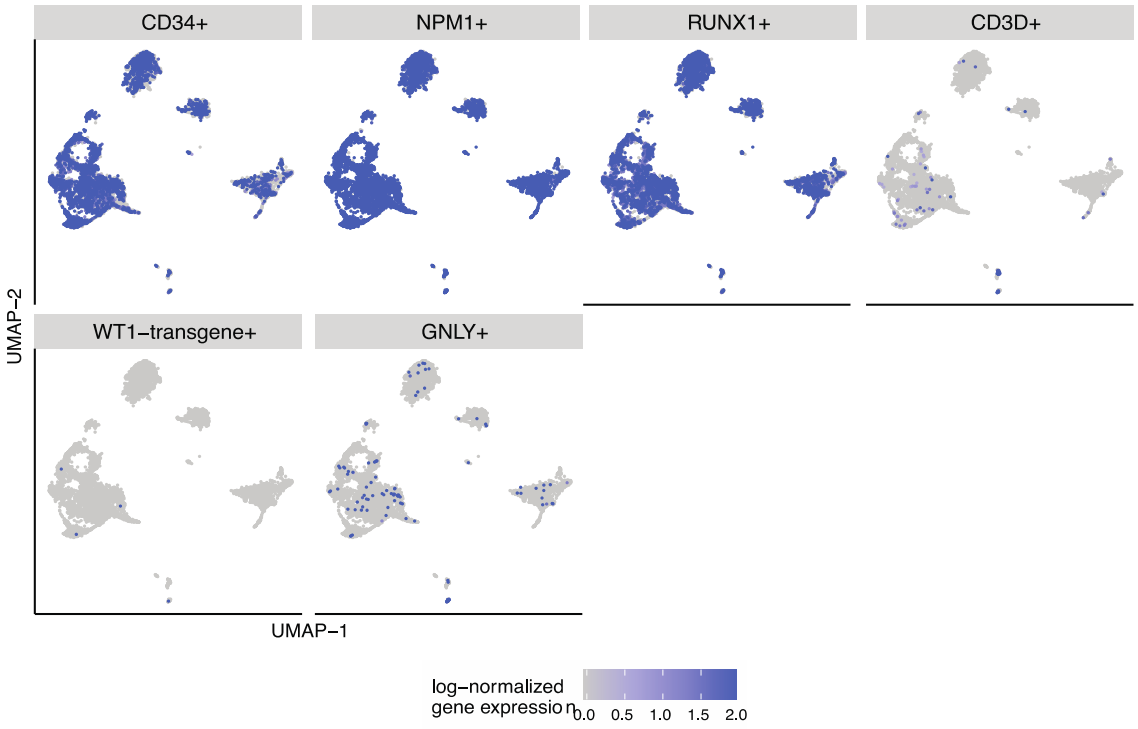


**Fig. S10: Identification of cell populations in patient 2 peripheral blood.** Selection of key markers that assisted in confirmation of clusters identified by principal component analysis and visualized with UMAP for both remission and relapse timepoints combined (n=10,700). Gene names are shown. Blue color shows cells expressing indicated gene, with darker blue indicating greater expression.

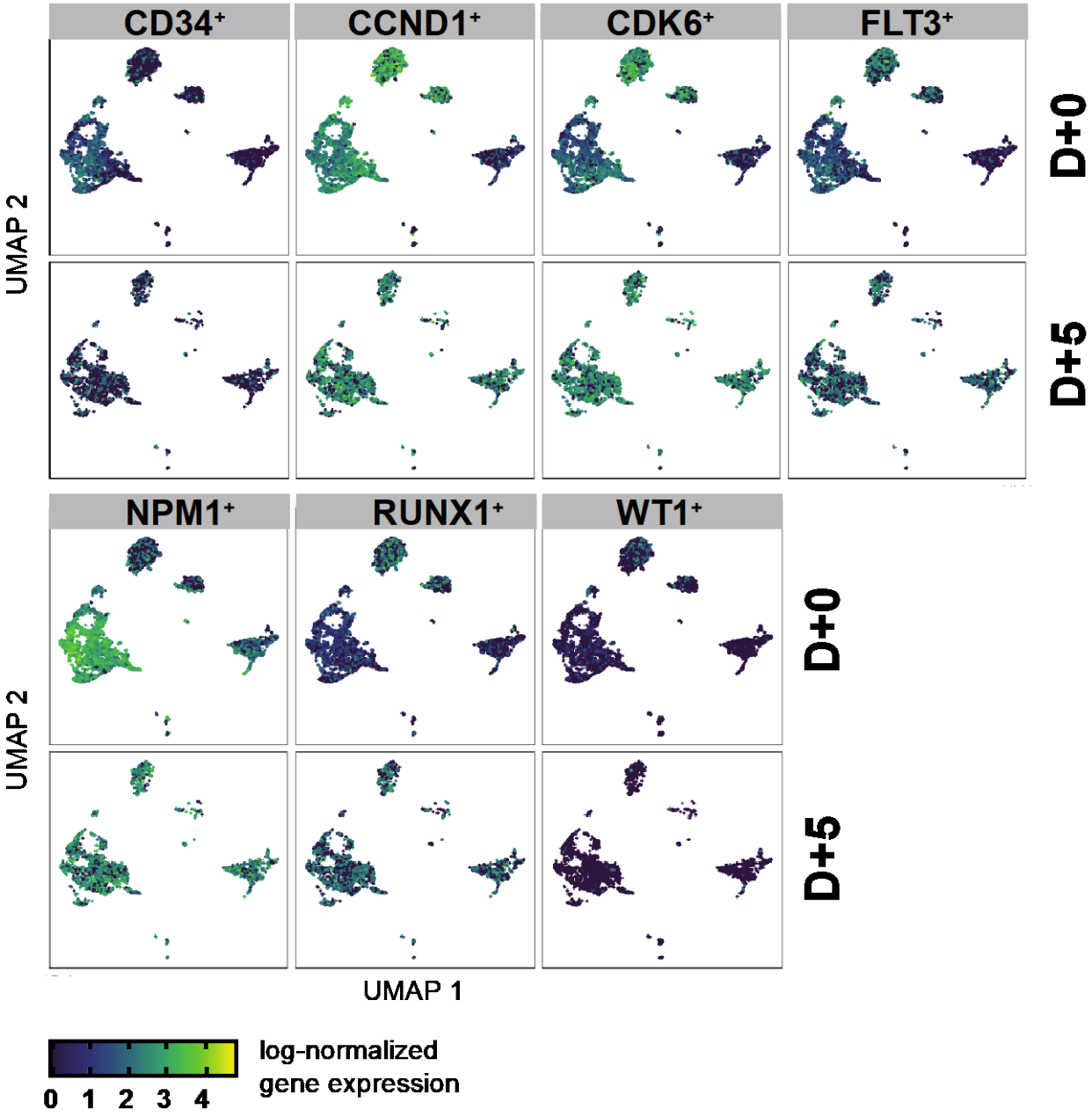


**Fig. S11: Gene expression of AML specific genes in patient 5 AML before and five days after $T_{TCR\text{-}C4}$ therapy.** Key markers associated with AML that assisted in confirmation of AML visualized with UMAP for both remission (D+0, n=7,381) and relapse (D+5, n=3,319) timepoints with each cell represented with a dot. Gene names are shown. Purple through yellow coloring color shows expression levels.

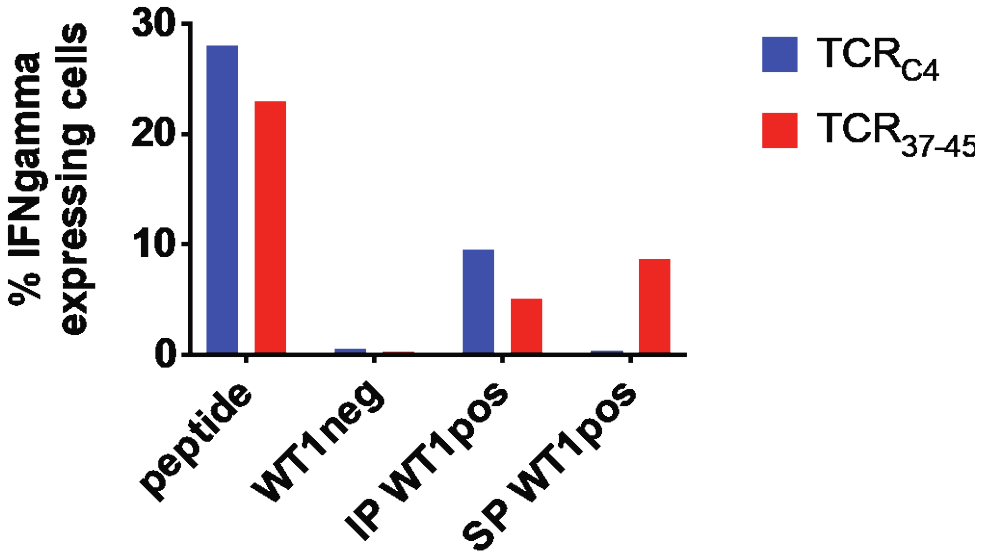


**Fig. S12: Recognition of HLA-A2- and WT1-transduced HEK293 cells expressing IP/SP by $T_{TCR-C4}$ and $T_{TCR37-45}$.** $CD8^+$ T cells from a healthy, HLA-A*02+ donor were selected and transduced with $TCR_{C4}$ and $TCR_{WT1-37-45}$. $T_{TCRC4}$ and $T_{TCR37-45}$ were co-cultured with target cell lines (x-axis). Targets are HLA-A2 T2 cells loaded with 10ng/mL respective peptide (peptide), HLA-A2-transduced HEK 293 expressing SP (WT1neg), HLA-A2- and WT1-transduced HEK 293 cells engineered to express IP (IP WT1pos), and HLA-A2- and WT1-transduced HEK 293 cells expressing SP (SP WT1 pos). Target cells were co-cultured with $T_{TCR-C4}$ or $T_{TCR37-45}$ for 20 hours at an E:T ratio of 1.5:1. Cells were subjected to ICS and assessed for IFNγ production with flow cytometry.

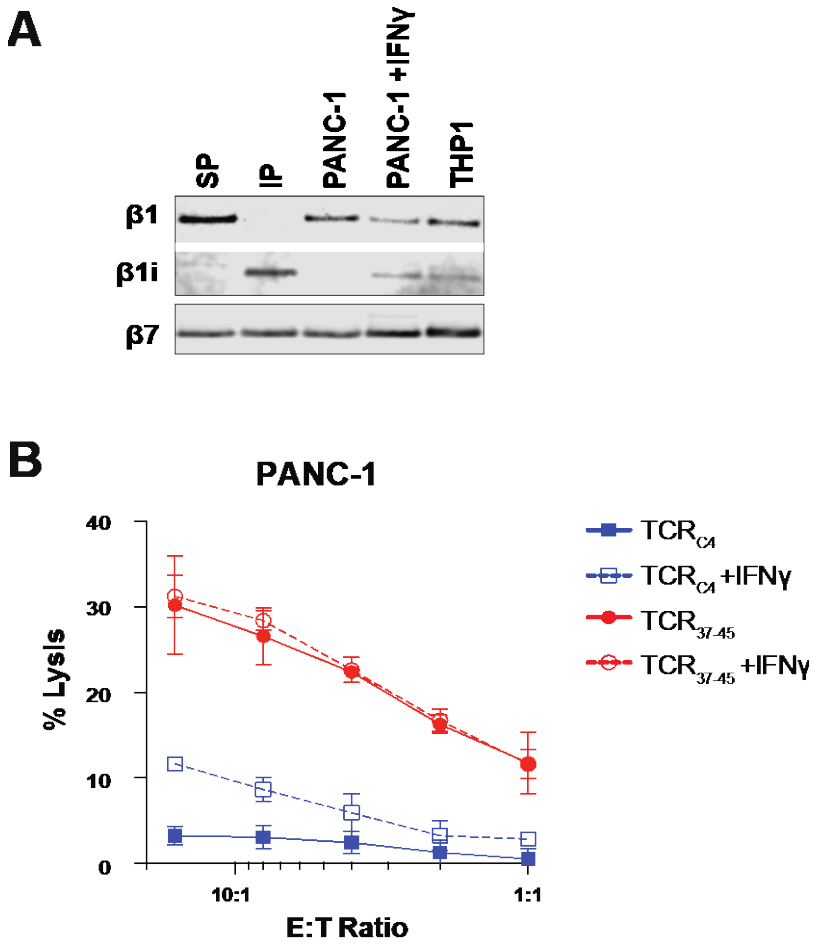


**Fig. S13: 48-hour exposure to IFNγ induces β1i expression and incorporation into proteasomes in PANC-1 but does not completely rescue recognition by $T_{TCR-C4}$ T cells.** (**A**) Immunoblot of standard and immunoproteasome subunits β1 and β1i respectively. Cells were lysed and assembled proteasome complexes were immunoprecipitated and analyzed. Proteasome subunit β7 is shared between both immunoproteasome and standard proteasome complexes and serves as a loading control of immunoprecipitated fractions. (**B**) PANC-1 cells that were either exposed to IFNγ for 48 hours (dotted lines) or untreated (solid lines) prior to culture with T cells expressing $TCR_{C4}$ or $TCR_{37-45}$ at various E:T ratios.

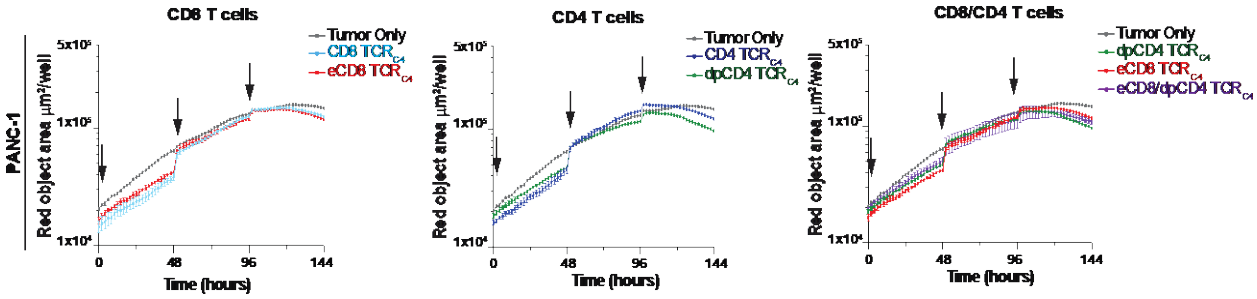


**Fig. S14: In the absence of addition of exogeneous IFNγ exposure, increased levels of CD8αβ does not rescue $TCR_{C4}$ in a PANC-1 solid tumor model.** Left: $CD8^+$ T cells transduced with only $TCR_{C4}$ (light-blue line) or a polycistronic construct containing $TCR_{C4}$ and CD8αβ (red line, $eCD8^+$). Middle: $CD4^+$ T cells transduced with only $TCR_{C4}$ (blue line) or a polycistronic construct containing $TCR_{C4}$ and CD8αβ (green line, $dpCD4^+$). Right: Comparison of $eCD8^+$ alone (red line), $dpCD4^+$ alone (green line) or $eCD8^+/dpCD4^+$ in combination (1:1 ratio, purple line). For all conditions, arrows indicate addition of tumor cells to culture. Standard error of triplicate wells are shown. 4:1 E:T ratio, total T cells was kept consistent for all conditions.

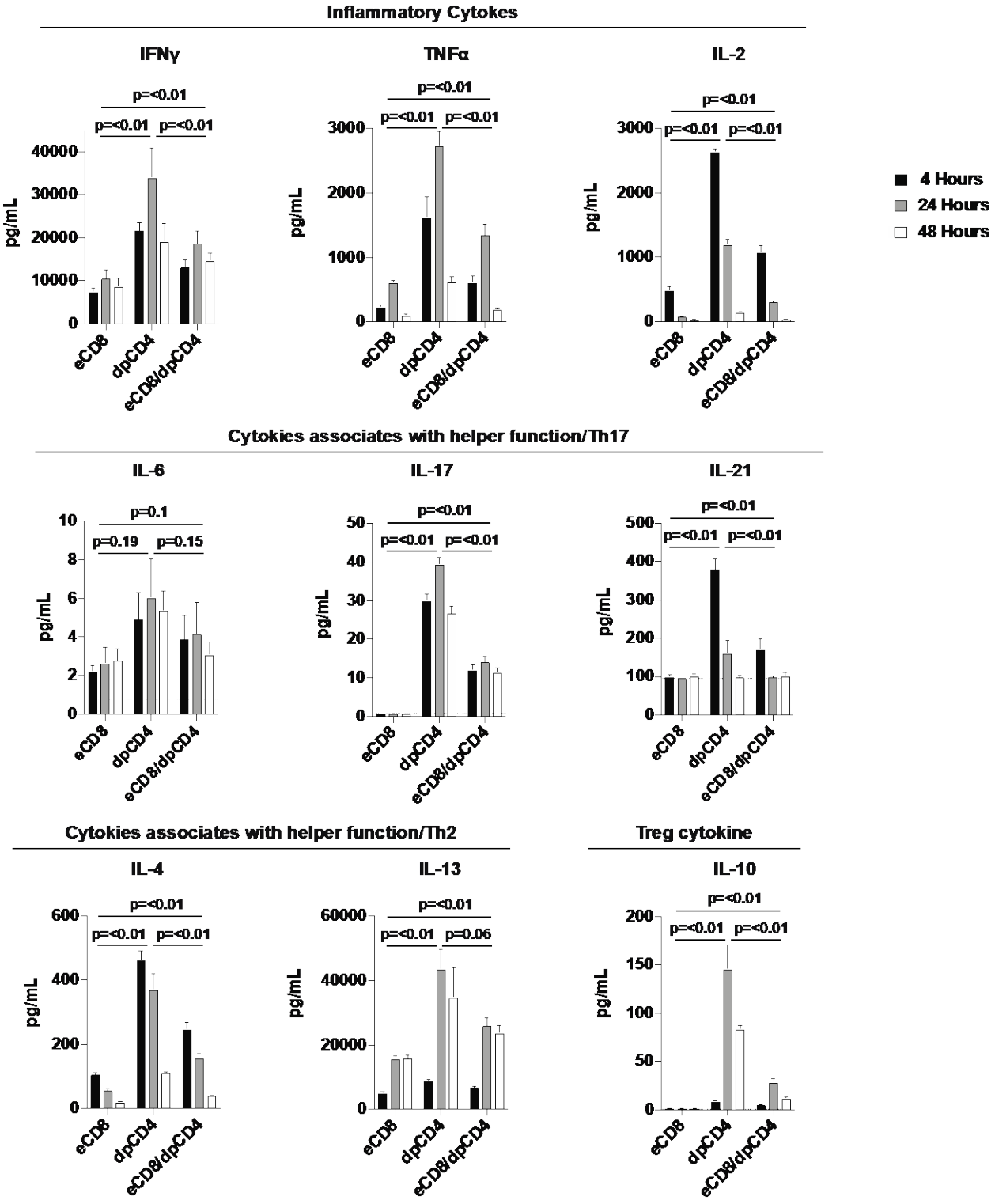


**Fig. S15: Cytokine profile of peptide stimulated eCD8$^+$, dpCD4$^+$ and eCD8$^+$/dpCD4$^+$ $T_{CR37-45}$ T cells.** Cytokine production by $T_{CR37-45}$ T cells after 4, 24, and 48 hours of

stimulation with T2 cells exogenously loaded with 10µg peptide. Except for IL-6 all cytokines are found at significantly higher levels in dpCD4$^{+}$ cells compared to eCD8$^{+}$ cells and the mixture of eCD8$^{+}$/dpCD4$^{+}$. The mixture of eCD8$^{+}$/dpCD4$^{+}$ does produce significantly more cytokine than eCD8$^{+}$ cells alone.

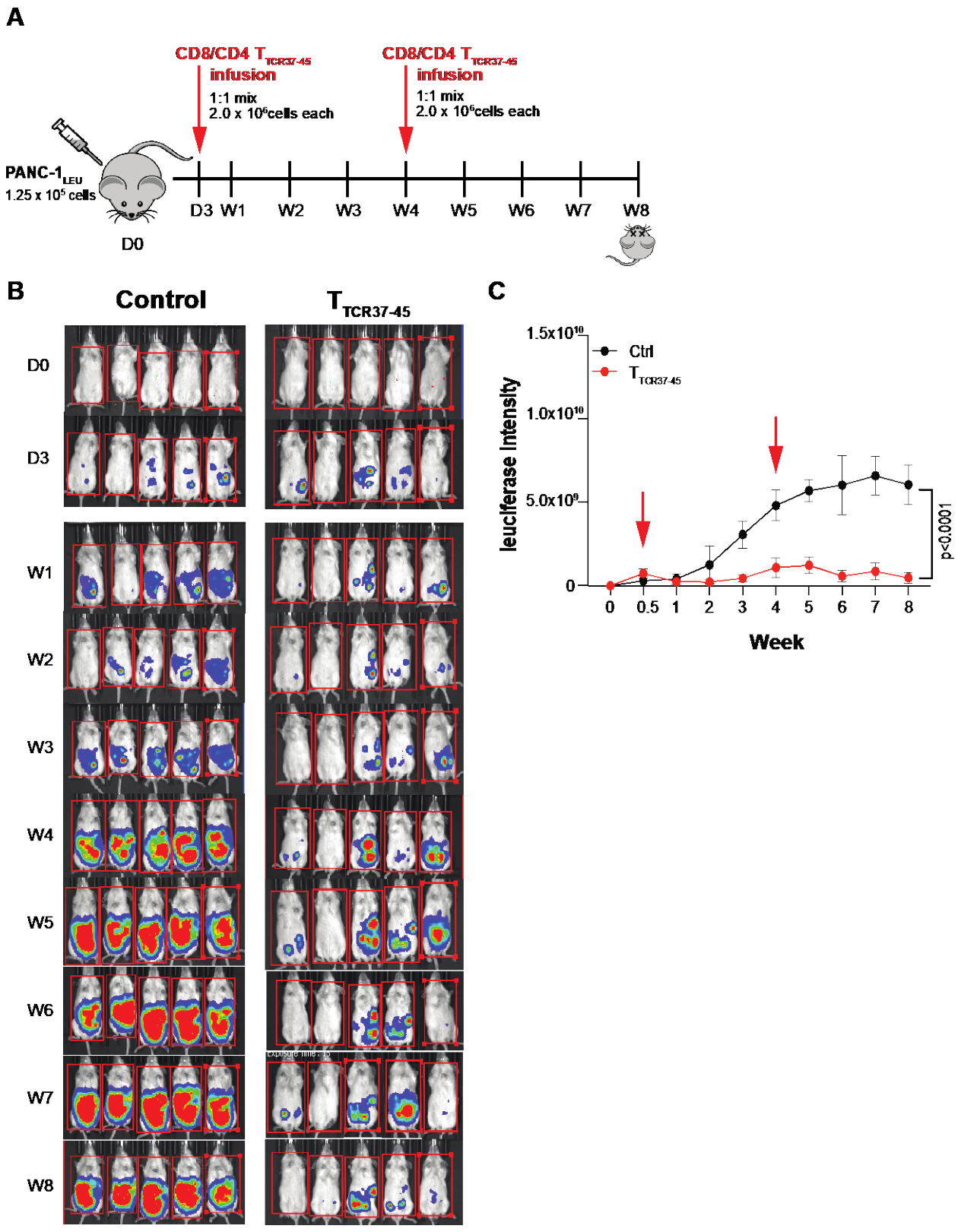


**Fig. S16: $T_{TCR37-45}$ controls PANC-1 tumor growth in a prevention model with NSG mice.**

**(A)** Schematic illustrating experimental time course. NSG (NOD-*scid* IL2Rgamma$^{null}$) mice were injected with 1.25 x $10^5$ Panc-1-Leu cells intraperitoneally. On day 3 post-injection, a subset of tumor-bearing mice were injected with a mix of $CD8^+$/dp$CD4^+$ $T_{TCR37\text{-}45}$ (2 x $10^6$ of each, 1:1 ratio), and received a second injection of $CD8^+$/dp$CD4^+$ $T_{TCR37\text{-}45}$ at week 4. Control mice did not receive therapeutic T cells **(B)** Mice were imaged weekly as shown for a bioluminescence signal to gauge progression/regression of tumor in vivo. The mice were administered 1uL of Luciferin per gram of body weight at 15 mg/mL of concentration intraperitoneal (I.P.), under isoflurane anesthesia. The incubation time was 15 minutes before the mice were imaged using IVIS, while still under isoflurane anesthesia. **(C)** Mean luciferase activity for the treated and untreated mice. Error bars indicate 95% confidence interval. The p-value was calculated by 2-way ANOVA. Of note: mice 3 and 5 of the $T_{TCR37\text{-}45}$ treatment group were originally imaged in the incorrect order on week 7. For clarity, the larger image for this week only was cropped to individual mice and ordered correctly

| Days after 1st $T_{TCR\text{-}C4}$ infusion | CMV (IU/mL) | EBV (IU/mL) |
|---|---|---|
| 0 | NDET | NDET |
| 1 | NDET | 130 |
| 7 | NDET | NDET |
| 14 | NDET | NDET |
| 24 | NDET | NDET |
| 180 | NDET | NDET |
| 210 | NDET | NDET |
| 254 | NDET | NDET |

**Table S1: Detection of CMV and EBV viremias after infusions.** Patient serum was analyzed for presence of CMV and EBV virus (see **Supplementary Methods**) over the course of treatment. NDET: none detected.